博士論文

太陽系初期進化段階における
有機物と鉱物の相互作用

Interactions between organic matter and minerals during early stages of the Solar System evolution

横浜国立大学大学院

理工学府

Yokohama National University

Graduate School of Engineering and Science

平川 尚毅

Naoki HIRAKAWA

2021 年 3 月

Contents

List of publications

Doctral Dissertation

1. **Hirakawa, N.**, Kebukawa, Y., Kobayashi, K., Nakano, H., 2020. Effects of minerals on metamorphism of organic matter during thermal processes in meteorite parent bodies. *Icarus*, 358, 114167. https://doi.org/10.1016/j.icarus.2020.114167

2. **Hirakawa, N.**, Kebukawa, Y., Furukawa, Y., Kondo, M., Nakano, H., Kobayashi, K., 2021. Aqueous alteration without initial water: Possibility of organic-induced hydration of anhydrous silicates in meteorite parent bodies. *Earth Planets Space*, 73: 16. https://doi.org/10.1186/s40623-020-01352-6

3. **Hirakawa, N.**, Shibuya, T., Ueda, H., Kebukawa, Y., Kobayashi, K., Synthesis of Fe-bearing olivine for experiments simulating conditions inside small bodies. in preparation.

Reference Article

4. Nakano, H., **Hirakawa, N.**, Matsubara, Y., Yamashita, S., Okuchi, T., Asahina, K., Tanaka, R., Suzuki, N., Naraoka, H., Takano, Y., Tachibana, S., Hama, T., Oba, Y., Kimura, Y., Watanabe, N., Kouchi, A., 2020. Interstellar organic matter: A hidden reservoir of water inside the snow line. *Scientific Report* 10, 7755. https://doi.org/10.1038/s41598-020-64815-6

Abbreviations

EDS	Energy Dispersive X-ray spectroscopy
FIB	Focused Ion Beam
FTIR	Fourier Transform Infrared Spectroscopy
ISM	Interstellar Medium
OM	Organic Mixture
SEM	Scanning Electron Microscope
TEM	Transmission Electron Microscope
XRD	X-Ray Diffraction

1. Introduction

1.1. Introductions into chondrites and the meteoritical organics

1.1.1. Chondrites and the classification

Evolution of our Solar System proceeded along (1) interstellar gas and submicron scale dusts in a molecular cloud, (2) gravitational contraction of molecular cloud core towards the formation of protostar and proto-solar nebulae, (3) accretion of the gas and dusts to proto-planetary disk, (4) accumulation to planetesimals (10 km size), (5) collision of planetesimals to form meteorite parent bodies (100 km size) and growth to planets (Hayashi et al. 1985; Figure1-1). Materials such as minerals, ice and organic matter were formed and evolved in each different stage. One of the most significant stages for interactions among materials was meteorite parent bodies, which meteorites came from.

Meteorites can be classified into various type and groups. Chondrite is a major meteorite group, they could avoid strong igneous processes in the parent bodies, thus various accreted components originated from molecular cloud and proto-solar nebulae can be observed. Chondrites can be also classified into carbonaceous chondrite, ordinary chondrite, enstatite chondrite and additional other chondrites (Rumuruti-like chondrites and Kakangari-like chondrites) primary based on chemical compositions, oxygen isotopic compositions, bulk stable-isotope anomaly, oxidation state and bulk carbon and nitrogen abundances (Table 1-1; Krot et al. 2014). Carbonaceous, ordinary and enstatite chondrites are additionally classified based on petrologic types (van Schmus and Wood 1967), which reflect the degree of thermal metamorphism and aqueous alteration in the parent bodies (Table 1-1). The least altered or metamorphosed chondrites are classified as type 3. Type 3 chondrites include some carbonaceous chondrites such as CV and CO chondrites, and unequilibrated ordinary chondrites. Type 1 and 2 are aqueously altered chondrites (type 1 was more altered than type 2 chondrites), such as CI, CM and CR chondrites, and thermally metamorphosed chondrites are type 4-6 (lager number means the larger metamorphic degrees). In terms of organic matter, however, there are some evidence of heating even in type 3 chondrites (Quirico et al. 2003, 2009; Bonal et al. 2006, 2007, 2016; Alexander et al. 2007; Busemann et al. 2007; Cody et al. 2008; Kebukawa et al. 2011; Homma et al. 2015), since organic matter is more sensitive to thermal conditions compared with minerals. With increase of metamorphic grade, the amount of organic matter decreased, and the chemical structure gradually changed. Thus, relatively weak thermal processes could have occurred in type 3 chondrites, which could induce the metamorphism of organic matter. Carbonaceous chondrites, especially CI, CM, CR, CV and CO chondrites, and ordinary chondrites with type 3 were focused on in present study to discuss the interactions between organic matter and minerals.

1.1.2. Organic matter in chondrites

Organic matter in chondrites is classified into soluble organic matter (SOM) and insoluble organic

matter (IOM). SOM involves prebiotic molecules such as amino acids, carboxylic acids and sugars. Most part of the organic matter is IOM (≧70%) with complex macromolecular networks (Derenne and Robert 2010). The structural and chemical diversity of organic matter in various chondrites reflect the physicochemical conditions such as temperature, time and oxidation state in meteorite parent bodies (Quirico et al. 2003, 2009; Alexander et al. 2007; Bonal et al. 2006; Busemann et al. 2007; Cody and Alexander 2005; Cody et al. 2008; Kebukawa et al. 2010b, 2011; Homma et al. 2015). Thermal processes in the parent bodies can lead to the loss of organic matter in chondrites. Type 1 and 2 chondrites contain relatively more amount of organic matter than heated chondrites. Type 3 chondrites are seldom or weakly heated, thus the amount of organic matter decreased with the increase of the effect of heating in type 3 chondrites.

Origin of these organic matter has been controversial; three synthetic processes are often discussed. One is that organic matter could have originate from molecular cloud via ion-molecule reactions and/or photochemical processes of amorphous ice (H_2O, CO, NH_3, CH_4 etc.) on grain surface (e.g. Herbst and van Dishoeck 2009). This process can explain the isotope anomalies of organic matter in many chondrites (Alexander et al. 2007, 2010), since isotopic fractionation processes could be possible only in low temperature regions such as molecular cloud (10 K). Fischer-Tropsch-type reaction of CO, H_2 and NH_3 gas on mineral grain surface in protoplanetary disk is the second one (Hayatsu and Anders 1981). In that case, organic matter could be formed at high temperature (500-900 K) in the nebulae. The third one proposes the complex organic matter formation in planetesimals through aqueous processes. Relatively simple molecules such as CH_2O and NH_3 from interstellar regions could react to macromolecular organic matter starting from Formose reactions (Cody et al. 2011; Kebukawa et al. 2013). Organic matter synthesized by these processes could have altered and/or metamorphosed in the meteorite parent bodies, then various chemical structures and compositions of meteoritical organics were formed.

1.1.3. Distribution of organic matter in the inner region of the early Solar System

Although various organic molecules are detected in chondrites (e.g. Alexander et al. 2017), the nature of the most primitive organic matter has not been revealed. The oldest origin of organic matter in Solar System could be molecular cloud. Such organic matter and the sourced ice on interstellar dust grains distributed to early disk of the Solar System. To know what types of organic matter could be existed at the time of accretion to small bodies, possible distributions of organic matter was theoretically and experimentally investigated in some studies (Nakano et al. 2003; Herbst and van Dishoeck 2009; Welsh et al. 2014; Gail and Trieloff 2017). Light molecular species such as H_2O, CO and NH_3 could evaporate under 100-300 K (Herbst and van Dishoeck 2009), which the boundary between these sublimation areas and non-sublimation area is called snow line of each molecule. Comparing with these light molecules, some complex organic molecules including polyaromatic

hydrocarbons, aliphatic hydrocarbons, alcohols, carboxylic acids, macromolecular organic matter could survive on the grain surface even inside sublimation area of these ice. Schematic image of the delivering of organic matter to inner Solar System was shown in Herbst and van Dishoeck (2009; Figure 1-2). In addition to these, some studies indicated the growth of rocky planetesimals inside H_2O snow line was realized by the sticky nature of rocky dust grains with organic mantles in a temperature range 200 K≦T≦400 K (Kouchi et al. 2002; Kudo et al. 2002; Gail and Trieloff 2017; Homma et al. 2019). Thus, survival of organic matter inside H_2O snow line should have had significant influences on the formation of early Solar System.

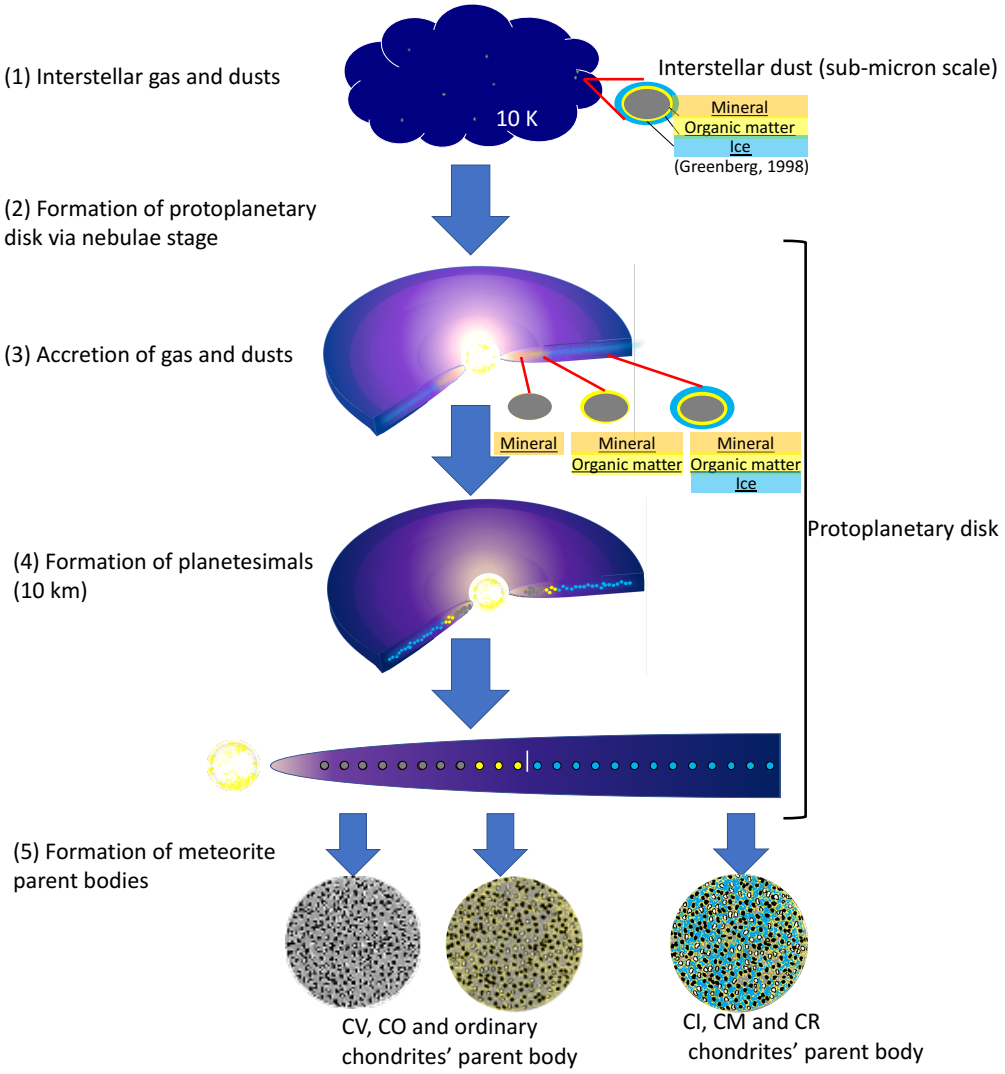

Figure 1-1. Schematic image of the evolution of the early Solar System.

Table 1-1. A framework of the classification of meteorites (Krot et al. 2014).

Class →	Carbonaceous								Ordinary			Enstatite			
Group →	CI	CM	CO	CR	CB-CH			CV	CK	H	L	LL	EH	EL	R	K
Petr. type →	1	1–2	3–4	1–2	3		3	3–4	3–6	3–6			3–6		3–6	3
Subgroup →					CB_a CB_b			CV_{OxA} CV_{OxB} CV_R								

Achondrites and other igneous meteorites

Primitive achondrites	*Differentiated achondrites*	*Irons and stony irons*	*Planetary*
Winonaites	Angrites	Mesosiderites	Martian
Acapodranites	Aubrites	Pallasites	Shergottites
Acapulcoites	Ureilites	Main group	Nakhlites
Lodranites	HED	Eagle Station	Chassignites
Brachinites	Howardites	IAB irons	Orthopyroxenite
	Eucrites	IC irons	Lunar
	Diogenites	IIAB irons	
		IIC irons	
		IID irons	
		IIE irons	
		IIG irons	
		IIIAB irons	
		IIICD irons	
		IIIE irons	
		IIIF irons	
		IVA irons	
		IVB irons	

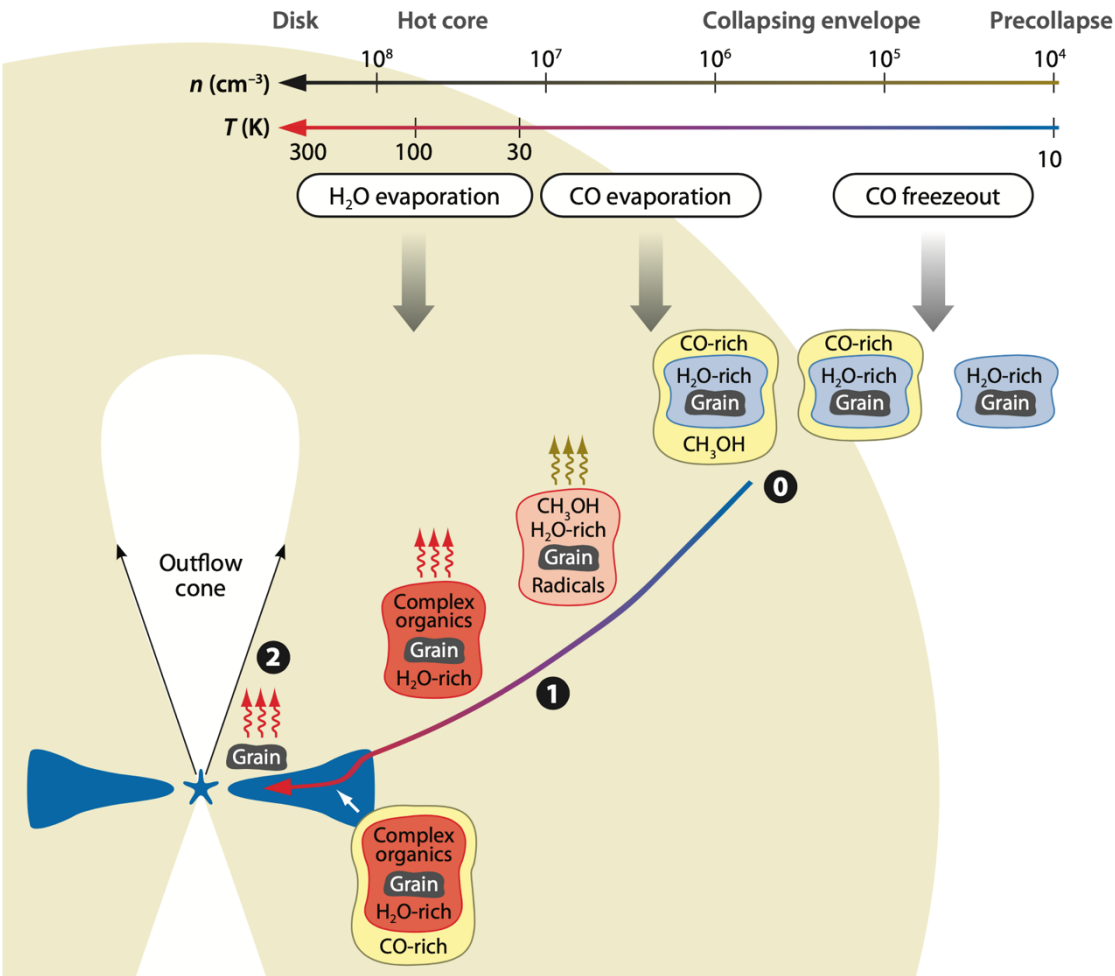

Figure 1-2. Schematic image of the survival of organic matter on grain surfaces (Herbst and van Dishoeck 2009).

1.2. Co-existence of organic matter and specific minerals

Microscopic and spectroscopic observations have revealed the close relationships among water, mineral and organic matter in the petrology of carbonaceous chondrites (Pearson et al. 2002, 2007; Garvie and Buseck 2007; Kebukawa et al. 2010a, 2019; Le Guillou et al. 2014, Le Guillou and Brearley 2014; Yesiltas et al. 2015; Yesiltau and Kebukawa 2016). Association of organic matter with phyllosilicates is well known (Figure 1-3), thus the phyllosilicate surface could act as an adsorbent during aqueous processes in the parent bodies (Pearson et al. 2002, 2007). On the contrary, organic matter distributed with anhydrous minerals was revealed to have relatively lower CH_2/CH_3 ratio compared with organic matter associated with phyllosilicates (Kebukawa et al. 2019a). The CH_2/CH_3 ratio can increase with the proceeding of alteration or metamorphism, thus organic matter associated with anhydrous minerals could be primitive (Kebukawa et al. 2019a, b). These observations could indicate that primordial organic matter and anhydrous minerals could evolve together to specific relationships such as the co-existence of phyllosilicates and organic matter. Phyllosilicates are the hydrous phase of silicate minerals, thus the relationship must have formed under the existence of water. However, such co-evolutional process is not simple, since the mutual influences between organic matter and minerals during alteration and metamorphism should be considered. Enhancement of several organic reactions by minerals in the parent bodies have been investigated experimentally or analytically (Pearson et al. 2002; Kebukawa et al. 2010b; Yamashita and Naraoka 2014; Le Guillou et al. 2014; Naraoka et al. 2015; Rotelli et al. 2016; Fuchida et al. 2017; Vinogradoff et al. 2020a, b) in according to some metamorphic processes such as the temperature, time and oxidation state (Quirico et al. 2003, 2009; Cody and Alexander 2005; Bonal et al. 2006;Alexander et al. 2007; Busemann et al. 2007; Cody et al. 2008; Kebukawa et al. 2010b, 2011; Homma et al. 2015). Organic matter and the associated minerals could directly influence each other, although the details have not been well known.

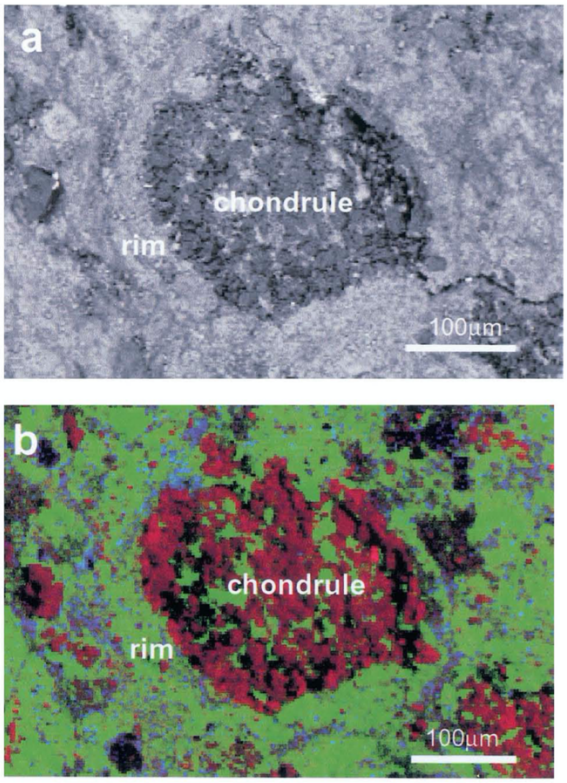

Figure 1-3. (a) Backscattered electron image of a Murchison chondrule surrounded by a fine-grained rim and matrix, which were majorly dominated by phyllosilicates. (b) Organic matter was stained by Os, which was concentrated in the rim and matrix (Fe = green, Si = red, Os = blue) (Pearson et al. 2002).

1.3. Examples of approaches for simulating the evolution of organic matter in meteorite parent bodies

There are various experimental approaches for simulating the evolution of primordial organic matter today. For example, Cody et al. (2011) performed condensation experiments of formaldehyde in water solution and detected the organic solid after heating at 50-250 °C. They suggested that primitive chondritic insoluble organic matter could have been formed via formose reaction and subsequent condensation, dehydration reactions in the extraterrestrial small bodies (Cody et al. 2011). Kebukawa et al. (2013) confirmed that adding NH_3 in the system could enhance the reactions. To investigate structural changes of insoluble organic matter during aqueous alteration in meteorite parent bodies, hydrothermal experiments of insoluble organic matter from meteorite Murray (CM2), which was the least altered chondrite in the parent body, at 300 °C for 6 days were performed in Yabuta et al. (2007). During the hydrothermal experiment, various soluble compounds were formed and the structure of the insoluble organic matter significantly changed to degradated (Yabuta et al. 2007). It could indicate that some soluble organic matter in meteorites could be formed by the decomposition of macromolecular insoluble organic matter. From these previous experiments, both synthesis and decomposition of insoluble organic matter could occur in response to the hydrothermal conditions.

1.4. An experimental study to investigate the evolution of primordial organic matter during thermal metamorphism

In addition to the previous experimental studies, Nakano et al. (2020) performed heating experiments of primordial organic matter analog, which was prepared by mixing some chemical reagents, without initial presence of water. They used two different experimental approaches, one method was by using diamond anvil cell to pursue the metamorphism of organic matter in-situ and another method was by using an autoclave to analyze the experimental products in detail. The suggestion in Nakano et al. (2020) that organic matter was the potential sources of water in early Solar System could be significant for considering mineral-organic matter relationships for present study. Thus, main points of Nakano et al. (2020) were summarized in this section.

1.4.1. Preparation of primordial organic matter analog

Primordial organic matter accreted on meteorite parent bodies such as precometary organic matter before metamorphic processes cannot be obtained directly. Thus, simulated organic mixture by mixing chemical reagents was prepared following several previous studies (Kouchi et al. 2002; Nakano et al. 2002; Nakano et al. 2003, hereafter called "OM", Table 1-2). The composition of the OM was determined based on the detected molecules found in the experiments simulating UV irradiation on interstellar ice analogs (H_2O: CO: NH_3 = 5: 5: 1) and warming (10 K to 300 K) from Briggs et al. (1992), Greenberg and Mendoza-Gomez (1993), and Mendoza-Gomez and Greenberg (1993). Although various other photolysis experiments such as Bernstein et al. (1995) used a CH_3OH-rich ice mixture (H_2O:CH_3OH:CO:NH_3 = 10:5:1:1), low mass protostar likely our Sun and molecular cloud were revealed to be rich in CO by infrared observations (Ehrenfreund et al. 2000; Gibb et al. 2004; Nakano et al. 2020). Nakano et al. (2020) insisted that the amount of CH_3OH, which is formed by the hydrogenation of CO in molecular clouds (Watanabe and Kouchi 2002), is expected to be only a certain extent (only a few percent CH_3OH) in the molecular cloud where our solar system was born, thus the ice mixture in Briggs et al. (1992) was considered to be more relevant for discussions of the organic matter in our Solar System than that in Bernstein et al. (1995).

In the refractory organic residue after the photolysis to interstellar ice analogs (H_2O: CO: NH_3 = 5: 5: 1), C2–C3 hydroxy acids and hydroxy amides, glycerol, urea, hexamethylenetetramine, and formamidine were identified (Briggs et al. 1992), as well as a complex mixture of aliphatic hydrocarbons from C5 to C30 and aromatic hydrocarbons with elemental compositions of C_9H_8, $C_{12}H_{12}$, $C_{12}H_{14}$, $C_{13}H_{16}$, $C_{13}H_{16}O$, $C_{14}H_{18}O$, $C_{14}H_{18}O_2$ (Greenberg and Mendoza-Gomez 1993; Mendoza-Gomez and Greenberg 1993). The OM was made by mixing chemical reagents based on these experimental products, but some compounds which could not be obtained were substituted by compounds with similar chemical characteristics. Some chemical reagents in the OM were also selected based on the compositional formula, although some of them such as hexamethylenetetramine, 4,4'-methylenebis-(2,6-dimethylphenol), α, α'-bis(4-hydroxyphenyl)-1, and 4-diisopropenylbenzene have not been detected in meteorites or interstellar media.

1.4.2. Water generation during the evolution of organic matter

One of the most significant results in Nakano et al. (2020) was the formation of water during the heating experiments. The heated product of OM using an autoclave (OM Labotec, MA type) at 400 °C showed clearly different two layers, a transparent fluid layer and a black sticky fluidal material layer floating on the transparent fluid (Figure 1-4). Through various analyses, the transparent layer was revealed to be an aqueous solution. Infrared absorption spectra of these layers were shown in Figure 1-5. The OH bending–vibration band of water [δ(OH)] at approximately 1700-1600 cm^{-1} was buried within strong bands at 1657 cm^{-1}, 1612 cm^{-1}, and 1550 cm^{-1} plausibly due to the amide I and II bands and to the antisymmetric COO^- stretching-vibration bands of carboxylate anions dissolved in the transparent aqueous product, respectively (Nakano et al. 2020).

The OM was also heated in a diamond anvil cell. The metamorphic process was observed in-situ by optical microscope and infrared spectroscopy during heated from room temperature to 400°C gradually. Change of the intensity of 5200 cm^{-1} band due to a combination of OH stretching and bending vibrations was chased with increasing temperature (Figure 1-6). Intensity ratios of a 5200 cm^{-1} band at reached temperature to the band at room temperature were also shown in Figure 1-7. The intensity of water increased at approximately 300 °C, it indicates the formation of much H_2O molecules at the temperature. Separation of two layers was subsequently observed above the temperature. The starting material was complex organic mixture, thus the formation process of H_2O molecules could not be decided in detail. However, one possible reaction process was dehydration-condensation reactions of alcohols and carboxylic acids. To confirm the hypothesis, additional experiments with new two compositional mixtures (an -OH and -COOH-bearing mixture and a mixture of amides and ketones without -OH and -COOH, Table 1-3) were performed. The OH-contents, defined as the ratio of the OH weight to the total sample weight, of the starting materials of an -OH and -COOH-bearing mixture, OM, and a mixture of amides and ketones without -OH and -COOH were 47.8%, 8.3%, and 0%, respectively (Nakano et al. 2020). The result clearly indicated that the amount of water depended on the -OH content of the starting materials.

1.4.3. Significant implications in terms of the water formation from organic mixture

The formation of water from organic mixture during simulated heating in meteorite parent bodies possibly suggests that organic matter could be one of water reservoirs to some small bodies. Some organic matter could survive inside H_2O snow line (Herbst and van Dishoeck 2009), thus such organic matter could bring water to inner Solar System where terrestrial planets were formed (Nakano et al. 2020). The possibility and the delivering route of water to Earth forming region have been controversial (O'Brien et al. 2006, 2014, 2018; Walsh et al. 2011), however at least accretion of organic matter on some small bodies in asteroidal region is more possible process, since some ordinary chondrites originated from S-type asteroids (Nakamura et al. 2011) contain organic matter (e.g. Alexander et al. 2017). Water from organic matter could be a potential source of alteration mechanisms. However, the evolution of organic matter could also be affected by surrounded minerals (Pearson et al. 2002; Kebukawa et al. 2010; Yamashita and Naraoka 2014; Le Guillou et al. 2014; Naraoka et al. 2015; Rotelli et al. 2016; Fuchida et al. 2017; Vinogradoff et al. 2020a, b). It is essential to understand

the evolution of primordial materials in terms of interactions between minerals and organic matter in early Solar System.

Table 1-2. Initial compositions of the organic mixture (OM) used in this study and the structural formulae of each compound.

Compounds	Molecular weight	Concentration (wt.%)
Alcohols		
(1) Ethylene glycol	62.07	1.9
(2) Glycerol	92.09	2.3
Phenols		
(3) 4-(1-Adamantyl) phenol	228.34	2.1
(4) 4,4'-Methylenebis-(2,6-dimethylphenol)	256.35	2.3
(5) αα'-Bis(4-hydroxyphenyl)-1,4-diisopropenylbenzene	346.46	0.2
Carboxylic acids		
(6) Glycolic acid	76.05	11.8
(7) Lauric acid	200.32	6.2
(8) Sebacic acid	202.25	6.3
(9) Eicosanoic acid	312.54	9.7
Ketones		
(10) Cyclohexyl phenyl ketone	188.27	8.1
(11) 4'-Cyclohexylacetophenone	202.30	7.1
Amides		
(12) Urea	60.06	0.9
(13) Acetamide	59.07	6.6
(14) Lactamide	89.09	8.8
N-containing cyclic compound		
(15) Hexamethylenetetramine	140.19	1.1
Aromatic hydrocarbons		
(16) 1,4-Diisopropenylbenzene	158.24	3.2
(17) Indene	116.16	7.6
(18) 1,2-Dimethylnaphthalene	156.22	2.6
(19) Phenanthrene	178.23	11.1

Structural formula	(1) 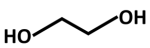	(2) 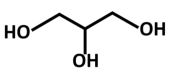	(3) 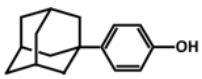
(4) 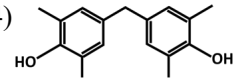	(5) 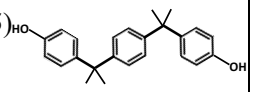	(6) 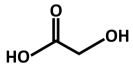	(7) 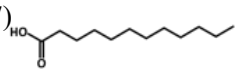
(8) 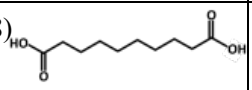	(9) 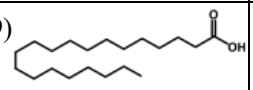	(10) 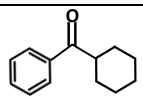	(11) 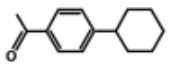
(12) 	(13) 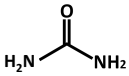	(14) 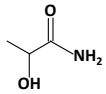	(15) 

(16) 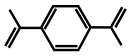	(17) 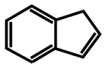	(18) 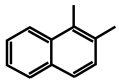	(19) 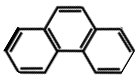

Table 1-3. Compositions for the additional experiments in Nakano et al. (2020). (a) an -OH and -COOH-bearing mixture, (b) a mixture of amides and ketones without -OH and -COOH.

Compounds	**Molecular weight**	**Concentration (wt.%)**
(a)		
Ethylene glycol	62.07	12.5
Glycerol	92.09	14.4
Glycolic acid	76.05	73.1
(b)		
Cyclohexyl phenyl ketone	188.27	35.5
4’-Cyclohexylacetophenone	202.30	31.6
Urea	60.06	3.5
Acetamide	59.07	29.4

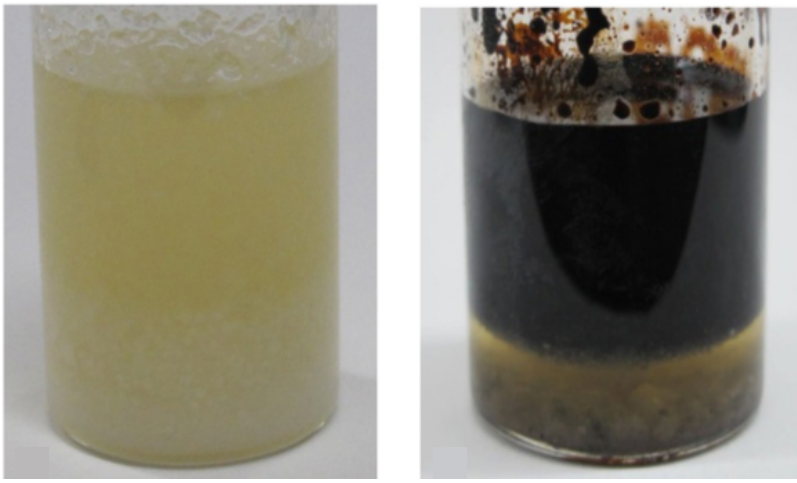

Figure 1-4. Photographs of the OM (left) and OM heated at 400 °C (right) (Nakano et al. 2020).

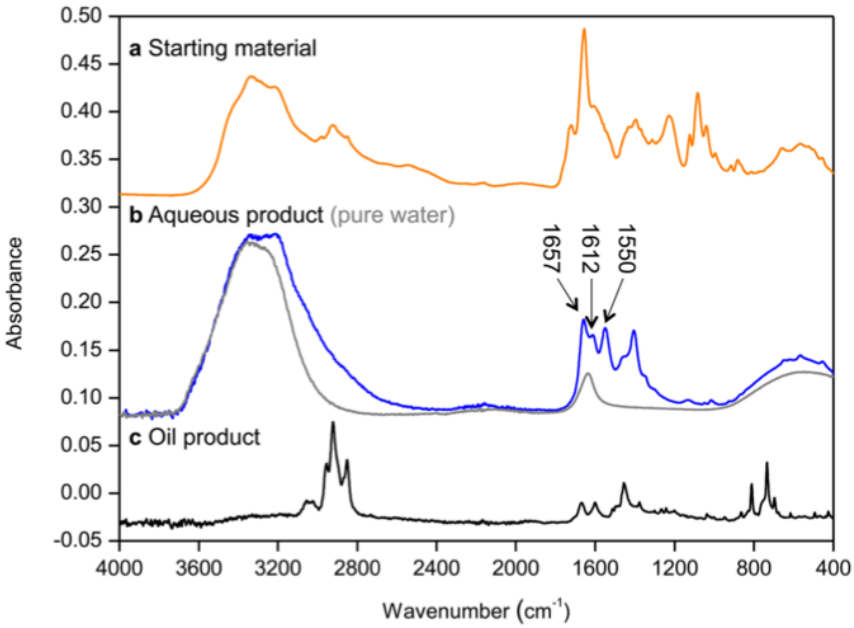

Figure 1-5. Mid-infrared absorption spectra of (a) the starting material (MC); (b) the recovered aqueous product, together with pure water; and (c) the recovered oil product (Nakano et al. 2020).

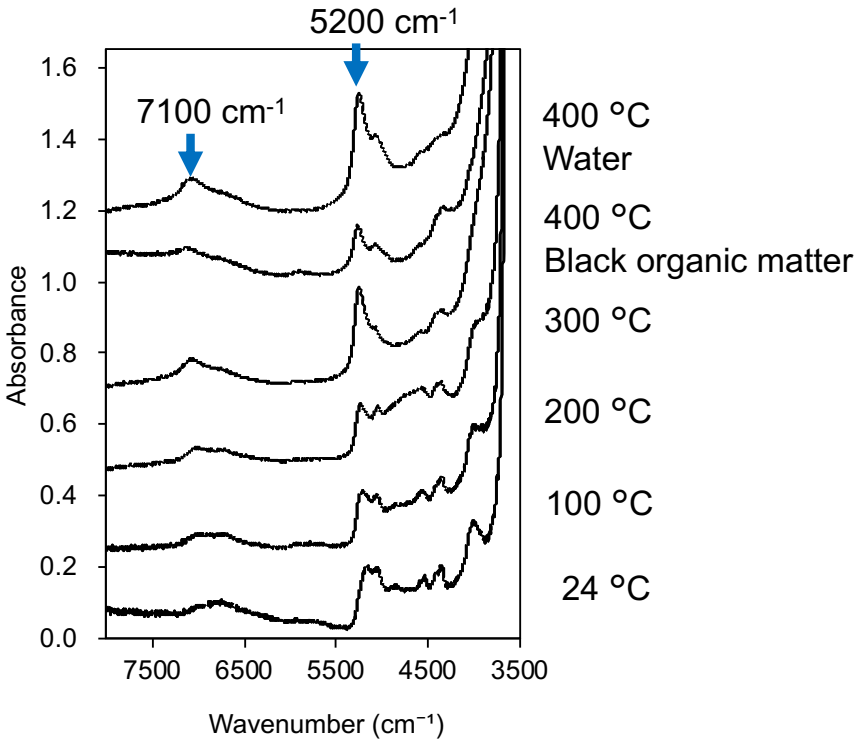

Figure 1-6. Near infrared absorption spectra of OM in diamond anvil cell at each temperature. Both 5200 cm^{-1} and 7100 cm^{-1} peaks with blue arrows were associated to H_2O, attributed to a combination of OH stretching and bending vibrations and to the OH stretching overtone of water, respectively (revision of Nakano et al. 2020)

1.5. Purpose and the outline of this study

As stated previously, evolution of organic matter and evolution of minerals did not occur alone. Evolution of materials should be considered in terms of their interactions. Various experimental studies have investigated the co-evolution of organic matter and minerals particularly simulating hydrous or hydrothermal conditions in parent bodies of CI, CM and CR chondrites, (Yamashita and Naraoka 2014; Naraoka et al. 2015; Rotelli et al. 2016; Fuchida et al. 2017; Vinogradoff et al. 2020a, b). On the other hand, dry environments in parent bodies of CV, CO and ordinary chondrites, which could have formed inside H_2O snow line, have not been considered in detail. Analyses of organic matter in various meteorites from dry parent bodies have revealed the evolution of organic matter accompanied with thermal metamorphism (Quirico et al. 2003, 2009; Bonal et al. 2006, 2007, 2016; Alexander et al. 2007; Busemann et al. 2007; Cody et al. 2008; Kebukawa et al. 2011; Homma et al. 2015), however the effect of surrounded minerals on organic matter during thermal processes has not been known well. In addition, the effect of organic matter on minerals has not been investigated. To provide fundamental insights into co-evolution of minerals and organic matter in parent bodies with dry environment, experiments simulating thermal processes in them were performed in this study.

As an initial step, primordial organic mixture analog (OM) described in section 1.3.1 and silicate minerals which is major mineral phase in chondrites were used in this study. In Chapter 2, effect of silicate minerals on the evolution of organic matter was investigated in functional group level. On the contrary, the effects of organic matter on minerals were investigated morphologically in Chapter 3, particularly focusing on the formation of water from organic matter. Additionally, preparation of a synthetic mineral (olivine) was conducted for future experiments in Chapter 4. At last, concluding remarks based on these results were described in Chapter 5.

2. Effects of minerals on metamorphism of organic matter during thermal processes in meteorite parent bodies.

2.1. Introduction

Primitive chondrites such as type 1 to 3 carbonaceous chondrites and type 3 ordinary chondrites contain up to a few wt. % of organic matter. The molecular structures and chemical compositions of the organic matter reflect the chemical and thermal conditions in the parent bodies. The majority of meteoritic organic matter consists of complex macromolecular organic matter, so-called insoluble organic matter (IOM). It is well known that elemental and isotopic compositions of IOM vary within and among chondrite groups, likely due to parent body processes that would have altered the initial elemental and isotopic compositions of IOM precursors (Alexander et al. 1998, 2007). Infrared and Raman characteristics of IOM from primitive chondrites also correlate well with the thermal and chemical environments of the meteorite parent bodies (Bonal et al. 2006, 2007, 2016; Busemann et al. 2007; Kebukawa et al. 2011; Quirico et al. 2003, 2009, 2018).

The association of phyllosilicates and organic matter in meteorites has been pointed out in several studies (Pearson et al. 2002, 2007; Garvie and Buseck 2007; Kebukawa et al. 2010a, 2019; Le Guillou et al. 2014; Yesiltas et al. 2015; Yesiltas and Kebukawa 2016). Some phyllosilicates are considered to enhance various organic reactions at low temperatures mostly due to its large specific surface area (Varma 2002). For example, cyclization of soluble organic matter into insoluble organic matter could be favored on the surface of phyllosilicates (Naraoka et al. 2000). Pearson et al. (2002) suggested that some phyllosilicates might act as absorbents of organic matter in the aqueous fluid and contribute to form complex organic networks during aqueous processes in the parent bodies of carbonaceous chondrites. Some experimental studies also showed the effects of minerals on aqueous alteration of organic matter. Vinogradoff et al. (2020a) conducted hydrothermal experiments of hexamethylenetetramine with phyllosilicates (smectites) and remarked that chemical evolution of organic matter strongly depends on the presence and the nature of smectites. Their experiments in the presence of carboxylic acids showed that amino acid formations were both enhanced and inhibited depending of the chemical composition of smectites (Vinogradoff et al. 2020b). Heterogeneity and diversity of organic matter in chondrites could be explained by the different reaction pathways when various phyllosilicates were present (Vinogradoff et al. 2020a). Furthermore, olivine could have enhanced the formation of pyridine carboxylic acids, long-chain alkylated pyridines, and lactams from an aqueous solution containing aldehydes (HCHO and CH_3CHO) and ammonia at 50-100 °C (Naraoka et al. 2015).

Effects of minerals on organic matter were not well investigated in dry and high temperature conditions such as in CV, CO, and type 3 ordinary chondrite parent bodies. The dominant mineral phases in CV, CO, and type 3 ordinary chondrites are olivine and pyroxene (Howard et al. 2010, 2014). CV, CO and ordinary chondrites contain up to ~0.7 wt.% of organic carbon as IOM (Alexander et al. 2007). Organic-bearing type 3 chondrites such as Semarkona (LL3.00) experienced ~260 °C, Kainsaz (CO3.2) experienced ~300 °C, and Vigarano (CV3 red) experienced 300-400 °C (Huss et al. 2006). The precursors of organic matter accreted in CV, CO, and type 3 ordinary chondrites were considered chemically similar (e.g., Alexander et al. 2007), though it may not be exactly the same. The origin of organic matter in these dry chondrites was probably in molecular clouds or protoplanetary disk, but one cannot exclude a possibility that the organics may have been modified by hydrous environments in their parent bodies before drying up—whether these dry chondrite parent bodies originally dry or dried after aqueous process is not clear. The maturity of IOM in these chondrites is apparently controlled by the degree of thermal metamorphism, and the metamorphic grade depends on the maximum temperature (Bonal et al. 2006, 2007, 2016).

Phyllosilicates also exist in CV, CO and type 3 ordinary chondrites, although they are much less abundant compared to CI and CM chondrites. Smectite exists in CV and serpentine exists in CO (Buseck and Hua 1993). Semarkona (LL3.00) and Bishunpur (LL3.15) contain smectite (Alexander et al. 1989). The origin of these phyllosilicates is not well understood due to their minor abundances. In-situ formation during aqueous processes in the parent bodies is considered to be reasonable (Bischoff 1998), although there is a possibility of nebula origin (Ciesla et al. 2003; Nagahara and Ozawa 2011).

In this study, heating experiments of organic matter with olivine and phyllosilicate (montmorillonite) were performed to evaluate the effects of minerals on thermal changes of organic matter in functional group level. It will be useful to understand the reactions of complex organic matter in dry environment such as during thermal metamorphism in CV, CO, and type 3 ordinary chondrite parent bodies. The experimental products were analyzed using infrared (IR) spectroscopy to follow the changes of organic matter in a functional group level, and the hexane soluble fractions were analyzed using gas chromatography mass spectrometry (GC/MS). In addition, the interlayer spacing of phyllosilicate was analyzed using X-ray diffraction (XRD), and the change of the chemical composition of olivine was also investigated by scanning electron microscope equipped with an energy-dispersive X-ray spectrometer (SEM/EDS).

2.2. Material and method

2.2.1. Starting materials

An organic mixture (OM) described in section 1.3.1 was used as a starting material (Table 1-2), to simulate primordial organic matter accreted to parent bodies before thermal metamorphism particularly focusing on the changes of molecular structure. Since the OM does not exactly represent

the primordial organic matter at molecular level, the purpose here was set to understand the reactions at functional group level. Nakano et al. (2002) showed that infrared spectra of IOM in carbonaceous chondrites could be reproduced by the OM after the experiments simulating aqueous alteration and subsequent thermal metamorphism. The OM is also similar to that of a cometary organic matter in elemental composition. The bulk elemental composition of the OM is H: C: N: O =148: 100: 5: 23 (O/C=0.23, N/C=0.05) and this is similar to a CHON particle of1P/Halley, O/C=0.2, N/C=0.04 (Kissel and Krueger 1987). Various functional groups (-OH, CH_3-, CH_2-, C=O, C=C, C=C-O, N-C=O, O-C=O) were detected in comet 81P/Wild 2 particles with IR and X-ray absorption near edge structure (Sandford et al. 2006). In addition, comets are known to contain alcohols, carbonyls, amines, amides, aliphatic hydrocarbons, and polycyclic aromatic hydrocarbons (PAHs), e.g., ethyleneglycol is detected in Hale-Bopp and 67P/Churyumov-Gerasimenko, acetamide is detected in 67P/Churyumov-Gerasimenko, and PAHs are detected in 21P/Giacobini-Zinner (Mumma and Charnley 2011; Goesmann et al. 2015; Grady et al. 2018; Otsubo et al. 2020). The OM could survive inside the snow line, which was shown by an evaporation experiment simulating an early solar nebula (Nakano et al. 2003). Thus, the OM could be a candidate for accumulated organic matter on the CV, CO, and type 3 ordinary chondrite parent bodies.

The olivine ($(Mg,Fe)_2SiO_4$) powder used here was from San Carlos, Arizona, USA, and Na-montmorillonite ($Na_{0.3}(Al,Mg)_2Si_4O_{10})(OH)_2$) powder was SWy-1, from the Clay Minerals Society Source. The particle size of olivine and montmorillonite in this study was approximately <200 μm and <2 μm, respectively, observed using a scanning electron microscope (SEM; Figure 2-1). Olivine was washed by hexane before use. Montmorillonite was pre-cleaned, and was not washed before use to avoid changes in chemical conditions by solvents. Many CV, CO, and type 3 ordinary chondrites contain minor phyllosilicates. Na-montmorillonite (a smectite-type phyllosilicate) was used to simulate the 2:1 type phyllosilicate structure in this study. Montmorillonite, for example, exists in Allende (CV3.2/3.6oxA) (Buseck and Hua 1993).

2.2.2. Heating experiments

Heating experiments were carried out within an autoclave (Figure 2-2, Tama-Seiki) whose reactor had a volume of 100 mL and was made of hastelloy. The following starting materials were prepared: (1) 0.5 g of OM, (2) 0.25 g of OM with 0.25 g of olivine (hereinafter referred to as OM + olivine), and (3) 0.25 g of OM with 0.25 g of montmorillonite (hereinafter referred to as OM + montmorillonite). These mixtures were subjected to heating experiments immediately after the preparation (<~20 min.), or stored in a refrigerator (<8 °C). Although the organic matter in chondrites is account for ~1 wt.% or less, the initial organic/mineral ratios in parent bodies before metamorphism was expected to be larger than these ratios in current chondrites, since a significant amount of organic matter could have been lost during thermal processes in the parent bodies. Thus, 1: 1 of the organic/mineral ratios were

simply adopted in this study, c.f., cometary particles have the organic/mineral ratio of ~45: 55 (in weight) (Bardyn et al. 2017). Each mixture was prepared in an unsealed Pyrex glass ampoule tube (AP20, Maruemu) and then placed in the reactor. Thus, reactions in the liquid and solid phases occur inside the ampoule tube, yet the generated gaseous species spread inside the reactor. The autoclave was purged with a N_2+H_2 gas mixture (99:1, v/v) at 60 atm three times to eliminate air completely before start heating. The samples were heated at 200 °C, 300 °C, or 400 °C in a closed system with the N_2+H_2 gas at around 1 atm for five hours. After cooling to room temperature, a valve of the autoclave was opened to release the inner gas, then the glass ampoule with the residual samples were recovered. To eliminate organic contaminants in the autoclave, the autoclave was heated over 500 °C for 5 hours in air without samples after each experiment. A new Pyrex glass ampoule was prepared for each experiment, after washed by pure water and heated at 500 °C for 5 hours in air. Reference mixtures were also prepared by mixing OM and minerals at room temperature (~25 °C) without any further treatments. The reference mixtures were analyzed immediately after the preparation (<~20 min).

To evaluate pressure dependence on changes in molecular structures, the experiments for the 5 g of OM (without minerals) under different pressures at 400 °C for five hours were performed. The experimental procedure was the same as described above, except the pressures were kept at 8 atm, 100 atm, and 268 atm at 400 °C with initial pressures of 1 atm, 50 atm, and 120 atm, respectively.

2.2.3. XRD analysis

Montmorillonite and the experimental products (mixtures of montmorillonite and OM) were analyzed by powder X-ray diffraction (XRD) using a SmartLab diffractometer, with a Hypix-3000 detector (Rigaku, Ltd., Japan) at 40 kV and 45 mA, by Cu $K\alpha$ radiation, with a scan speed of 5.0 °/min and a resolution of 0.01. Mineral species were identified by using the SmartLab Studio II by searching the diffraction patterns from ICDD card data through the Hanawalt search method. The interlayer spacing (*d*-spacing) of the montmorillonite samples was calculated by Bragg's law defined here as *d*-spacing = λ / 2sin θ, where θ is the scattering angle and λ is the wavelength of the X-ray.

2.2.4. FTIR analysis

Heated OM was viscous fluids, and therefore those products were analyzed using a Fourier transform infrared spectrometer (FTIR; FT/IR-6100, JASCO) with a single-reflection attenuate total resonance (ATR) device (ATR PRO ONE, JASCO), a high intensity ceramic IR light source, a Ge/KBr beam splitter, and a triglycine sulfate (TGS) detector. The ATR-IR spectra were accumulated 128 times with a wavenumber range of 4000-800 cm^{-1} and a spectral resolution of 4 cm^{-1}. The background spectra were obtained through air before each measurement.

To obtain the IR spectra exclusively from organics, OM + olivine and OM + montmorillonite

products were analyzed by FTIR-microspectroscopy (micro-FTIR; FT-IR-6100+IRT-5200, JASCO) with a mercury-cadmium-telluride (MCT) detector and ×16 Cassegrainian mirrors. IR transmission spectra were accumulated approximately 100-300 times, with a spectral resolution of 4 cm^{-1} in the range of 4000-800 cm^{-1}, and with a 20 × 15 μm^2 aperture in transmission mode. Samples were set on CaF_2 plates, and then the background spectra were acquired through the CaF_2 plates adjacent to the samples. Each spectrum was an average of the spectra taken from at least three different points.

All spectra were normalized to the peak height of the aromatic C=C band (~1600 cm^{-1}) relative to an appropriate baseline. To conduct semi-quantitative comparison of C=O abundances, peak heights of C=O were divided by aromatic C=C after subtracting the linear baselines at 1800-1500 cm^{-1}. The error bar is the standard deviation (1σ) of the spectra from different analytical points for each sample (only applicable for the data from micro-FTIR). Note that, it was confirmed that these peak height ratios obtained by ATR-IR spectra and IR transmission spectra were comparable and did not show significant differences.

2.2.5. GC/MS analysis

Five mg of heated OM, 30 mg of OM + olivine, or 30 mg of OM + montmorillonite samples were extracted by using 500 μL of hexane. Extractions using dichloromethane and methanol were also confirmed, and hexane was the most effective to follow the changes in groups of molecules such as long-chain carboxylic acids, esters, alkanes, amides, and nitriles. An aliquot of 0.1 μL from each solution was analyzed with a gas chromatography mass spectrometer (GC/MS; QP-2020, Shimadzu) equipped with a non-polar column DB-5 (purchased from Agilent J & W) with a 30 m × 0.25 mm internal diameter and 0.25 μm film thickness. A splitless injection was employed at an inlet temperature of 200 °C with a purge delay of 5 min. The column temperature was initially 40 °C, increasing at a rate of 3 °C/min up to 60 °C and then 6 °C/min up to 320 °C. He (>99.999 %) was used as a carrier gas with a flow rate of 1.23 mL/min. Electron ionization (EI) was applied at 70 eV with an ion source temperature of 200 °C. Data processing was conducted using GCMSsolution software (Shimadzu). The solvent background (hexane) taken at 10 min was subtracted and peaks were selected based on a signal-to-noise ratio of >10. Peak identifications were conducted using NIST2017 library (2017 edition).

2.2.6. SEM/EDS analysis

Change of the elemental compositions of the olivine after experiments were characterized using a scanning electron microscope (JSM-6510LA, JEOL) equipped with an energy-dispersive X-ray spectrometer (JED-2300, JEOL). Grains were fixed on a 10 mm brass stub with a carbon tape and were coated by Au sputtering. All grains were observed by secondary electron imaging at 20 kV. An elemental analysis was conducted by EDS at 20 kV.

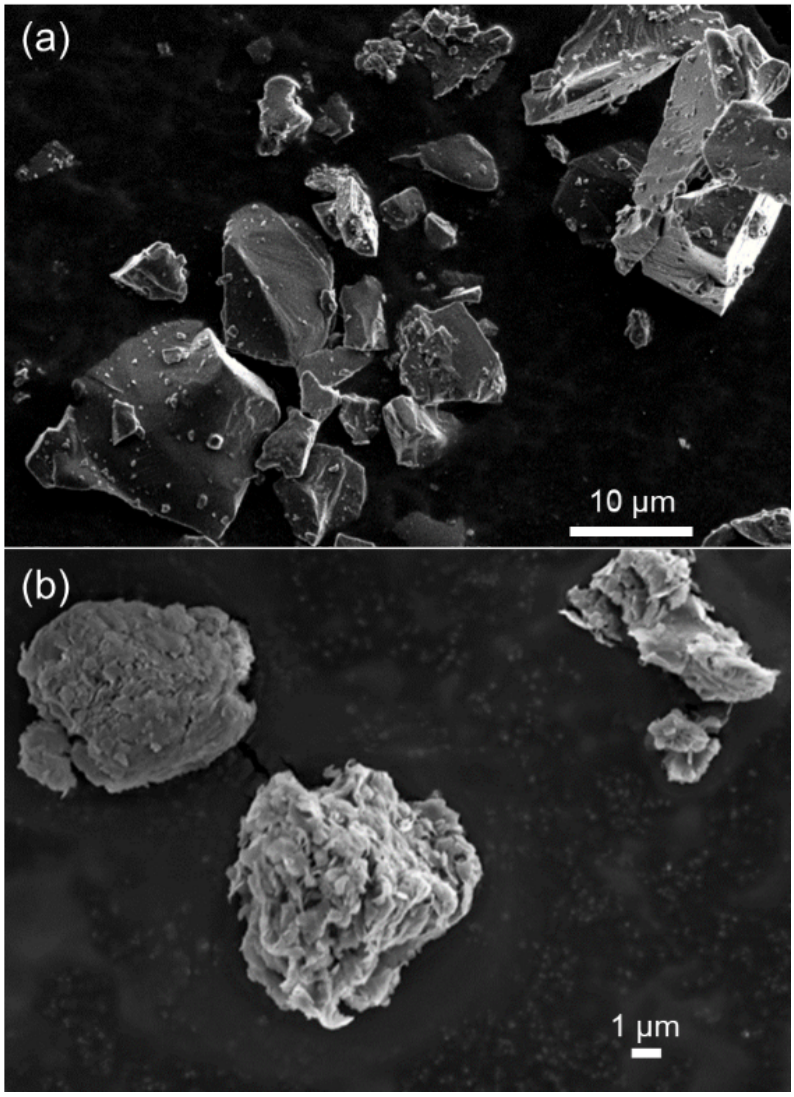

Figure 2-1. SEM images of (a) olivine and (b) montmorillonite used in this study.

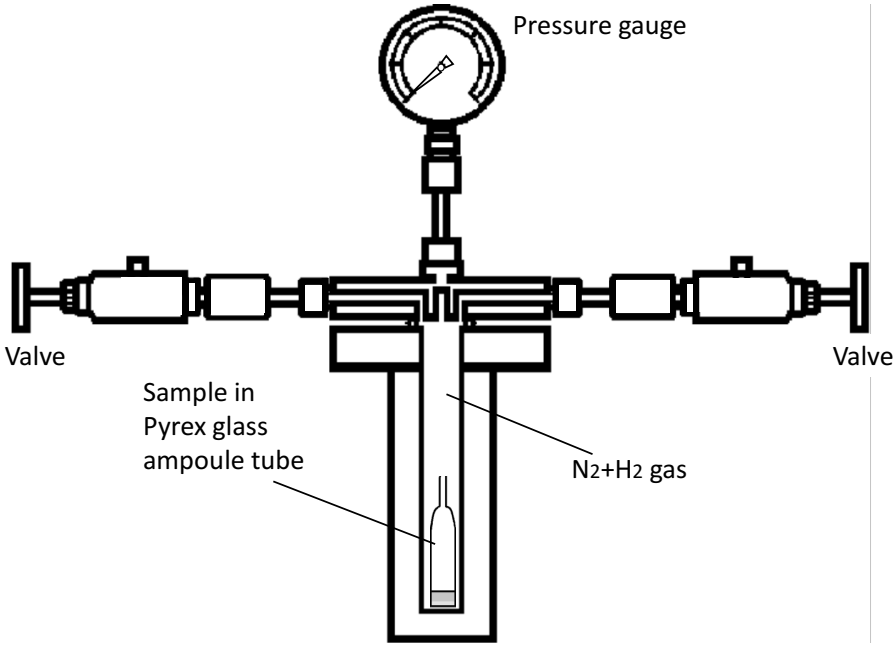

Figure 2-2. Schematic image of the autoclave used in this study. Each sample was heated in a closed system at ~1 atm with a N_2+H_2 gas mixture (99:1, v/v).

2.3. Results

2.3.1. XRD analysis

XRD patterns of montmorillonite and montmorillonite heated with the OM are shown in Figure 2-3. Intercalation of the OM in the montmorillonite interlayer space is evidenced by shifts in the 001 XRD reflections at 2θ = 6.8-7.4° to smaller 2θ. The 001 reflection angle (2θ) of montmorillonite is 7.06° and is shifted to smaller 2θ (6.09°) by mixing with the OM. The angles shifted to higher 2θ after heating at each temperature. Figure 2-4 shows the changes in their *d*-spacing. The *d*-spacing of the initial montmorillonite sample was 12.52 Å, and then expanded to 14.51 Å by mixing with the OM. The *d*-spacing of montmorillonite heated with the OM decreased with increasing temperature: 13.96 Å at 200 °C, 13.68 Å at 300 °C, and 12.79 Å at 400 °C. Some peaks in the XRD pattern of OM + montmorillonite were due to crystals of organic compounds, however all organic peaks disappeared after heating. Peak identification of these organics was not conducted, since it is out of the scope of this study. The changes in the 001 reflection angle indicate that the *d*-spacing was increased by intercalation of some compounds from the OM (Block et al. 2015; Michels et al. 2015), and decreased with an increase in temperature. To evaluate modification of montmorillonite by heating, a heating experiment at 400 °C for 5 hours without OM was also conducted. The XRD pattern of montmorillonite did not change except the 001 reflection peak which reflects the *d*-spacing of montmorillonite decreased to 9.73 Å (2θ = 9.09°) after heating at 400 °C without OM (Figure 2-3, 2-4).

To investigate the change of the basal space in response to the intercalation of each chemical reagent, mixing of montmorillonite and some reagents (ethyleneglycol, acetamide, hexamethylenetetramine, 1,2-dimethylenaphtharene, lauric acid, sebacic acid and phenenthrene) from the OM were additionally performed. The XRD patterns were shown in Figure 2-5a-c and the change of basal space was shown in Figure 2-6. The comparison of XRD pattern of initial montmorillonite with vacuum heated montmorillonite and montmorillonite mixed with OM was shown in Figure 2-5a. After vacuum heating, the basal space of montmorillonite became narrower than initial montmorillonite (Figure 2-6). Montmorillonite mixed with acetamide, hexamethylenetetramine (Figure 2-5b), lauric acid, sebacic acid and phenanthrene (Figure 2-5c) showed sharp peaks in each XRD pattern due to the crystalline. The basal space of montmorillonite mixed with lauric acid, sebacic acid and phenanthrene did not change significantly. These chemical reagents were solid materials, thus only mixing did not induce the intercalation of these compounds. Compared with these compounds, the basal space changed broader after mixing with acetamide, ethyleneglycol, 1,2-dimethylnaphtharene and hexamethylenetetramine. Ethyleneglycol and 1,2-dimethylnaphtharene were liquid reagents and small molecules, thus these molecules could easily enter the basal space of montmorillonite. However, acetamide and hexamethylenetetramine were initially solid reagents. These molecules were highly hygroscopic and soluble in water. Thus, these molecules could partially

be intercalated through the adsorbed water during mixing or analyzing.

2.3.2. FTIR analysis of heated OM with/without minerals

The IR absorption spectra revealed numerous organic functional groups in each product (Figure 2-7a). Functional groups detected in this study are summarized in Table 2-1 (Socrates 2001; Djomgoue and Njopwouo 2013; Maina et al. 2015; Laine et al. 2016; Bunin et al. 2017). The bands with no significant shifts at different temperatures were considered from the same functional group. fixed bands were chosen to compare these spectra.

The IR absorption spectra (normalized with aromatic C=C band) of heated OM changed significantly with increasing heating temperature (Figure 2-7a). The aliphatic C-H bands at 2925 cm^{-1} and 2855 cm^{-1}, and aromatic C-H band at 3060 cm^{-1} are higher at 300 °C and 400 °C compared to those at 25 °C and 200 °C. At 200 °C and 300 °C, the 1740 cm^{-1} C=O peak appeared, which can be attributed to ester. While the peak at 1683 cm^{-1} (ketone) and 1665 cm^{-1} amide did not change significantly. These results indicate that heating caused some structural changes in the organic matter containing C=O bonds.

Figure 2-7b shows the IR spectra of OM + olivine. The aliphatic C-H bands at 2925 cm^{-1} and 2855 cm^{-1}, and aromatic C-H band at 3060 cm^{-1} increased at 200 °C and 300 °C, and decreased at 400 °C. The C=O peak at 1740 cm^{-1} (ester) appeared at 200 °C, and a peak appeared at 1705 cm^{-1} attributed to carboxyl and/or aldehyde at 300 °C. The peak at ~1680 cm^{-1} (ketone) was most intense at 200 °C. The 1665 cm^{-1} band (amide C=O) decreased at 200 °C, and were not observed at 300 °C and 400 °C. No C=O peaks are detected at 400 °C. The blank spectrum of olivine did not show organic peaks, thus organic contaminations did not affect the results in this study (Figure 2-7b).

Figure 2-7c shows IR spectra of OM + montmorillonite. The 3060 cm^{-1} aromatic C-H band did not appear at 200 °C and higher temperatures, and the aliphatic C-H bands at 2925 cm^{-1} and 2855 cm^{-1} decreased at 400 °C. The C=O peak at 1740 cm^{-1} due to ester appeared at 200 °C. Only a weak shoulder of ketone at 1675 cm^{-1} can be observed at 300 °C. These C=O peaks are not detected at 400 °C. The blank spectrum of montmorillonite did not show organic peaks, thus organic contaminations did not affect the results in this study (Figure 2-7c).

Figure 2-8a and b show peak height ratios of C=O (ester at ~1740 cm^{-1} and ketone at 1680 cm^{-1}, respectively) to aromatic C=C (1600-1580 cm^{-1}) at each temperature. These ratios at 400 °C were not plotted, since there were little or no peaks of C=O at 400 °C. In addition, aromatic C=C bands at ~1600 cm^{-1} of OM + olivine and OM + montmorillonite at 400 °C are ambiguous. The ester C=O/C=C ratios (Figure 2-8a) of OM increased at 200 °C and 300 °C. The ester C=O/C=C ratio of OM + olivine significantly increased at 200 °C, then decreased at 300 °C. However, the ester C=O/C=C ratio of OM + montmorillonite did not increase at 200 °C, and the ratio decreased at 300 °C. The ketone C=O/C=C ratio (Figure 2-8b) of the OM did not change significantly by the heating up to 300 °C. The ketone

C=O/C=C ratio of OM + olivine slightly increased at 200 °C, then decreased at 300 °C. With montmorillonite, ketone C=O/C=C decreased with a rise in temperature.

2.3.3. GC/MS analysis

Figure 2-9 shows total ion chromatograms obtained by GC/MS of the OM and heated OM with and without minerals. Compounds identified in the heated OM are shown in Table 2-2 and Figure 2-9. The GC/MS analysis of the OM without heating identified indene (17.42 min), 1,4-diisopropenyl benzene (29.50 min), 1,2-dimethylnaphthalene (33.42 min), cyclohexyl phenyl ketone (36.88 min), phenanthrene (40.33 min), and 4-(1-adamantyl)phenol (45.62 min). All compounds detected by GC/MS of the starting mixture were initial OM compounds, except for a small peak of 3,4-dihydro-2-methyl-1(2H)-naphthalenone (32.45 min).

2.3.3.1. Products from heated OM

New peaks were identified with heating of the OM without minerals, in particular an acetate and monoaromatic hydrocarbons with side chains before 35 min and long chain aliphatic compounds after 35 min. From the OM heated at 200 °C, numerous new compounds were detected primarily after 35 min. The number of ester compounds in the OM heated at 200 °C was the highest among all of the heated OM.

The OM heated at 300 °C gave some new GC peaks. Ester compounds and amide compounds were detected after 35 min. Nitrile compounds such as dodecanenitrile and nonadecanenitrile (48.50 min) were detected. The intensities of nitrile compounds were more than 5-10 times higher than ester compounds or amide compounds.

All the ester compounds such as dodecanoic acid ethyl ester (36.52 min), were not present in the case of the OM heated at 400 °C. In contrast to the loss of the ester compounds, several alkanes were detected after heating at 400 °C. Mono-, di-, and tri-aromatic hydrocarbons were detected including derivatives of indene, 1,4-diisopropenylbenzene, 1,2-dimethylnaphthalene, cyclohexyl phenyl ketone, and phenanthrene.

2.3.3.2. Products from heated OM + olivine

Hydrocarbons such as indene, 1,4-diisopropenylbenzene, 1,2-dimethylnaphthalene, cyclohexyl phenyl ketone, and phenanthrene were the main compounds detected from the OM + olivine heated at 200 °C. Ester compounds such as dodecanoic acid ethyl ester and cyclopropane carboxylic acid pentadecyl ester were identified, and a nitrile compound (dodecanenitrile) was identified at 200 °C. Dodecanenitrile and dodecanoic acid ethyl ester were also identified, as well as in the heated OM products at 300 °C. Many compounds including alkanes and nitriles in the heated OM products at 400 °C (with no minerals) were not detected in the heated OM with olivine products. Note that signals

in the blank analysis of raw olivine extract before heating experiments was background level.

2.3.3.3. Products from heated OM + montmorillonite

Similar to the OM heated with olivine, hydrocarbons such as 1,4-diisopropenylbenzene, 1,2-dimethylnaphthalene, cyclohexyl phenyl ketone, and phenanthrene were the main compounds detected from OM + montmorillonite heated at 200 °C. Dodecanenitrile was newly detected at 200 °C. Dodecanenitrile increased at 400 °C; however, the other peaks detected in heated OM without minerals or with olivine significantly decreased with montmorillonite. Note that signals in the blank analysis of raw montmorillonite extract before heating experiments was background level.

2.3.3.4. Pressure dependence of heated OM

To evaluate the pressure dependence for changes in the molecular structure of organic matter by heating, the OM samples were heated under 8 atm, 100 atm, and 268 atm with the N_2+H_2 gas at 400 °C. All spectra were similar to the spectra obtained at 8 atm and 400 °C (Figure 2-10). This indicates that the pressure effects on the changes in the OM structure from heating were slight.

The GC/MS analysis showed mostly similar peaks from the OM heated products at 8 atm, 100 atm, and 268 atm (Figure 2-11). Although some slight differences were observed—indene (17.42 min) and 1-(1-methylethenyl)-4-(1-methylethyl)benzene (27.27 min) were detected at 268 atm—the most of the compounds were not affected by pressure.

2.3.4. SEM/EDS analysis

Comparison of the elemental composition of olivine was shown in a ternary diagram (Figure 2-12a, b). Plots of the chemical compositions of the olivine heated at 200 °C (Figure 2-12b) showed similar or slightly Si-rich composition compared with initial olivine (Figure 2-12a). Some plots were on the serpentine compositions in the ternary diagram. Olivine heated at 300 °C (Figure 2-12b) showed more Si-rich compositions than olivine heated at 200 °C, the plots were between serpentine and saponite. Olivine heated at 400 °C (Figure 2-12b), on the other hand, showed similar composition or Mg-rich compositions compared with initial olivine.

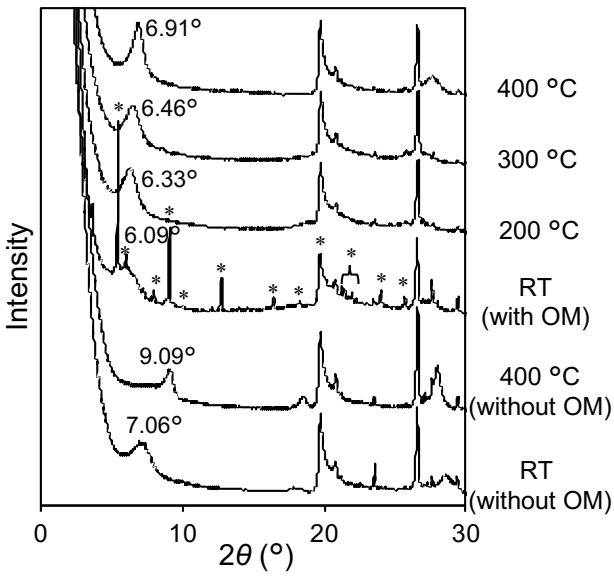

Figure 2-3. XRD patterns of montmorillonite, montmorillonite heated at 400 °C, montmorillonite with OM, and montmorillonite with OM heated at 200 °C, 300 °C and 400 °C. 2θ of 001 reflections from montmorillonite are indicated in the figure. Peaks due to organic crystals are shown with *.

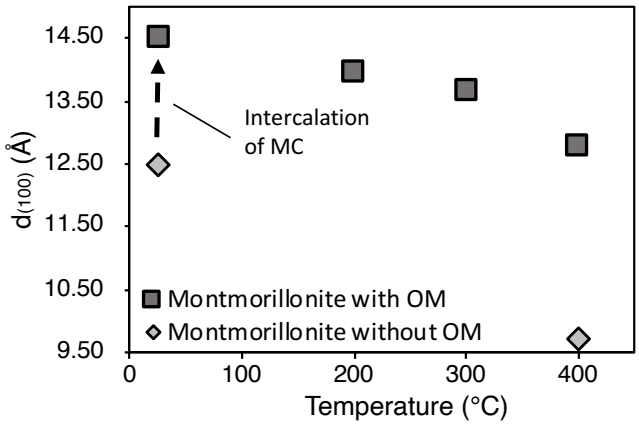

Figure 2-4. Changes in *d*-spacing of montmorillonite by intercalation of OM (broken line) and heating.

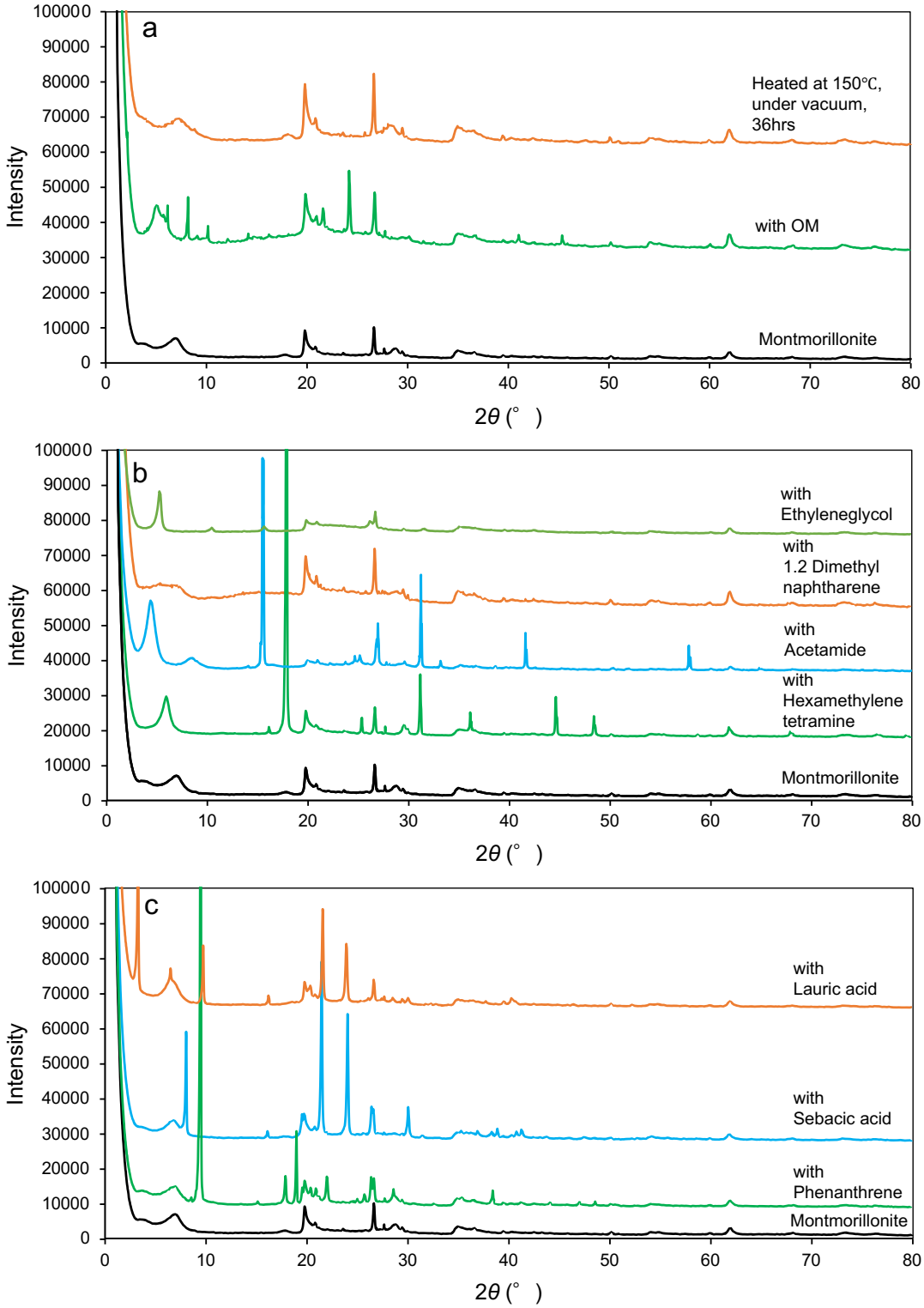

Figure 2-3. (a) XRD patterns of the initial montmorillonite, montmorillonite mixed with OM and montmorillonite heated at 150 °C under vacuum for 36 hours. (b) XRD patterns of the montmorillonite mixed with ethyleneglycol, 1,2-dimethylnaphtharene, acetamide and hexamethylenetetramine. (c) XRD patterns of the montmorillonite mixed with lauric acid, sebacic acid and phenanthrene.

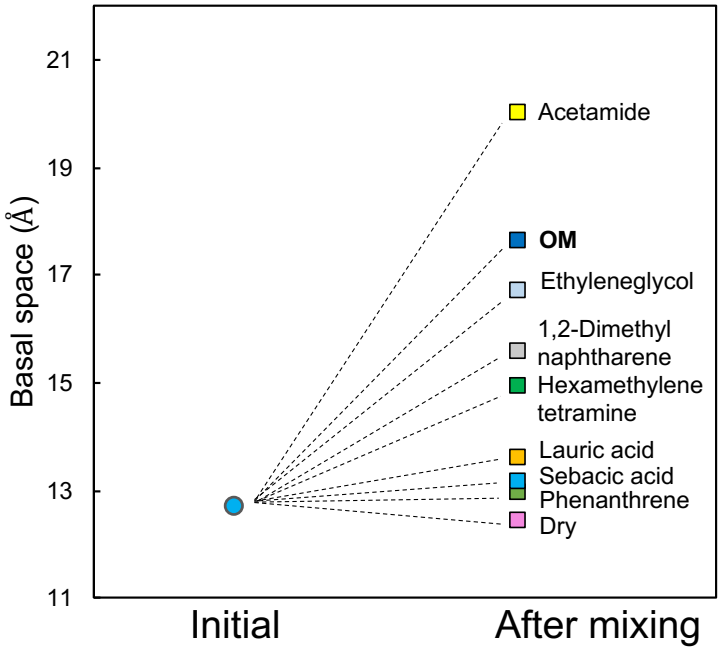

Figure 2-4. The change of the basal space of montmorillonite by mixing each chemical reagent. The initial basal space of the montmorillonite (left) changed after mixing with each reagent (right).

Table 2-1. Peak positions and assigned functional groups of the FTIR spectra (Socrates, 2001; Djomgoue and Njopwouo, 2013; Maina et al., 2015; Laine et al., 2016; Bunin et al., 2017).

Peak position (cm^{-1})	Vibrational mode	Functional group
3620	Al-OH stretch	Inter octahedral
~3400	O-H stretch	Alcohol, carboxyl, water
3060	C-H stretch	Aromatic CH
2955	C-H asymmetric stretch	Aliphatic CH_3
2925	C-H asymmetric stretch	Aliphatic CH_2
2870	C-H symmetric stretch	Aliphatic CH_3
2855	C-H symmetric stretch	Aliphatic CH_2
1740	C=O stretch	Ester
1720-1690	C=O stretch	Carboxylic acid
1715-1685	C=O stretch	Aldehyde
1700-1660	C=O stretch	Ketone
1665	C=O stretch	Amide
1600-1580	C=C stretch	Aromatic
1455	C-H asymmetric bend	Aliphatic CH_3
1375	C-H symmetric bend	Aliphatic CH_3
1230-1030	C-N stretch	Amines
~1210	Aromatic skeletal	
1150-1020	C-O stretch	
1045	Si-O-Si asymmetric stretch	Montmorillonite
980, 940	Si-O-Si asymmetric stretch	Olivine

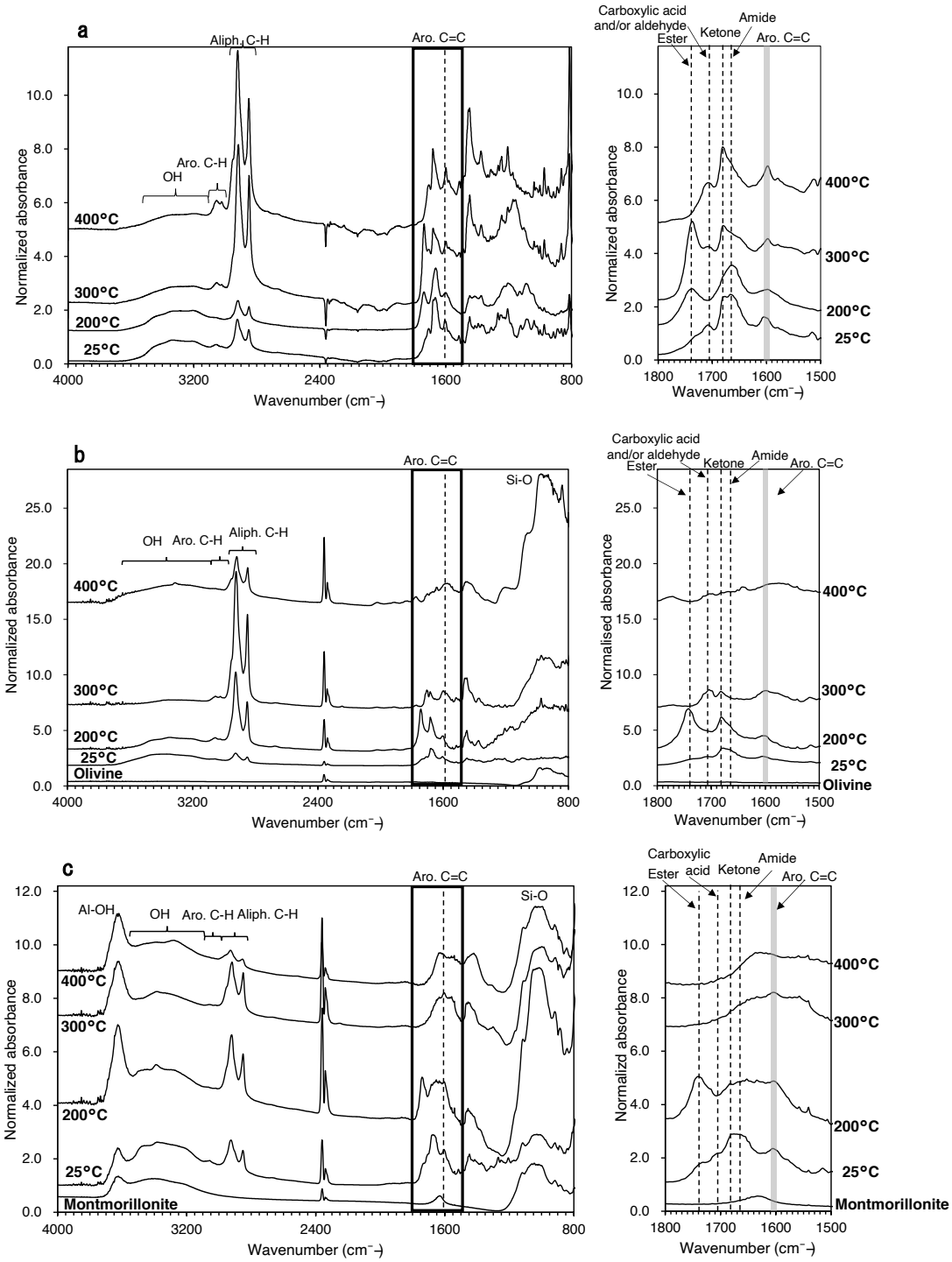

Figure 2-7. (a) ATR-IR spectra of OM, (b) Micro-FTIR spectra of OM + olivine, and (c) Micro-FTIR spectra of OM + montmorillonite. The enlarged spectra between 1800-1500 cm^{-1} (C=O and aromatic C=C region) are shown in the right panels. All spectra were normalized to the peak height of the aromatic C=C band (~1600 cm^{-1}).

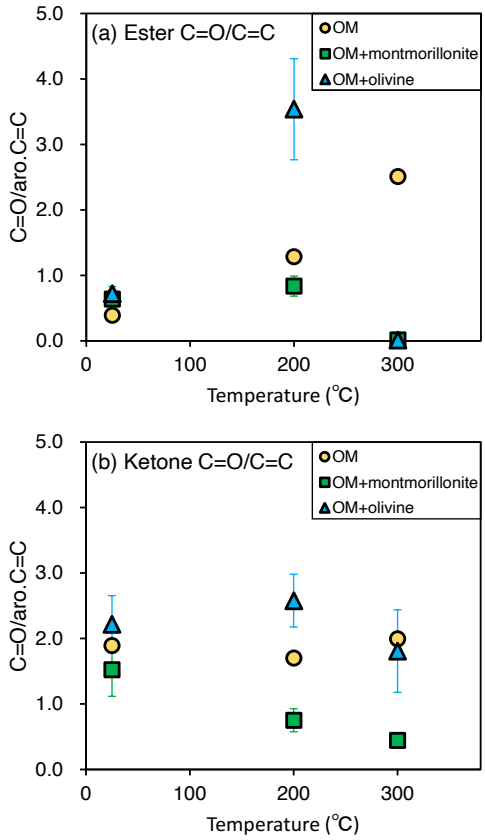

Figure 2-8. The peak intensity ratios obtained from IR spectra of the heated OM, OM + olivine, and OM + montmorillonite after heating at 200 °C and 300 °C. (a) Ester C=O at ~1740 cm^{-1} over aromatic C=C at ~1600 cm^{-1}, and (b) ketone C=O at ~1680 cm^{-1} over aromatic C=C at 1600-1580 cm^{-1}.

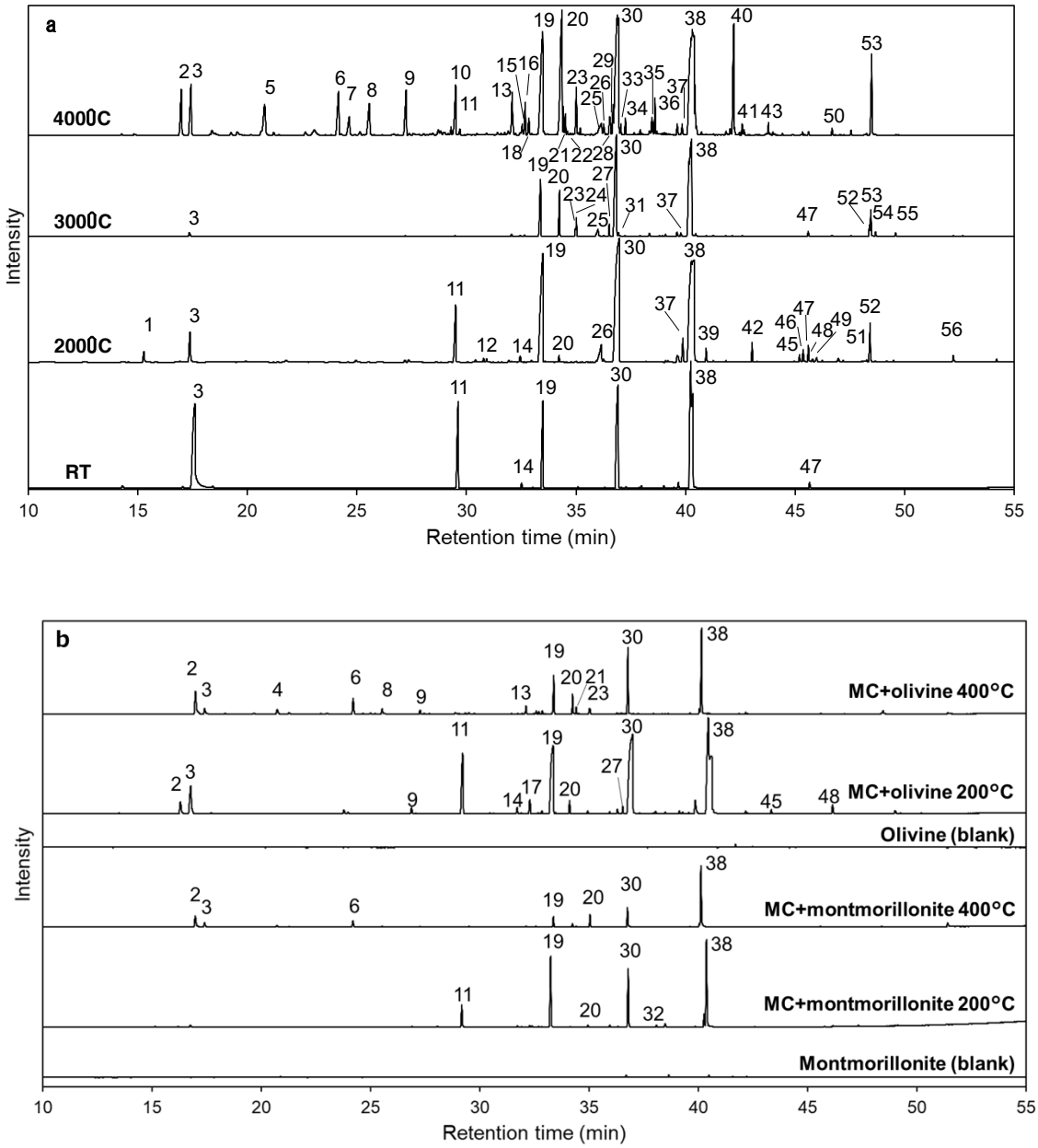

Figure 2-9. (a) Total ion chromatograms (TIC) obtained by GC/MS of hexane extracts from OM and heated OM at 200 °C, 300 °C, and 400 °C. (b) TIC of OM + olivine (200 °C and 400 °C) and OM + montmorillonite (200 °C and 400 °C). The both samples were heated at around 1 atm. The chromatograms of blank extractions from olivine and montmorillonite are shown to confirm that there was no contamination. The peak numbers correspond to compounds listed in Table 2-2.

Table 2-2. Compounds detected from heating OM experiments, with and without minerals in the hexane fraction by GC/MS. Asterisks (*) indicate initial compounds in OM. Pluses (+) indicate detected compounds in the different mixtures.

Number	Retention time (min)	Compounds	OM			OM+olivine		OM+montmorillonite	
			200 (°C)	300 (°C)	400 (°C)	200 (°C)	400 (°C)	200 (°C)	400 (°C)
1	15.23	1,2-Ethanediol diacetate	+						
2	16.98	Indane			+	+	+		+
3 *	17.42	Indene	+	+	+	+	+		+
4	20.72	4-(Octyloxy)- benzaldehyde					+		
5	20.78	2,5-Dimethylphenol			+				
6	24.20	1,4-Bis(1-methylethyl)benzene			+		+		+
7	24.65	Nonanenitrile			+				
8	25.57	2,3,5-Trimethylphenol			+		+		
9	27.27	1-(1-Methylethenyl)-4-(1-methylethyl)benzene			+	+	+		
10	29.30	Tridecane			+				
11 *	29.50	1,4-Diisopropenylbenzene	+		+	+		+	
12	30.78	Triacetin	+						
13	32.09	(Cyclohexylmethyl)benzene			+		+		
14 *	32.45	3,4-Dihydro-2-methyl-1(2H)-naphthalenone	+			+			

15	32.55	[(Cyclohex-1-en-1-yl) methyl]benzene			+				
16	32.68	(1.4-Dimethylpent-2-enyl)benzene			+				
17	32.72	1-(2.3-Dihydro-1H-inden-5-yl)ethenone				+			
18	32.85	Diphenylmethane			+				
19 *	33.42	1.2-Dimethylnaphthalene	+	+	+	+	+	+	+
20	34.25	Dodecanenitrile	+	+	+	+	+	+	+
21	34.43	2-Tridecanone			+		+		
22	34.52	Pentadecane			+				
23	34.97	Exo-7-(1-cyclohexen-1-yl)-bicyclo[4.2.0]oct-1-ene		+	+		+		
24	35.02	Dodecanoic acid methyl ester		+					
25 *	36.16	Dodecanoic acid	+	+	+				
26	36.27	Fluorene			+				
27	36.52	Dodecanoic acid ethyl ester		+		+			
28	36.55	2-Octyldodecyl butyrate			+				
29	36.69	Heptadecane			+				
30 *	36.88	Cyclohexyl phenyl ketone	+	+	+	+	+	+	+
31	36.94	Nonanoic acid 9-hydroxy methyl ester		+					
32	36.96	1,2,3,4,4a,9,10,10a-Octahydrophenanthrene (trans)						+	
33	37.05	2-Phenyl 2,4-octadienol			+				
34	37.26	Benzophenone			+				
35	38.47	2-Methyl 3H-Benz[e]indene			+				

36	38.61	Octadecane			+				
37	39.85	Dodecanamide	+	+	+				
38 *	40.33	Phenanthrene	+	+	+	+	+	+	+
39	40.95	Octadecanoic acid 2-hydroxyethyl ester	+						
40	42.20	Nonadecane			+				
41	42.59	3-Methylphenanthrene			+				
42	43.05	4,4-Ethylenedioxy-1-pentylamine	+						
43	43.79	Heneicosane			+				
44	44.35	Cyclopropane carboxylic acid pentadecyl ester				+			
45	45.21	Dodecanoic acid ethenyl ester	+						
46	45.38	Hexanoic acid tridecyl ester	+						
47 *	45.62	4-(1-Adamantyl)phenol	+	+		+			
48	45.81	1,2-Diphenyl-1,2-di(morpholin-4-yl)ethane (threo)	+						
49	46.00	1,4-Dioxo-1,2,3,4-tetrahydrophthalazine	+						
50	46.69	4-Methyl-2-tricyclo[3,3,1,1(3,7)]dec-1-yl-phenol			+				
51	46.99	Eicosanoic acid 2,3-bis(acetyloxy)propyl ester	+						
52 *	48.40	4,4'-Methylenebis[2,6-dimethylphenol]	+	+					
53	48.50	Nonadecanenitrile		+	+				
54	48.68	Methyl 18-methylnonadecanoate		+					

55	49.59	Eicosanoic acid ethyl ester		+					
56	52.23	Octadecanamide	+						

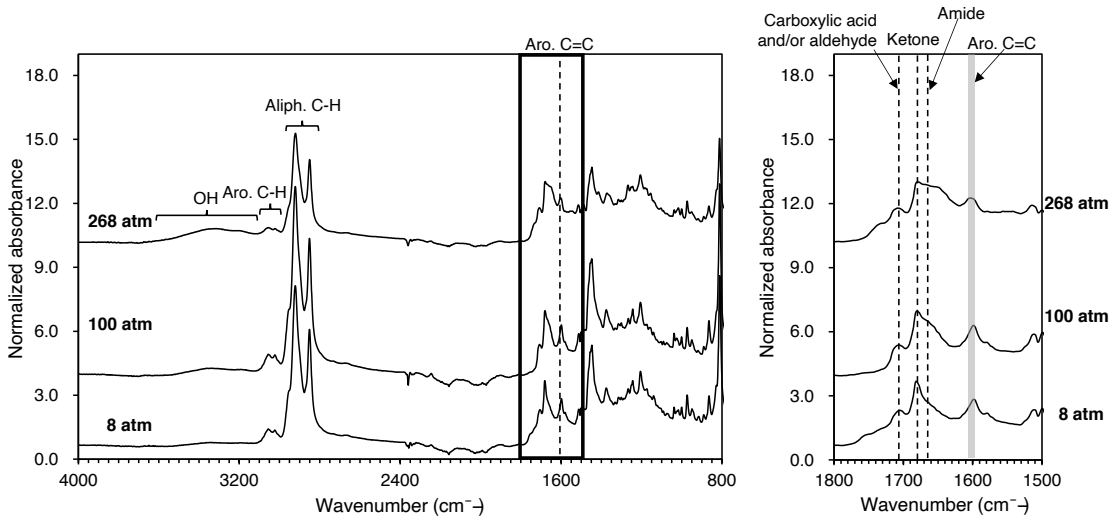

Figure 2-10. ATR-IR spectra of OM heated products heated at 400 °C under different pressures. The enlarged spectra between 1800-1500 cm^{-1} (C=O and aromatic C=C region) are shown in the right panels. All spectra were normalized to the peak height of the aromatic C=C band (~1600 cm^{-1}).

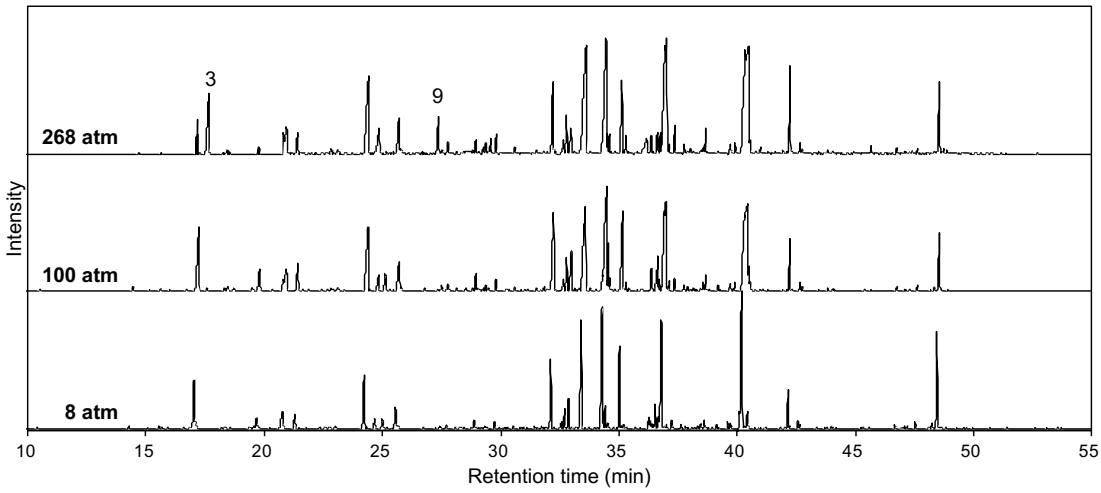

Figure 2-11. TIC obtained by GC/MS of hexane extracts from OM heated products heated at 400 °C under different pressures (8 atm, 100 atm and 268 atm). Different peaks with numbers at 17.42 min (3) and 27.27 min (9) correspond to compounds listed in Table 2-2.

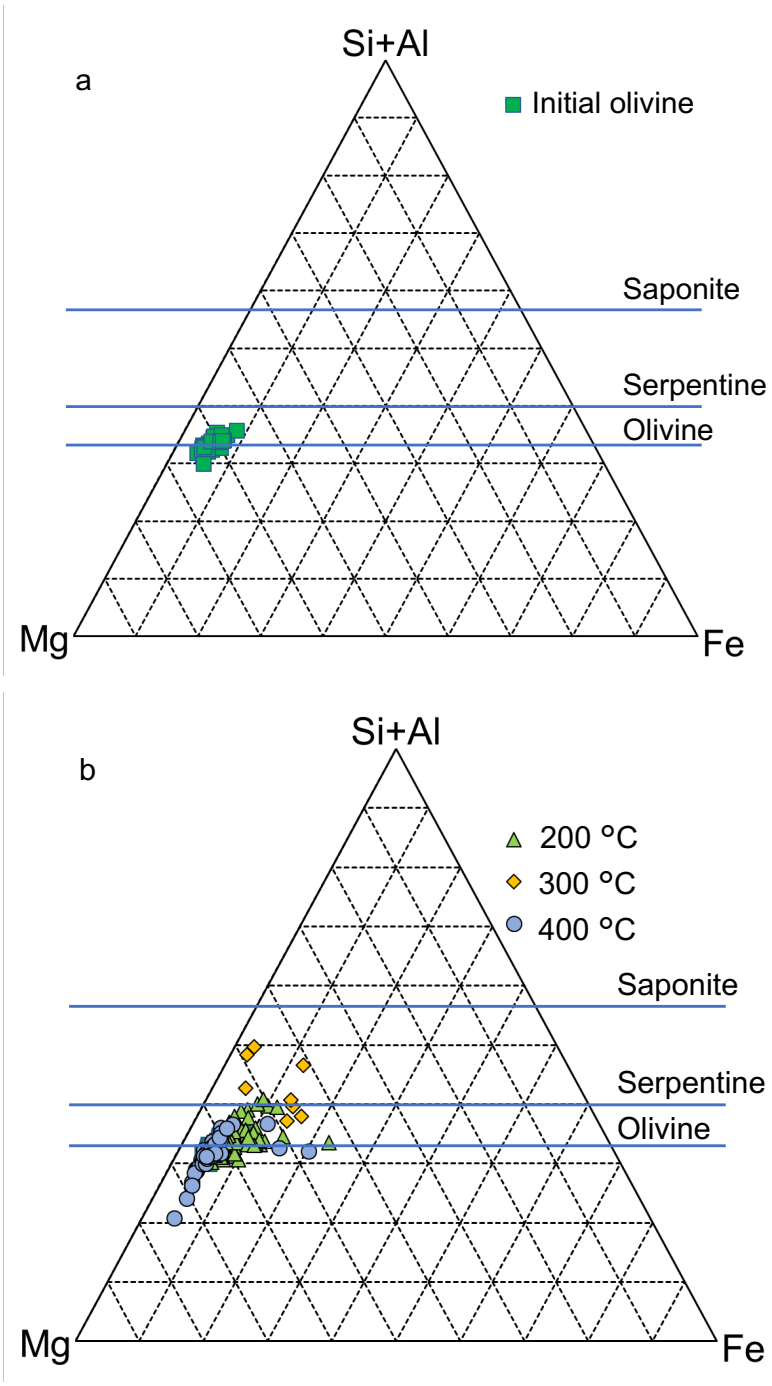

Figure 2-12. (a) A ternary diagram of initial olivine (square). (b) A ternary diagram of the heated olivine at 200 °C (triangle), 300 °C (diamond) and 400 °C (circle) with presence of organic mixture.

2.4. Discussion

2.4.1. Changes in molecular structures of OM by heating

Ester compounds detected at 200 °C and 300 °C by GC/MS could be formed through dehydration condensation of carboxylic acids with alcohols from the initial OM. In IR spectra, the intensity ratios of ester C=O/C=C in the OM increased at 200 °C and 300 °C as compared to the OM at room temperature (Figure 2-8a). However, the ester C=O was not observed at 400 °C (Figure 2-7a), indicating that carboxylic acids were decomposed due to decarboxylation before ester formation, and thus ester did not form at this temperature. In addition, the O-H band relative to aliphatic C-H at 300 °C is smaller than those at lower temperatures (Figure 2-7a), and indicated that significant dehydration from aliphatic compounds occurred at 300 °C. Dehydration was also induced by N-containing compounds. Newly detected amide compounds at 200 °C such as dodecaneamide and octadecaneamide could be formed through nucleophilic reaction followed by dehydration of carboxylic acids with amines. Amine compounds such as trimethylamine could be formed through the thermal decomposition of hexamethylenetetramine (included in the initial OM) over 200 °C (Iwakami et al. 1968). Then, dehydration of amides produced nitriles mainly at 300 °C and 400 °C.

Alkanes with 15-19 carbons detected from the OM heated at 400 °C may be evidence of thermal cracking and decarboxylation of eicosanoic acid ($C_{20}H_{40}O_2$). 2,5-dimethylphenol and 2,3,5-trimethylphenol at 400 °C could be formed through the cracking of 4,4'-methylenebis(2,6-dimethylphenol), which has a bridged structure of two phenols. 4-(1-adamantyl)phenol was also the candidate for the precursor of these phenols at 400 °C. Thus, a cleavage at a bridged part of each aromatic compound likely occurred at 400 °C.

2.4.2. Pressure effects on changes in molecular structures of the OM by heating

As an example, 200 km asteroidal interiors could reach up to 100 atm (10 MPa) (Grimm and McSween 1989). Thus, the effects of pressure on changes in molecular structures of organic matter was evaluated. Significant influences of increasing pressure (8-268 atm) for the OM without minerals were not observed in the infrared spectra and GC/MS (Figure 2-10, 2-11). Thus, pressure effects could be negligible for organic matter without minerals at 400 °C. Higher pressure (> a few GPa) could lead to the formation of renewed intra- or inter-molecular bonds (Tao et al. 2014; Potiszil et al. 2017). Pressure unlikely affects the organic chemistry during long-term thermal metamorphism in a few hundred km parent bodies, and thus minerals and the other physicochemical factors are possibly more significant (Figure 2-7, 2-8, 2-9), but pressures may affect in the case of shock metamorphism.

2.4.3. Effects of minerals

Some minerals are known to enhance various chemical reactions (e.g. Almon and Johns 1975; Davis and Stanley 1982; Heller-Kallai et al. 1984; Sanna and Andrésen 2012; Varma 2002; Bu et al.

2017). In this study, changes in C=O groups at each temperature could be enhanced by the minerals. The possible effects of minerals on organic matter observed in this study were summarized in Table 2-3.

The significant increase of ester C=O/C=C with olivine could indicate that esterification was enhanced by olivine at 200 °C. Depletion of C=O bands at 300 °C and 400 °C could indicate that decarboxylation was enhanced by olivine. Decarboxylation could be enhanced when olivine acted as an acid catalyst (Kluger et al. 2013). Olivine is known as a strong cracking catalyst under gasification conditions of biomass at high temperatures (> 410 °C) (Sanna and Andrésen 2012; Lancee 2014). Thus, in the case of OM + olivine at 400 °C, decarboxylation could be induced by the loss of carboxylic moieties through the cleavage of C-C bonds of long-chain carboxylic acids.

Decrease in C=O in the OM was enhanced by montmorillonite with heating (Figure 2-8). Industrial studies have revealed the role of phyllosilicate for decarboxylation of carboxylic acids during thermal processes at 250 °C and higher temperatures (Almon and Johns 1975; Heller-Kallai et al. 1984). Cracking was also known to be promoted by phyllosilicates (Heller-Kallai et al. 1984), thus cracking-induced decarboxylation of the OM could be enhanced by montmorillonite, similar to olivine. Phyllosilicates as a cracking catalyst has been well studied and utilized in the petroleum industry to decompose heavy crude oil (e.g. Haresnape 1948; Milliken et al. 1952; Davis and Stanley 1982).

Olivine and montmorillonite are fundamentally different silicate groups—olivine is a nesosilicate and montmorillonite is a phyllosilicate. Such differences cause large differences in physicochemical properties. The noticeable differences between olivine and montmorillonite are likely (1) structural properties and (2) surface area. These physical and chemical differences are further examined in the following discussion.

Meanwhile, reactions of organics may induce transformation of minerals—at least the *d*-spacing of montmorillonite was enlarged by OM. It is also possible that water generated through heating of the OM (Nakano et al. 2020) could alter olivine. For example, serpentine is formed from olivine thorough aqueous alteration, but complete transformation of olivine to serpentine demands much longer time than 5 hours (Malvoisin et al. 2012). However, the evidences of transformation of minerals were not studied here in detail.

2.4.3.1. Structural properties

Olivine and montmorillonite show different structural properties originated from different silicate structures. Layered structures in phyllosilicates, which show electric charges with some cations in the layer space, can show various structural properties such as swelling, cation-exchange, and intercalation (Varma 2002). Some organic matter could make Van der Walls and cationic bonds with montmorillonite (Hendricks 1941; Varma 2002). Olivine, on the other hand, does not show such properties. In addition to these properties, acidity of the minerals should be compared, since it could

have significant effects on organic reactions. Thus, the structural property is remarked in terms of acidity in this section.

The interlayer cation in montmorillonite act as Brønsted-Lowry acid (Varma 2002). Surface and edge defects of montmorillonite result in Lewis acid sites. Lewis acid sites also appears in olivine (Tian et al. 2012). These acidities could promote different chemical reactions in accordance with temperature.

The enhancement of esterification of the OM by olivine at 200 °C is likely due to Lewis acid sites of olivine, since esterification is known to be promoted by acid catalysts (Trejda et al. 2019). Esterification could be enhanced by interlayer protons (Brønsted-Lowry acid) and Lewis acid sites of montmorillonite (Varma 2002). However, enhancement of esterification of the OM by montmorillonite was not observed in this study. Unlike olivine, decomposition effects of montmorillonite might be stronger than the esterification effect at 200 °C.

Decarboxylation can be promoted by Lewis acid sites (Johns 1979)—both olivine and montmorillonite have Lewis acid sites. At 300 °C, the ester abundances in OM + olivine and OM + montmorillonite were significantly lower than the OM without minerals (Figure 2-8a). It is probably because olivine and montmorillonite acted as a solid acid for decarboxylation of carboxylic acids—precursors of esters. In the case of montmorillonite, the degree of decarboxylation depends on the chemical compositions of the octahedral sheets (Heller-Kallai et al. 1984). Al^{3+} and/or Fe^{3+} ions in octahedral sheets of montmorillonite can capture an electron from adsorbed molecules containing carboxyl groups, which results in the formation of radical intermediates. These radical intermediates then produce alkyl radicals and CO_2 (Alomon and Johns 1975; Bu et al. 2017). Bu et al. (2017) reported that thermal degradation of fatty acids with carboxyl groups can be catalyzed by montmorillonite. This catalytic activity of montmorillonite leads to lower decomposition temperatures of fatty acids. Therefore, in the present study, decarboxylation of fatty acids in the OM was promoted by montmorillonite even at 200 °C.

Cracking is also the significant catalytic effects driving the decrease in C=O. Cleavage of C-C bonds in long chain carboxylic acids could lead to the formation of small volatile molecules. In case of olivine, Lewis acid sites in olivine might lead to cleavage of C-C and/or C-O at 400 °C (Sanna and Andrésen 2012). Heller-Kallai et al. (1984) reported that acidity of the phyllosilicate interlayers affected the amount of cracking. In addition to Lewis acid sites on mineral surface, interlayer cations in montmorillonite which act as Brønsted-Lowry acid could also enhance a cracking reaction. Brønsted-Lowry acid sites first acted as proton-donors, and then they could catalyze cracking via the carbonium ion mechanism (Liu et al. 2013). These decomposition effects of montmorillonite explain that less compounds were detected by GC/MS when the organic mixture heated with montmorillonite compared to these with olivine and without minerals.

2.4.3.2. Contact surface area

The activity of a catalyst is closely associated with surface area. The catalytic activity decreases when particle size increases (Shankland 1954). The particle size of olivine and montmorillonite in this study was approximately <200 μm and <2 μm, respectively, observed using a SEM. It is roughly comparable to the actual grain size of these minerals in meteorites (Buseck and Hua 1993). In addition, organic molecules could enter the interlayer of clay minerals to form organo-clay complexes (Cai et al. 2007). In this study, the interlayer space of montmorillonite increased when mixed with the OM. This result indicates that organic compounds were intercalated into the interlayer space of montmorillonite (Figure 2-3, 2-4). Hence, contact surface area of montmorillonite with the OM was much higher than that of olivine. Although one cannot evaluate the effects of contact surface area in the present study, it is highly plausible that the higher surface area of montmorillonite could result in stronger effects compared to olivine.

2.4.4. Possibility of alteration of olivine

Based on the result of the EDS, the chemical composition of olivine was affected by the organic matter at 200-400 °C. The Si-rich chemical compositions of the experimental products at 200 °C and 300 °C could indicated the dissolution of Mg^{2+}, and it may subsequently induce the precipitation of some hydrous minerals such as serpentine and/or saponite. However, the dissolution of Mg^{2+} was not observed in the experiment at 400 °C.

This trend could be explained by Yada and Iishi (1974). In the experiment, 50 mg of natural olivine (Fo90) was heated at 250-450 °C for 30 min-30 day with 0.1 mL of pH controlled water. Serpentine was formed in 10 days at 250-400 °C under pH7 solution, however most olivine remained at 450 °C. The result clearly indicate that serpentine could not be formed at high temperature. Result that Mg-depleted composition was not observed in present study was possibly due to the high temperature effect. To confirm the formation of such secondary minerals in this study, investigation using SEM/EDS and heating duration for 5 hours was insufficient. Thus, possibility of the alteration of olivine induced by organic matter was investigated in detail in chapter 3.

2.4.5. Insight into carbonyl groups in CV, CO and type 3 ordinary chondrites

Differences in the effects of olivine and montmorillonite for decarboxylation and esterification implied that there would be differences in the C=O structures between organic matter coexisting with olivine and montmorillonite in meteorites heated under 300 °C, however, these structures would be the same in the meteorites heated over 400 °C. Type 3 chondrites were divided into four groups (groups A to D) in Kebukawa et al. (2011) based on the infrared spectra of their IOM. Groups C and D, which included CV, CO, and ordinary chondrites, were divided based on the peak positions of C=O. Group C contains Kaba (CV3.0/3.1ox), Vigarano (CV3.3/3.1-3.4red), Mokoia (CV3.2/3.6ox), Allende

(CV3.2/>3.6ox), and Bishunpur (LL3.15). A weak C=O band was observed at 1725 cm^{-1} possibly due to lactones in group C. Group D contains Leoville (CV3.0/3.1-3.4red), Kainsaz (CO3.2/3.6), ALHA77003 (CO3.6), Tieschitz (H/L3.6), and Chainpur (LL3.4). C=O with variable intensity was observed at 1667 cm^{-1} due to ketone in group D. The metamorphic temperatures of these groups C and D chondrites were similar—200-400 °C and 250-450 °C, respectively. The difference in carbonyl structures in spectral groups C and D was explained by the local activity of water during thermal metamorphism. Preservation of lactones in spectral group C might suggest low H_2O activity during parent body processing. Alternatively, higher H_2O activity could lead to the extensive decarboxylation in group D chondrites.

The results of the present study show a possibility of mineral effects on organic reactions in meteorite parent bodies. If the precursor of chondritic IOM is similar to the OM, some of these variations might be explained by coexisting minerals. Mineralogy of both groups C and D is mainly composed of olivine and pyroxene. CVox chondrites such as Kaba (CV3.0/3.1ox) and Mokoia (CV3.2/3.6ox) in group C contain phyllosilicates and magnetite, which could be formed through aqueous alteration. These minerals might be explained by H_2O generated through organic reactions—dehydration of carboxylic acids and amides, as shown by the previous study (Nakano et al. 2003, 2020). Phyllosilicates in such meteorites could have been produced with the H_2O generated from organic compounds during thermal metamorphism. C=O bonds in group C IOM appear at 1725 cm^{-1}, which is attributed to lactone (Kebukawa et al. 2011). An ester bond in lactone could be formed through dehydration condensation of carboxyl and alcohol. If the lactone was formed faster than phyllosilicates, esterification reaction could be enhanced by olivine at lower than 300 °C in group C chondrites based on the present study. Then, the olivine could gradually be altered to phyllosilicates with generated water from organic reactions. On the contrary, lactones could not be formed if there were phyllosilicates before organic reactions at 200-300 °C, since the phyllosilicates could enhance the decomposition of organic compounds. In case at around 100 °C, phyllosilicates possibly enhance esterification (Varma 2002), which could be lower temperature than the temperatures of group C or D chondrites.

The group D IOM shows ketone C=O but does not show ester C=O (Kebukawa et al. 2011). Thus, the organic matter in group D could be metamorphosed at higher than 300 °C with olivine, since decomposition of organic matter could be enhanced by olivine at the temperature based on the present study. In addition, there could be another case. Phyllosilicates in primitive type 3.0 CO chondrites are known to be several wt. % more abundant than in CV chondrites (Howard et al. 2014; McAdam et al. 2018), and thus CO chondrites in group D such as Kainsaz (CO3.2/3.6) and ALHA77003 (CO3.6) could have contained more abundant phyllosilicates than CV chondrites before thermal metamorphism. In this study, esterification did not proceed well in the presence of phyllosilicates at 200 °C. Thus, phyllosilicates in CO chondrites might contribute to the lack of ester C=O in the IOM (Kebukawa et

al. 2011). A similar process could be applied to Leoville (CV3.0/3.1-3.4red) in group D, since it also contains phyllosilicates locally (Kracher et al. 1985).

Metamorphic conditions such as temperature, time, and oxidation processes have been investigated to determine how they influence the final structure of the IOM (e.g. Alexander et al. 2007; Bonal et al. 2006; Busemann et al. 2007; Cody and Alexander 2005; Cody et al. 2008; Homma et al. 2015; Kebukawa et al. 2010b, 2011; Quirico et al. 2003, 2009). Oxygen containing parts are difficult to understand because O/C in chondritic IOM is not completely correlated with the maturity within the metamorphosed chondrite group (Quirico et al. 2009). In addition to those expected maturation parameters, the present study proposes effects of co-existing minerals for oxygen correlated evolution of organic matter in meteorite parent bodies. Enhancements of oxygen expulsion through decarboxylation and cracking of organic matter by minerals may lead to the metamorphism of oxygen-containing moieties in meteoritic organic matter. It should be noted that the heated OM does not represent full characteristics of chondritic IOM, but the effects of minerals presented here could be useful to understand the reactions involving the common structures such as carbonyl moieties. Further studies are needed to understand the precise effects of minerals for organic matter during thermal metamorphism.

Table 2-3. Summary of the effects of olivine and montmorillonite observed in this study.

Temperatures	Minerals	Characteristics enhanced by minerals in this study	Possible effects	References
200 °C	Olivine	Significant increase of ester C=O/C=C ratio Enhances of ester and nitrile compounds	Esterification	1, 2
	Montmorillonite	Decrease of ketone C=O/C=C	Decarboxylation of carboxylic acids	3
300 °C	Olivine	Significant decrease of ester C=O/C=C	Decarboxylation of carboxylic acids	1, 4
	Montmorillonite	Decrease of ester C=O/C=C and ketone C=O/C=C	Decarboxylation of carboxylic acids and cracking	5, 6, 7, 8
400 °C	Olivine	Loss of C=O peaks Decrease of soluble compounds	Decarboxylation of carboxylic acids and cracking	9, 10
	Montmorillonite	Loss of C=O peaks Significant decrease of soluble compounds	Decarboxylation of carboxylic acids and cracking	5, 6, 7, 8

[1] Tian et al., 2012, [2] Trejda et al., 2019, [3] Johns, 1979, [4] Kluger et al., 2013, [5] Almon and Johns, 1975, [6] Heller-Kallai et al., 1984, [7] Bu et al., 2017, [8] Liu et al., 2013, [9] Sanna and Andresen, 2012, [10] Lancee, 2014

2.5. Conclusions

A precometary organic matter analog was heated with olivine and montmorillonite using an autoclave to investigate the effects of minerals on the metamorphism of organic matter during thermal processes in meteorite parent bodies. The experimental products were analyzed using XRD, FTIR, and GC/MS. Results were interpreted mostly based on the functional group chemistry. With increasing heating temperature, the molecular structures of the OM changed significantly. Changes in C=O bands in IR spectra were affected when the OM was heated with minerals. These results indicated that olivine enhanced esterification at 200 °C, decarboxylation at 300 °C and 400 °C, and cracking-induced decarboxylation at 400 °C, and montmorillonite enhanced decarboxylation at 200 °C, 300 °C and 400 °C, cracking-induced decarboxylation at 300 °C and 400 °C. The presence/effect of montmorillonite implied a stronger decrease in C=O than olivine in the OM produced. This could be due to the physicochemical differences between olivine and montmorillonite—olivine is a nesosilicate and montmorillonite is a phyllosilicate. Montmorillonite has much larger contact surface area than olivine. In addition, montmorillonite has both Brønsted-Lowry acid sites and Lewis acid sites, while olivine has only Lewis acid sites. The effect of pressure on the degradation of the OM was also tested, however no significant differences were observed in the FTIR spectra of the OM heated at 400 °C under pressures up to 268 atm. The results might further imply that decreases in O-bearing functional groups in organic matter in chondrites were enhanced by co-existing minerals during thermal processes in CV, CO, and type 3 ordinary chondrite parent bodies. Although further studies are needed, the differences in co-existing minerals might have contributed to the variations in molecular structures of organic matter in chondritic meteorites, particularly on oxygen containing moieties.

3. Aqueous alteration without initial water: Possibility of organic-induced hydration of anhydrous silicates in meteorite parent bodies.

3.1. Introduction

Minerals, water, and organic matter are the initial building blocks of our Solar System. Evolution of the early-stage Solar System proceeded with their interactions. Following accretion to planetesimals, H_2O ice melted by the heating mostly due to the decay of short-lived radioactive nuclides (Brearley 2006; Trigo-Rodrigez et al. 2019). The water fluid contributed to the aqueous alteration of minerals with distributing and migrating some elements (Brearley 2006; King et al. 2017). Alteration of anhydrate silicates results in the formation of phyllosilicates. Phyllosilicates are abundant in CI, CM, and CR chondrites; thus, these chondrites experience strong aqueous activities (Brearley 2006). Phyllosilicates also exist in some "dry" chondrites such as CV, CO, and unequilibrated ordinary chondrites (Buseck and Hua 1993; Brearley 2006), although they are much less abundant compared with CI and CM chondrites. These phyllosilicates in such dry chondrites may be evidence of water in their parent bodies (Bischoff 1998); however, the origin of the water in these chondrites is not well understood.

These "dry" chondrites are known to be thermally metamorphosed in their parent bodies (Huss 2006). The main heat source is considered to be the decay of short-lived nuclides after accretion to planetesimals (Huss 2006). Thermal metamorphism by the heating could gradually affect the nature of meteorites. For example, the least metamorphosed chondrites (unequilibrated ordinary chondrites) experienced slight heating, such as Semarkona meteorite (LL3.0, ~260 °C, Alexander et al. 1989), Vigarano (CV3, 300-400 °C, Tomeoka and Tanimura 2000; Huss 2006) and Kainsaz (CO3.2, ~300 °C, Huss 2006). Although these temperatures can result in low-degree effects on petrology or mineralogy, they can have significant influence on the structure and composition of organic matter in meteorites via various chemical reactions. Additionally, impact-induced heating could be another heat source. Impact compactions could occur during the formation of small bodies prior to most of aqueous alteration (Trigo-Rodriguez et al. 2006; Beidz et al. 2016). Some carbonaceous chondrites also show post-alteration heating shown by evidences such as dehydration of phyllosilicates, recrystallization of olivine, carbonization and graphitization of organic matter (Kitajima et al. 2002; Nakamura 2005; Rubin et al. 2007; Nakato et al. 2008; Quirico et al. 2018). Hydrous minerals could remain in weakly heated chondrites (<250 °C; Nakamura 2005). In case of equilibrated chondrites, subsequent heating at high temperature after extensive shock events could induce annealing of crystal fractures of minerals (Rubin 2004).

In terms of interactions among minerals, water, and organic matter, the role of organic matter for alteration of minerals is not well understood. Recent studies suggested that minerals act as catalysts for the formation and evolution of organic matter (Pearson et al. 2002; Kebukawa et al. 2010; Yamashita and Naraoka 2014; Le Guillou et al. 2014; Fuchida et al. 2017; Rotelli et al. 2016; Vinogradoff et al. 2020a, b). Chemical reactions of organic matter are frequently accompanied by simultaneous generation of by-products. Nakano et al. (2020) performed heating experiments of organic mixtures up to 400 °C, which simulated the evolution of primordial organic matter in meteorite parent bodies, and they found various by-products including CO, CO_2, and H_2O during the experiments. These compounds in turn could have influence on mineral alterations.

In this study, a heating experiment of an anhydrous silicate (olivine) with an organic mixture was performed simulating thermal metamorphism in meteorite parent bodies. The reaction products were analyzed using X-ray diffraction (XRD), secondary electron microscopy with energy-dispersive X-ray spectroscopy (SEM/EDS), and transmission electron microscopy with energy-dispersive X-ray spectroscopy (TEM/EDS). Insoluble organic matter on mineral grains were additionally analyzed by pyrolysis gas chromatography mass spectrometry technique (PY-GC/MS). Through this study, it was shown that minerals could be altered by organic matter in meteorite parent bodies without the initial presence of water.

3.2. Experimental

3.2.1. Starting materials

In this study, olivine was used as a typical anhydrous silicate in chondritic meteorites. San Carlos olivine powder (Fo91) was heated in an autoclave (Tama-Seiki) with a molecular cloud organic matter analog (Table 1-2, Nakano et al. 2002), which simulated the primordial organic matter accreted to meteorite parent bodies before thermal metamorphism. The olivine powder, the initial grain size of which was <200 μm, was ground before the experiments using an agate mortar to obtain a typical grain diameter of <50 μm. The organic mixture was prepared following the method of Kouchi et al. (2002), Nakano et al. (2002, 2003, 2020).

3.2.2. Heating experiment

For the heating experiment, 0.2 g of ground olivine powder with 1.0 g of organic mixture was sealed in a stainless-steel Swagelok tube fitting union (3/8 in.) with 316 stainless-steel plugs (3/8 in., 3.0 cm^3) under N_2 gas atmosphere. The tube fitting was placed in an autoclave (Tama-Seiki) and then heated at 300 °C for 10 days (Figure 3-1). After the tube fitting was cooled, the experimental product was recovered. The product was rinsed with hexane (3 mL) and methanol (3 mL) to eliminate the organic matter from the surface of the olivine.

To estimate the amount of water generated in heated product, a heating experiment without olivine

and the distillation of water were additionally performed following the procedure of Nakano et al. (2020). The organic mixture (28.9 g) was heated at 300 °C in an autoclave (OM Labotec, MM-100 special type) for 5 h. After cooling to the room temperature by turning off the electric power supply, the autoclave was opened, and the product was recovered. To separate the water from the product, the product (2.0 g) was heated at 100 °C. The water was subsequently distillated to the other sample vial.

3.2.3. Characterization techniques

3.2.3.1. XRD

The initial olivine and experimental product rinsed with hexane and methanol were analyzed by powder XRD using a SmartLab diffractometer with a Hypix-3000 detector (Rigaku, Ltd.) at 40 kV and 45 mA by Cu Kα radiation with a scan speed of 5.0°/min and a resolution of 0.01. Identification of the mineral phase was performed using SmartLab Studio II by searching the diffraction patterns from International Center for Diffraction Data (ICDD) database through the Hanawalt search method.

3.2.3.2. SEM/EDS

Grain size, morphology, and elemental composition of the experimental products were characterized using a scanning electron microscope (JSM-6510LA, JEOL) equipped with an energy-dispersive X-ray spectrometer (JED-2300, JEOL). Grains were fixed on a 10 mm brass stub with resin and were coated by Au sputtering. All grains were observed by secondary electron imaging at 15 kV. An elemental analysis was conducted by EDS at 20 kV.

3.2.3.3. Focused ion beam (FIB) processing

Focused-ion-beam preparations were performed with an NX2000 (Hitachi High-Tech Global) at the Japan Aerospace Exploration Agency. First, the surface of the target area in an olivine grain on an SEM stub was covered with a carbon deposition layer. Three sides of the target area were milled on the surface of the SEM stub (~10 μm depth). After the bottom edge was cut, the section was suspended by a cantilever and then attached to a silicon nanomesh. The sample was thinned to the thickness that allows electron transparency (<100 nm) using successively lowered Ga^+ ion beam currents of 12 nA, 1.5 nA, 280 pA, and 100 pA at 30 kV, and final polishing was done using a current of 20 pA at 10 kV and 20 pA at 5 kV of ion energy.

3.2.3.4. TEM/EDS

FIB thin sections were analyzed using TEM (JEM-2100F, JEOL) equipped with EDS (JED-2300T, JEOL) at Yokohama National University and Tohoku University. High-resolution images were obtained at 200 kV. EDS spectra were accumulated for approximately 1 hour.

3.2.3.5. PY-GC/MS

After recovering the heated product and rinsing with hexane (3 mL) and methanol (3 mL), several amount of the sample was separately collected. The fraction was additionally rinsed by hexane (2 mL), methanol (2 mL) and pure water (2 mL) under sonification to eliminate soluble organic compounds completely. During the sonification, soluble parts were resolved into solvents and insoluble solid precipitates were divided from the collected product. The solid fraction, which included mineral grains and insoluble organic matter, was dried at 60 °C. Approximately 3 mg of the insoluble organic matter with mineral grains was inserted in a pyrolyzer (PY-2020iD, Frontier Lab) and pyrolyzed at 600 °C for 0.3 minutes. The pyrolyzer was directly connected to a gas chromatography mass spectrometer (GC/MS; QP-2020, Shimadzu) equipped with a non-polar column DB-5 (purchased from Agilent J & W) with a 30 m × 0.25 mm internal diameter and 0.25 μm film thickness. The pyrolysates were carried through the column by helium (>99.999 %) with a flow rate of 1.23 mL/min. The column temperature was initially 40 °C, increasing at a rate of 3 °C/min up to 60 °C and then 6 °C/min up to 320 °C. Electron ionization (EI) was applied at 70 eV with an ion source temperature of 200 °C. Data processing was conducted using GCMSsolution software (Shimadzu). The background (sample cup) taken at 10 min was subtracted and peaks were selected based on a signal-to-noise ratio of >3. Peak identifications were conducted using NIST2017 library (2017 edition).

3.3. Results

3.3.1. XRD

While the bulk structure of olivine did not change significantly after heating with organic mixture, there were some evidences of mineral replacement in the XRD pattern of the olivine after the experiment (Figure 3-2). A wide loose curve from 15° to 50° in the baseline could indicate the existence of amorphous phase with crystalline olivine. Magnesite has strong peaks at 32.5°, 43° and 54 ° (Lafey et al. 2014; Ulrich et al. 2014), thus small peaks around 43° and 54° were diffraction from magnesite, which are secondary minerals formed during the heating of olivine with organic matter. The peak at 32.5° could be overlapping with olivine. Peaks of olivine and magnesite are indicated in Figure 1 and the other peaks could be impurities originally contained in natural olivine samples. A broad small peak at 7° was unidentified.

3.3.2. SEM/EDS

Clearly visible cracks with SEM images and abundant etch pits are the typical dissolution features on olivine grains (Malvoisin et al. 2012; Oelkers et al. 2018). SEM observation revealed these dissolution characteristics on the surface of olivine (Figure 3-3). Initial olivine used as the starting material in the heating experiment had angular shapes with smooth surfaces (Figure 3-3a, b). Numerous residual olivine grains after the experiment apparently showed the alteration features.

Isolated conical etch pits are shown in Figure 3-3c, d (hereafter called grain A) and mammillated topography are shown in Figure 3-3e, f (hereafter called grain B). Most of the etch pits detected in this study were conical to polyhedral or pyramidal features.

Precipitation features, which had a webbed structure, covered the surface of the heated grains (Figure 3-3c, d). This structure gradually suffered damage during SEM observation, indicating the presence of materials that interact with the electron beam. Irregularly shaped fragile materials 1–10 μm in diameter, likely organic residues, were also on the surface of the olivine (Figure 3-3e–h). Such fragile materials were easily damaged by an electron beam, and commonly contained in the experimental product. Details of the changes in the molecular structures of organic mixture and the effects of minerals were in chapter 2.

The chemical composition of olivine obtained by EDS had a 1:2 Si/(Mg + Fe) molar ratio (Figure 3-4). Flat surface areas of the grains in the experimental product showed similar compositions as the starting materials, while the areas covered with precipitation features showed Mg-poor and Si-rich compositions. Note that the information depth of SEM/EDS is approximately 1 μm, however precipitation layers were <1 μm (Figure 3-4). Thus, the chemical compositions of the precipitation areas obtained by EDS could include the information from the olivine surface.

3.3.3. TEM/EDS

TEM investigations revealed a change of morphologies near the grain surface areas. Figure 3-5 is a TEM image with elemental mappings of the FIB section taken from the etch pit area shown in Figure 3-3g, h. A matrix of flake-like particles constituting an anastomosing network was observed in this area. C was entirely distributed in the mapping area, while Si, O, Mg and Fe showed an irregular distribution feature. Si was concentrated in the flake-like particles (Figure 3-5c). Iron oxides were on the etch pits (Figure 3-5e, f). Mg was clearly depleted in the surface area of olivine, however there were a few Mg, Si, O and Fe concentrated areas, which are independent from flake-like particles (Figure 3-5). Differences in chemical compositions of these areas were shown in Figure 3-6 (Points 1-4). Point 1 was richer in Mg than the other areas, however the mineral phase was not identified. Point 2 and Point 3 were flake-like particles, these chemical compositions were plotted between serpentine and talc. Point 4 was the surface area of olivine and its composition was slightly Mg-depleted compared to the initial olivine. Nanoscale spherical black particles in Figure 3-5a were Au from the coatings on the surface of grain B for SEM observations. A TEM image of the other area in the FIB section showed tubular fibers (<100 nm thick) on the surface of olivine that were anastomosed and were poorly crystalline (Figure 3-7). The lattice fringes were unclear and were easily damaged by the electron beam during TEM observation. The electron diffraction spots (Figure 3-7), were not clear enough for identifying crystal structure. These features were significantly similar to those of proto-serpentine reported by Lafey et al. (2016), which could be formed in the first step of serpentinization

of olivine (Lafey et al. 2012, 2016).

3.3.4. PY-GC/MS

Many pyrolysates involving alkane, alkene, nitrile, amide and cyclic compounds were detected. The total ion chromatogram was shown in Figure 3-8a and the detected compounds were listed in Table 3-1. The most predominant compound was 1,2,4,5-tetramethyl-1H-imidazole, and valuably alkylated nitrogen containing aromatic compounds such as alkylated pyrazole (1,3,5-trimethyl-1H-pyrazole (19.18 min), 1,3,5-trimethyl-1H-pyrazole (22.74 min), 4-ethyl-3,5-dimethyl-1H-pyrazole (23.64 min) 1H-, 4-(2-bromoethyl)-3,5-dimethyl-pyrazole (27.48 min), 4-ethyl-3,5-dimethyl-1H-pyrazole (27.86 min) , 1-ethyl-5-methyl-pyrazole-4-carboxaldehyde (28.17 min), 1,3,4,5-tetramethyl-1H-pyrazole (31.20 min), 4-ethyl-3,5-dimethyl-1H-pyrazole (32.54 min)), imidazole (1,2,4,5-tetramethyl-1H-imidazole (22.42 min), 2-ethyl-4-methyl-1H-imidazole (23.53 min)), pyrazine (2-methoxy-3-(1-methylethyl)-pyrazine (30.14 min), 2,3-Dimethyl-5-ethylpyrazine (30.35 min), 2-Oxo-1-methyl-3-isopropylpyrazine (30.63 min), 2-methoxy-3-(1-methylethyl)-pyrazine (30.70 min), 2-ethyl-3,5-dimethyl-pyrazine (31.94 min)) and benzimidazole (2,5-dimethyl-1H-benzimidazole (34.44 min), 1,2-Dimethylbenzimidazole (35.79 min)) were also detected. There were also many alkanes and alkenes. Alkene and alkane appeared in pair, alkene had a little shorter retention time than alkane as shown in Figure 3-8b. These alkenes and alkanes were C9-19, which indicated that cracking of long chain aliphatic compounds in starting material produced these compounds. In an average mass spectrum between 10-55 min (Figure 3-8c), peaks appeared repeatedly every m/z 14.

3.3.5. Amount of water generated from organic matter

The experimental product was black sticky liquid, generated water could be solved in the liquid (Figure 3-9a). Recovered water through the distillation was 0.05 g (Figure 3-9b), thus at least 2.5 wt.% of water was generated from the organic mixture at 300 °C. The water could contribute to the alteration of olivine. Based on the amount of recovered water, water/rock ratio in this study could be 0.13. The water was pH 8, measured with a pH test paper (Johnson, TEST PAPERS Universal pH1-pH14).

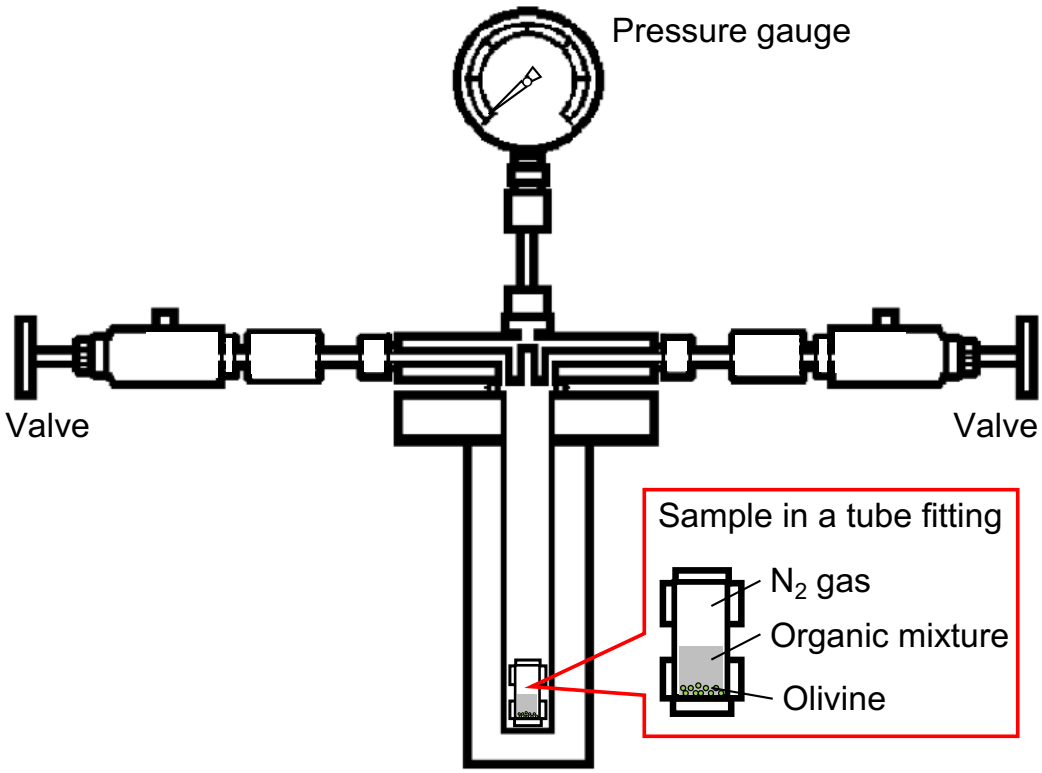

Figure 3-1. Schematic image of the experimental setup. Samples were placed in a stainless-steel tube (inner volume: 3.0 cm^3) sealed with Swagelok tube fitting union (3/8 in.) and 316 stainless-steel plugs (3/8 in.) under N_2 gas, and then heated inside an autoclave.

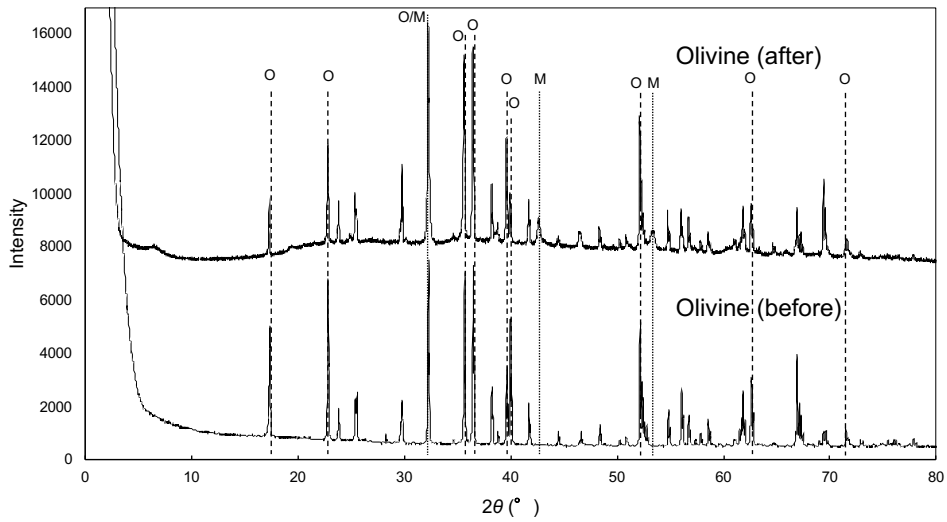

Figure 3-2. XRD patterns of olivine before (lower) and after (upper) the experiment. The bulk structure of olivine did not change after heating with organic mixture. New peaks due to magnesite appeared in the XRD pattern of olivine (after) are indicated with *. O: Olivine, M: Magnesite.

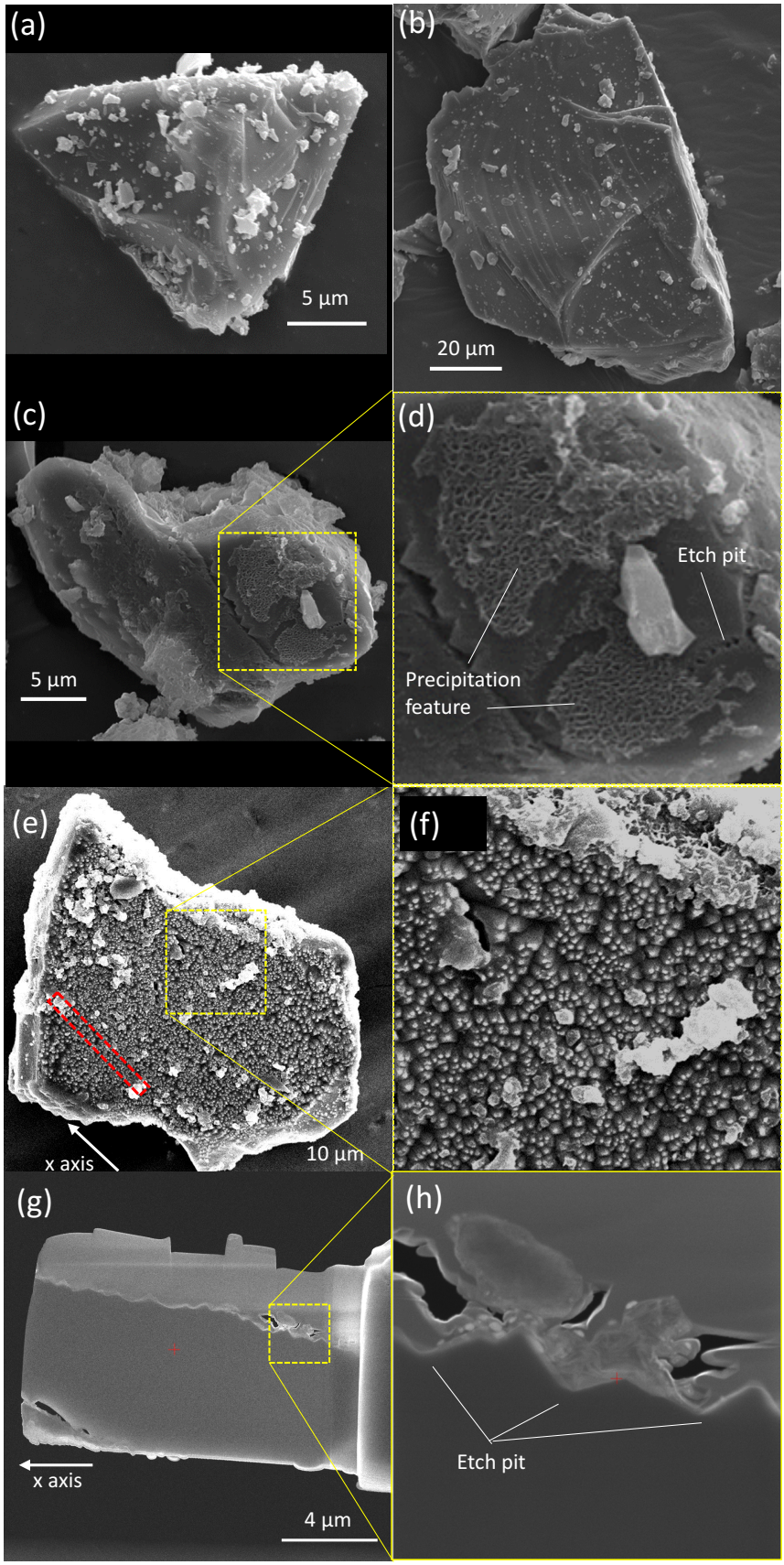
(a)
5 µm
(b)
20 µm
(c)
5 µm
(d)
Etch pit
Precipitation
feature
(e)
x axis
10 µm
(f)
(g)
x axis
4 µm
(h)
Etch pit

Figure 3-3. Microstructure of initial olivine grains (a, b), olivine grains after the experiment (grain A: c, d; grain B: e,f), and an FIB section from grain B (g, h). (a, b) Typical olivine grains used as the starting materials. These grains had a smooth surface with smaller olivine particles (~1 μm) attached to them. (c, d) Grain A was partially covered with precipitation features. Conical etch pits were also detected. (e, f) Grain B was entirely covered with polyhedral etch pits. Irregularly shaped carbonaceous materials (1–10 μm, white particles) were attached to the surface. (g, h) An FIB section obtained from grain B (red broken area).

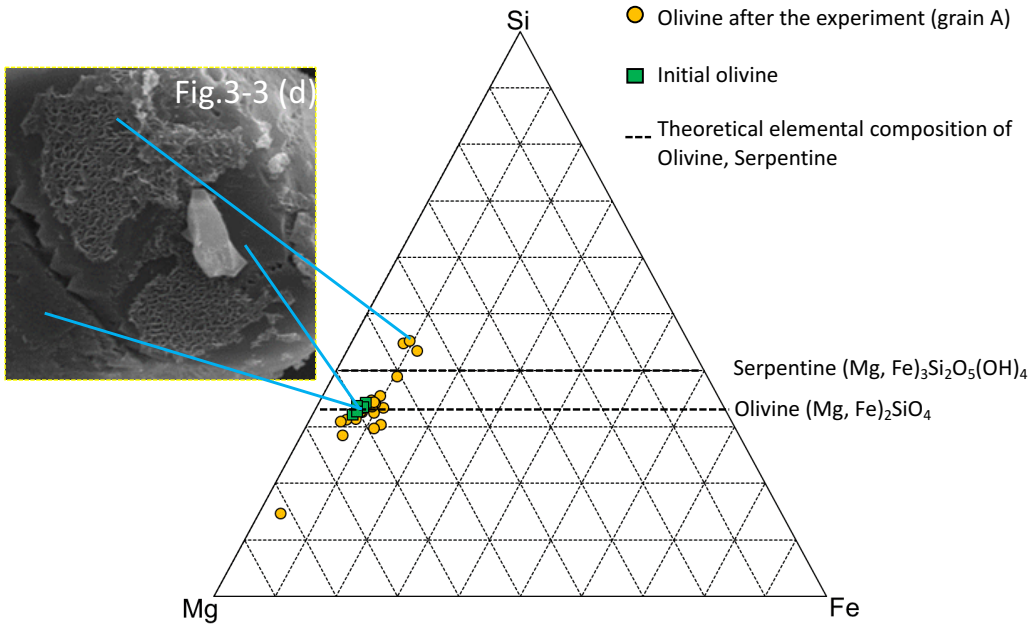

Figure 3-4. A plot from SEM/EDS analyses of the initial olivine and an olivine after the experiments (grain A). EDS plots for a flat surface of a reacted olivine had chemical compositions similar to those of typical olivine. Olivine surface with precipitation features had Si-rich and Mg-poor compositions as compared with a typical olivine.

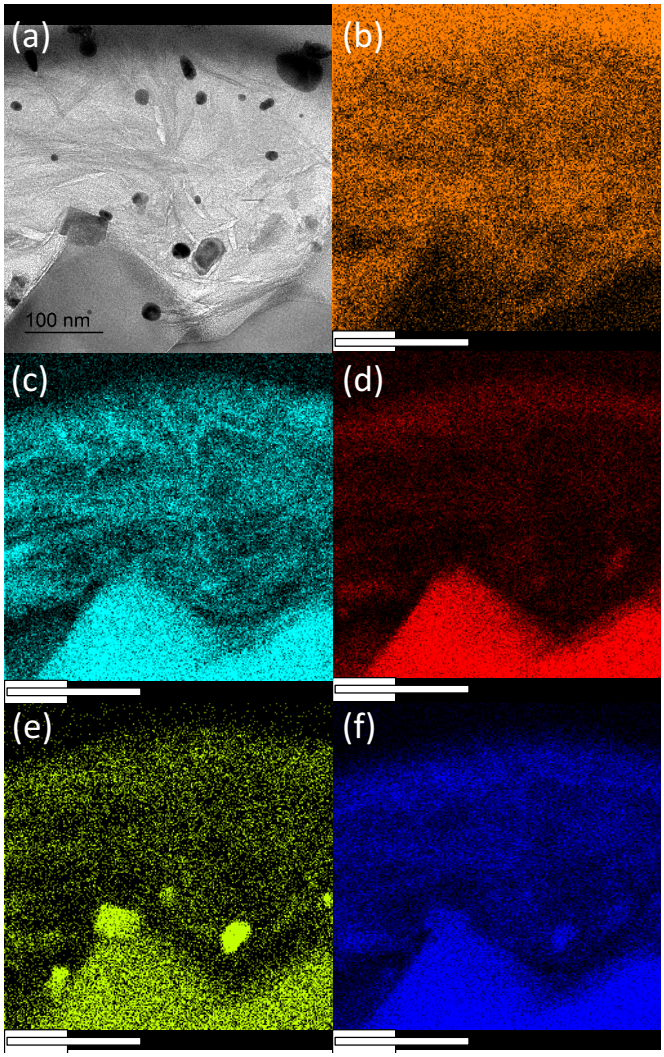

Figure 3-5. (a) A TEM image of the boundary area between etch pits of grain B and a precipitation feature. Flake-like particles can be observed in this area. (b–f) EDS C, Si, Mg, Fe, and O elemental mappings of the area (a).

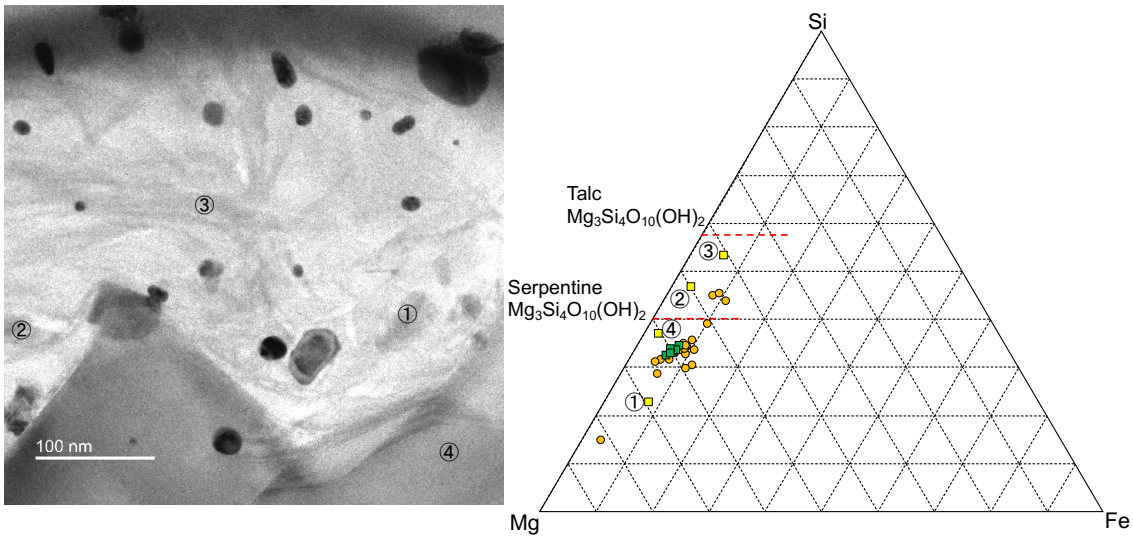

Figure 3-6. Chemical compositions of the four different textures in Figure 3-5. Point 1: Mg, Si, O and Fe concentrated area, Point 2: a part of flake like particles, Point 3: another part of flake like particles, and Point 4: the surface area of olivine.

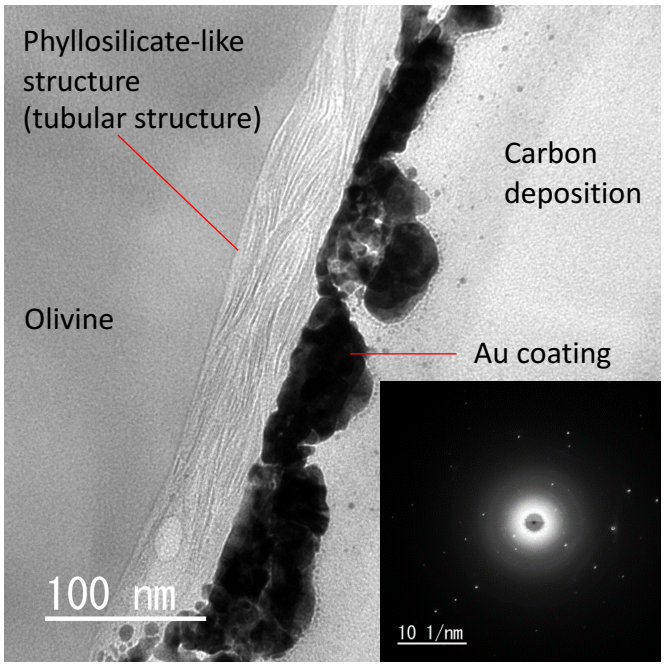

Figure 3-7. A TEM image of a phyllosilicate-like structure near the surface area of olivine that had reacted (grain B), along with a diffraction pattern of the structure (lower right). The phyllosilicate-like structure was a tubular anastomosed feature.

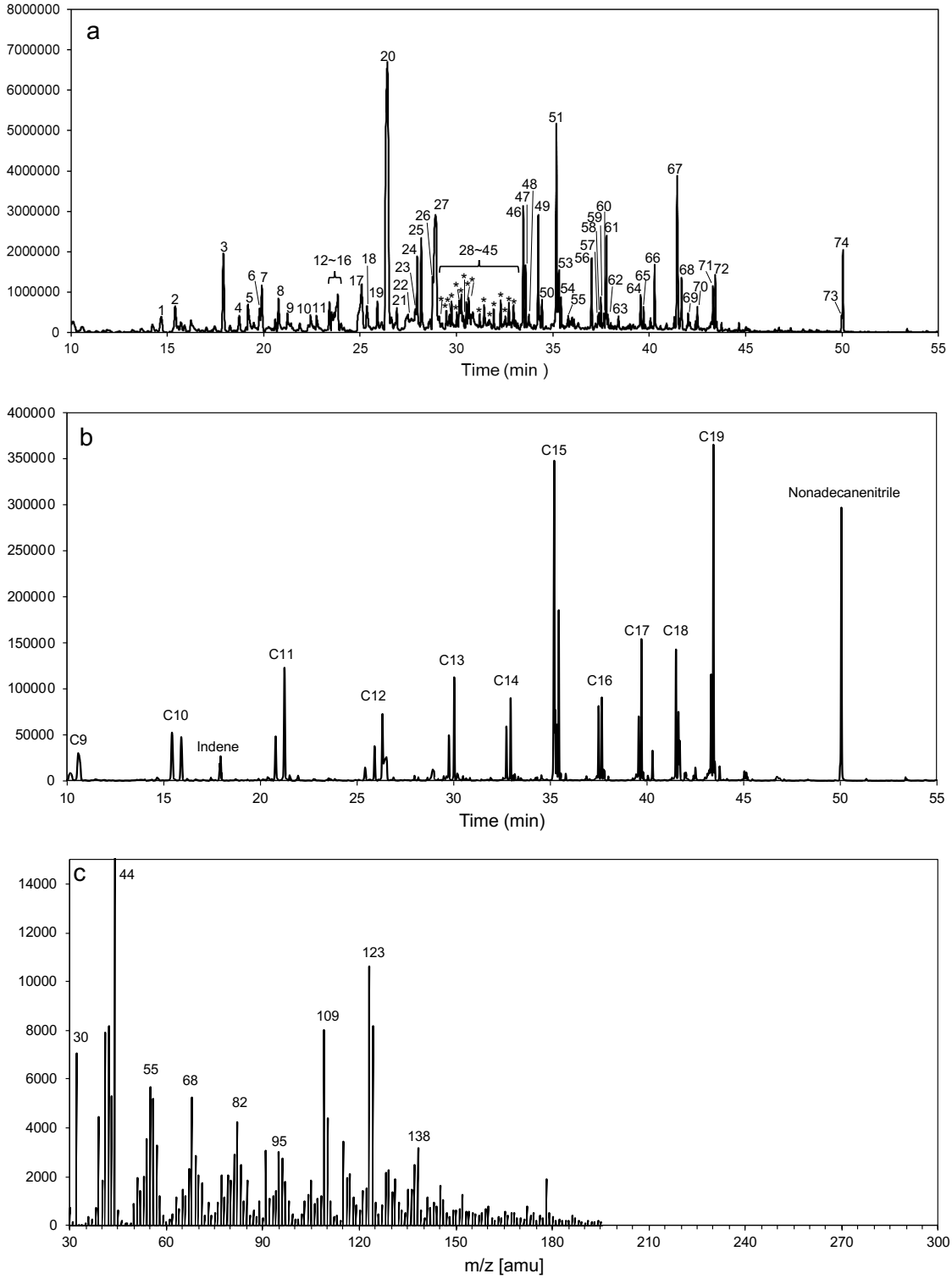

Figure 3-8. (a) Total ion chromatogram (TIC) of pyrolyzed insoluble organic matter with mineral grains after rinsing by hexane, methanol and pure water. (b) The m/z 57 ion chromatogram of pyrolyzed insoluble organic matter with mineral grains after rinsing by hexane, methanol and pure water. (c) Average mass spectrum between 10-55 min in Figure 3-8a.

Table 3-1. Compounds detected by the pyrolysis of insoluble organic matter with mineral grains after rinsing by hexane, methanol and pure water.

Number	Retention time (min)	Compounds
1	14.68	Benzonitrile
2	15.05	1-Decene
3	17.91	Indene
4	18.74	Tetracyclo[3.3.1.1(3,7).0(2,4)]decane
5	19.18	1,3,5-Trimethyl-1H-pyrazole
6	19.79	7-Octene-1-nitrile
7	19.90	Adamantane
8	20.77	1-Undecene
9	21.23	Undecane
10	22.42	1,2,4,5-Tetramethyl-1H-imidazole
11	22.74	1,3,5-Trimethyl-1H-pyrazole
12	23.41	(1-Methyl-2-cyclopropen-1-yl)-benzene
13	23.53	2-Ethyl-4-methyl-1H-imidazole
14	23.64	4-Ethyl-3,5-dimethyl-1H-pyrazole
15	23.78	Naphthalene
16	23.84	1-Methyl-4-(1-methyl-2-propenyl)-benzene
17	25.08	3,4,5-Trimethylpyrazole
18	25.36	1-Methyl-4-(1-methyl-2-propenyl)-benzene
19	25.90	1-Tetradecene
20	26.42	1,2,4,5-Tetramethyl-1H-imidazole
21	26.90	1,2-Dihydro-6-methyl-naphthalene
22	27.48	4-(2-Bromoethyl)-3,5-dimethyl-1H-pyrazole
23	27.86	4-Ethyl-3,5-dimethyl-1H-pyrazole
24	27.97	1-(1-Methylethenyl)-3-(1-methylethyl)-benzene
25	28.17	1-Ethyl-5-methyl-pyrazole-4-carboxaldehyde
26	28.76	4-Ethyl-1,3-benzenediol
27	28.92	2,3,4,5-Tetramethyl-2-cyclopenten-1-one
28	29.12	1-Benzosuberone
29	29.48	3,5-Dimethyl-4-allylpyrazole
30	29.64	2-Methyl-naphthalene

31	29.74	1-Tridecene
32	30.02	Tridecane
33	30.14	2-Methoxy-3-(1-methylethyl)-pyrazine
34	30.25	1,3-Bis(1-methylethenyl)-benzene
35	30.35	2,3-Dimethyl-5-ethylpyrazine
36	30.52	Cyclohexyl-benzene
37	30.63	2-Oxo-1-methyl-3-isopropylpyrazine
38	30.70	2-Methoxy-3-(1-methylethyl)-pyrazine
39	30.85	1-Ethylidene-1H-indene
40	31.20	1,3,4,5-Tetramethyl-1H-pyrazole
41	31.94	2-Ethyl-3,5-dimethyl-pyrazine
42	32.29	Biphenyl
43	32.54	4-Ethyl-3,5-dimethyl-1H-pyrazole
44	32.72	1-Pentadecene
45	32.96	(Cyclohexylmethyl)-benzene
46	33.47	[(Cyclohex-1-en-1-yl)methyl]-benzene
47	33.59	(1,4-Dimethylpent-2-enyl)benzene
48	33.76	Diphenylmethane
49	34.24	1-Phenylbicyclo(4, 1, 0)heptane
50	34.31	1,2-Dimethyl-naphthalene
51	34.44	2,5-Dimethyl-1H-benzimidazole
52	35.18	Undecanenitrile
53	35.32	2-Tridecanone
54	35.43	Tetradecane
55	35.79	1,2-Dimethylbenzimidazole
56	37.01	1,2,3,4,4a,9,10,10a-Octahydrophenanthrene (trans)
57	37.36	Fluorene
58	37.40	2-Dodecanone
59	37.49	1-Pentadecene
60	37.65	Hexadecane
61	37.78	Decanedinitrile
62	37.85	Phenyl cyclohexyl ketone
63	38.41	4-Ethenyl-1,1'-biphenyl
64	39.56	9-Nonadecene
65	39.70	Heptadecane

66	40.28	N-(2-Hydroxyethyl)-dodecanamide
67	41.45	Phenanthrene
68	41.68	N-Methyldodecanamide
69	42.01	N-(2-Hydroxyethyl)-decanamide
70	42.50	N-Ethyl-dodecanamide
71	43.31	1-Nonadecene
72	43.43	Heneicosane
73	49.98	2-Nonadecanone
74	50.05	Nonadecanenitrile

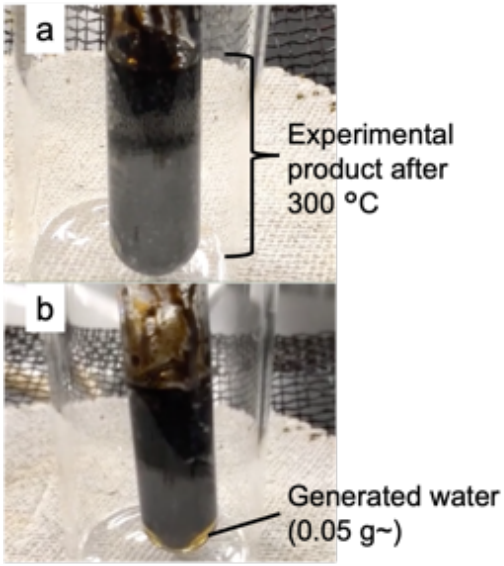

Figure 3-9. (a) the organic product after heating at 300 °C (2.0 g), and (b) organic product with separated water.

3.4. Discussion

3.4.1. Alteration of olivine

It is well known that mineral replacements such as serpentinization take place primarily by dissolution–precipitation processes (Putnis 2002; Lafay et al. 2012). Etch pits confirmed by SEM (Figure 3-3c–f) on the surface of product grains could be the preferential dissolution features at the first step of serpentinization. The dissolution process is crystallographycally controlled (Velvel 2009; Malvoisin et al. 2012; Lafey et al. 2018). Thus, these etch pits become deeper and elongate in the [010] and [001] direction as alteration proceeds (Velvel 2009; Malvoisin et al. 2012). Isolated conical etch pits (Figure 3-3c, d) would evolve to a network of polyhedral and pyramidal mounts and ultimately to a mammillated (sawtooth) topography (Figure 3-3e, f, Malvoisin et al. 2012). It indicates that the alteration degree in grain B (Figure 3-3e, f) is advanced as compared with grain A (Figure 3-3c, d).

Olivine dissolution proceeds by the breaking of Mg–O bonds and an early rapid reversible exchange of Mg for protons on the olivine surface, which then liberates the SiO_4^{4-} anions directly into solution in acidic to neutral solution (Luce et al. 1972; Oelker et al. 2018). In contrast, Si–O structures preferentially dissolved ahead of cation dissolution in alkaline solution (Oelkes et al. 2018). These processes could result in depletion of Mg or Si on the olivine surface. Mg-poor and Si-rich webbed-like structure covering the surface of olivine after the experiments could be precipitation features of dissolved silicate (Lisabeth et al. 2017). Although in-situ pH condition of generated water during heating was not clear in this study, carboxylic acids could contribute to weakly acidic water. Decomposition of amides and hexamethylenetetramine, on the contrary, could generate NH_3 (Iwakami et al. 1968), which could result in alkaline water. However enough amount of water for pH measurement was not recovered, since the water from 1.0 g of organic matter was too small. Water obtained in an additional experiment through distillation in this study was approximately at pH8, and in Nakano et al. (2020) was at pH 9.3 because of dissolved NH_3. Thus, the pH of water could strongly depend on the composition of the initial organic matter.

Amorphous proto-phyllosilicates precipitated onto the etch pits; thus, growth and crystallization of serpentine or talc proceeded in the precipitation area within or on the etch pits (Plümper et al. 2012). Talc could grow with higher silica activity and CO_2 concentration (Moore and Rymer 2007; Oelker et al. 2018). Thus, Si-rich flake-like particles in Figure 3-5 and tubular fibers in Figure 3-7 were precipitated features of proto-phyllosilicates, and these features could be the same material for the Mg-poor and Si-rich precipitation features in Figure 3-3c, d. The formation of tubular structures (Figure 3-7) also indicated the incipient formation of serpentine or talc on the surface of olivine grains. However, highly crystalline phyllosilicate was not confirmed by electron diffraction because the incomplete crystallization structures resulted in unclear lattice images and electron diffraction spots (Lafey et al. 2016). A schematic image of serpentinization based on obtained characteristics in this study is shown in Figure 3-9.

The rate of serpentinization typically depends on temperature, pH, water/rock ratio, and initial grain size (Malvoisin et al. 2012). Reaction progress of serpentinization from olivine with 38–50 μm grain size reached nearly 40 % in 250 days at 300 °C, and the major serpentine was lizardite (Malvoisin et al. 2012). Duration of the reaction in this study was 10 days and was likely too short to reach complete serpentinization, although serpentinization rate was the highest at 300 °C compared with those at higher or lower temperature (Wegner and Ernst 1983; Malvoisin et al. 2012). Yada and Iishi (1974, 1977), however, confirmed the formation of serpentine in shorter time (30 minutes to 10 days) at 250–400 °C at pH 3–13. In that case, conical chrysotile was the major serpentine in fairly wide ranges of pH and temperature, and lizardite existed at higher temperatures and longer durations. Under the alteration conditions in this study, finding proto-serpentine was reasonable, and it could grow toward chrysotile in several months.

3.4.2. Role of organic matter

Serpentinization demands water, but water was not present in the starting material in this study. Water, which is required for serpentinization, could be generated through organic reactions such as dehydration condensation of carboxylic acids and alcohols in the starting material at 300 °C (Chapter 2). Nakano et al. (2020) showed the formation of water from the same organic mixture used in this study (Table 1-2). The amount of water formed depended on the content of hydroxy group (–OH) of the starting materials (Nakano et al. 2020). Decomposition of these organic compounds could form smaller molecules such as CO, CO_2, CH_4, H_2, C_2H_6, and C_3H_8 (Nakano et al. 2003). It is consistent with the generation of CO, CO_2, CH_4, and H_2O through the destruction of insoluble organic matter in thermally metamorphosed chondrite parent bodies suggested by Alexander et al. (2010). In addition, the previous study showed that decarboxylation was promoted by olivine at 300 °C (Chapter 2). Magnesite, which could be formed via aqueous carbonation of olivine (see details below), as detected by XRD, also indicates the formation of CO_2 from the organic mixture.

Insoluble organic matter was left after rinsing by hexane, methanol and pure water, although all chemical compounds in the starting organic mixture were solvent soluble species. Thus, insoluble organic matter was formed after mixing of each reagent and heating in the tube fitting. If graphitization was proceeded, a strong peak around 27 ° could be observed (Sayah et al. 2018) in the upper XRD pattern in Figure 3-1. However, it did not show such new peaks, but the base line showed amorphous feature. It could indicate that the chemical structure of the organic matter was not ordered. The pyrolysates contained many alkylated aromatic compounds and average mass spectrum showed strong peaks every m/z 14, which accord with $-CH_2-$. The insoluble organic matter could have had weakly bridged structures by alkyl chains. Additionally, Naraoka et al. (2015) reported that the olivine surface could serve reaction sites to support elongation of alkyl-chains during the formation of nitrogen containing aromatic compounds through aldol condensation. The presence of olivine in this study

could have also had the similar effects on the organic matter.

Phyllosilicates and magnesium carbonate (magnesite) are thermodynamically stable solids in the $MgO–SiO_2–H_2O–CO_2$ closed system at 300 °C and under 1–100 bar of partial pressure of CO_2 (Oelkers et al. 2018). Magnesium olivine (forsterite) favors reactions that form serpentine and magnesite in accordance with:

$$2Mg_2SiO_4 + CO_2 + 2H_2O \rightarrow Mg_3Si_2O_5(OH)_4 + MgCO_3$$

(Forsterite) (Serpentine) (Magnesite)

or talc and magnesite in accord with:

$$4Mg_2SiO_4 + 5CO_2 + H_2O \rightarrow Mg_3Si_4O_{10}(OH)_2 + 5MgCO_3$$

(Forsterite) (Talc) (Magnesite)

under higher CO_2 concentration in water (Oelkers et al. 2018). Organic-induced serpentinization is possible with simultaneous water formation from dehydration of organic compounds. It indicates the possibility of in situ formation of phyllosilicates inside the H_2O snow line because refractory organic compounds, in contrast to H_2O, could survive during accretion of planetesimals in the area, as discussed below. However, it should be noted that there could be some differences of alteration conditions between present experiment and environments in the chondrite parent bodies. For example, only olivine was used, however organic compounds could react and dissolve metal ions from other minerals to form other secondary minerals.

3.4.3. Possible aqueous alteration in the "dry" parent bodies

Recent astronomical observations revealed the existence of organic molecules with hydroxy groups such as CH_3OH (Walsh et al. 2016), HCOOH (Favre et al. 2018) in protoplanetary disk, as well as CH_3CH_2OH, CH_3COOH, and $HOCH_2CHO$ were suggested by model calculation (Walsh et al. 2016). CH_3CH_2OH, CH_3COOH and $HOCH_2CHO$ were detected from the low-mass protostar IRAS 16293–2422 (Bisschop et al. 2008; Jerry Shiao et al. 2010; Jørgensen et al. 2012). They could be delivered inside the snow line on dust particles. Water and highly-volatile organic compounds evaporated inside the snow line, but the other organic molecules could remain on the grain surfaces. At least, organic compounds such as polyaromatic hydrocarbons, aliphatic hydrocarbons, alcohols, carboxylic acids, and macromolecular organics detected in cometary dusts could survive inside the sublimation area of water ice (Herbst and van Dishoeck, 2009; Welsh et al. 2014). In that case, organic matter could accumulate on planetesimals without water or with little water.

Water/rock ratio of ordinary chondrites is estimated as ~0.1-0.2 (Doyle et al. 2015). Water/rock

ratios of carbonaceous chondrites are estimated by Marrocchi et al. (2018), the ratio of CM chondrite is 0.4, CR is 0.1-0.4, CV is 0.1-0.2, and CO is 0.01-0.10. Glavin et al. (2018) also summarized the water/rock ratio of carbonaceous chondrites based on Brearley (2006) and Krot et al. (2006), the ratio of CI is 1.1-1.2, CM is 0.3-0.6 and CR is 0.4-1.1. Thus, water/rock ratio in this experiment (0.13) could be consistent with CV, CO and ordinary chondrites.

Ordinary chondrites originate from S-type asteroids located in the inner region of the asteroid belt inside the snow line. However, some ordinary chondrites show aqueous alteration features. For example, the Semarkona meteorite (LL3.0) has phyllosilicates (Alexander et al. 1989; Piani et al. 2015). The major phyllosilicate phases in Semarkona is smectite, and carbonate is calcium carbonate (Hutchison et al. 1987; Alexander et al. 1989), although proto-phyllosilicate and magnesium carbonate formed in the present study. These differences could be due to the glassy mesostases in Semarkona (Hutchison et al. 1987). The glassy mesostases are highly susceptible to hydration compared with crystalline olivine (Dobrica and Brearley 2020). The total amount of water generated from organic matter could be much less than that present in aqueously altered carbonaceous chondrite parent bodies. The Semarkona parent body could have heterogeneous textures with variable porosity (Dobrica and Brearley 2020), and thus water could move through the grain boundaries, while the alteration condition in present experiment was static with only one mineral (olivine) in a closed system. Thus, in the case of Semarkona, the small amount of water generated from organic matter could contribute to dissolution of glassy mesostases and some metal ions from the other minerals to form smectite and calcium carbonate (Hutchison et al. 1987), preceding the dissolution of olivine.

Water abundance in the bulk Semarkona was estimated as 0.2-0.7 wt.% (Alexander et al. 2010). Assuming that primordial organic matter accumulated in the Semarkona parent body was similar to the organic mixture used in this study, at least 8.0-28.0 wt.% of organic matter have to initially present in the parent body necessary for producing the amount of water in Semarkona, since the water produced from the organic mixture was 2.5 wt.%. Organic carbon in the bulk Semarkona meteorite as insoluble organic matter is 0.36 wt.% (Alexander et al. 2007), thus if the water was delivered from organics, some of organic matter should have been lost through subsequent thermal processes. Some thermally metamorphosed chondrites classified in CV and CO chondrites with alteration features could have captured water near, or in some case inside, the snow line (Marrocchi et al. 2018), thus the role of organic matter to generate water to produce hydrated silicates would be minor. The water generated from organic matter could significantly contribute to alteration of anhydrous minerals, only in case of the accretion inside the snow line.

Results in the present study indicate that the hydration of anhydrous silicate was possible in their parent bodies with organic matter at least locally, even if water ice did not accumulate on them. However, there could be some differences in conditions between parent bodies and the experiment—such as mineral compositions and static/flow of water, and thus further studies are needed to evaluate

the details of such alteration processes. The results further implied that organic matter was one of the possible sources of deuterium-rich water in ordinary chondrites. For example, water in CM chondrites are homogeneously D-poor (Alexander et al. 2012). The water could have originated from isotopic re-equilibration in the inner disk between gaseous H_2O and the D-depleted solar H_2 (Jacquet and Robert 2013). In contrast to these, the D/H ratios of water in ordinary chondrites are highly heterogeneous (Alexander et al. 2017). Some of them show significantly high D/H ratios, similar to some comets (Piani et al. 2015). The existence of D-rich water in ordinary chondrites was explained by an oxidation reaction of Fe metal ($3Fe + 4H_2O = Fe_3O_4 + 4H_2$; Alexander et al. 2010, 2017). Loss of isotopically light H_2 gas would have enriched the residual water in deuterium (Alexander et al. 2017). Piani et al. (2015), however, pointed out that the process would have required a large amount of initial water and a significant amount of oxidation reactions to explain the high D/H values. Their suggestion was that the D-rich water could originate from isotopically heterogeneous ice inherited from the interstellar ice (Piani et al. 2015). Alternatively, Remusat et al. (2016) suggested that the D-rich, recalcitrant organic matter in some ordinary chondrites, could be interstellar origin. In addition to these hypotheses, Nakano et al. (2020) suggested that precometary organic matter could be another water source in ordinary chondrite parent bodies. High deuterium concentration in organic matter is well known in the interstellar medium (ISM) and the outer region of the Solar System (Owen et al. 1986; Mauersberger et al. 1988; Cecilia 2002; Parise et al. 2004). These organic molecules could be enriched in deuterium by ion-molecular reaction (Millar 2003) in the gas phase and/or by grain surface reactions in molecular clouds (Parise et al. 2004; Watanabe and Kouchi, 2008; Taquet et al. 2012). Based on a study of carbon rich clast in Antarctic CR2 chondrite LaPaz Icefield (LAP) 02342, transportation of organic matter and ice in outer solar system could occur into CR chondrite region during the formation of the planetesimals (Nittler et al. 2019). Thus, some organic matter could survive the inner region of the solar nebula (Walsh et al. 2014). Although deuterium tends to concentrate on methyl or ethyl group more than on hydroxy groups in alcohols in molecular clouds (Nagaoka et al. 2005; Oba et al. 2016), deuterated molecules such as CH_3OD were confirmed in ISM (Mauersberger et al. 1988). Thus, both D-poor and D-rich water could be generated from hydroxy groups in organic matter, and such water could then contribute to both D-rich and D-poor hydrated minerals, as well as explain the heterogeneous D/H distribution in ordinary chondrites. Further studies are needed to understand the D/H fractionation between organic matter and phyllosilicates. Organic matter in ordinary chondrites is generally ^{15}N-poor as compared with ^{15}N-rich organic matter in the outer Solar System. However, nitrogen abundances in ordinary chondrites are small, and ^{15}N-rich organic matter may be preferentially removed during thermal metamorphism (Alexander et al. 1998).

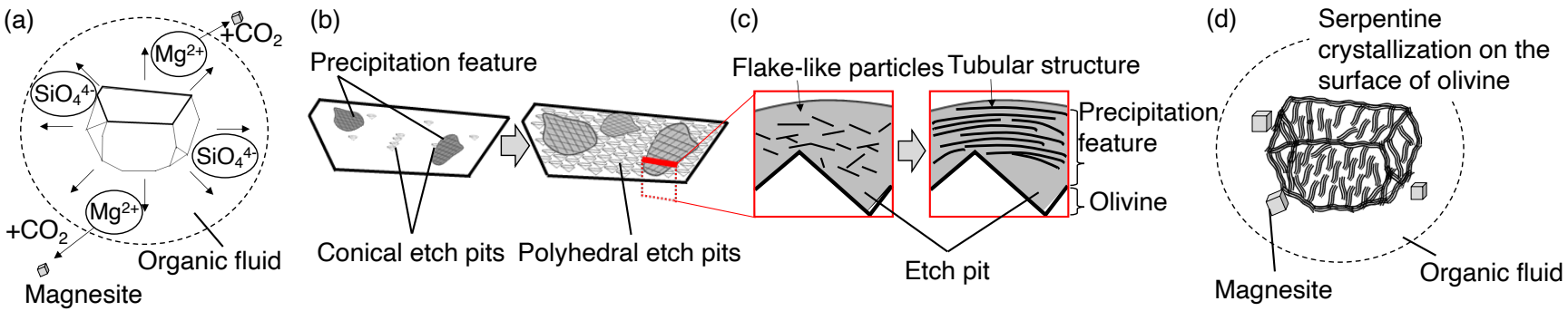

Figure 3-9. Schematic image of serpentine formation on the olivine surface. (a) Dissolution of olivine into the organic fluid. Magnesite formation also proceeded. (b) Precipitation features cover the olivine surface. Etch pits evolved with the dissolution progress. These features were confirmed using SEM. (c) Flake-like particles evolved to a tubular structure, from amorphous to crystalline, in the precipitation features. These features were confirmed using TEM. (d) Growth of crystalline serpentine on the olivine surface.

3.5. Conclusions

To investigate the possible hydration of anhydrous silicates by organic matter in meteorite parent bodies, a heating experiment using olivine with precometary organic matter analog was performed. In situ formation of proto-phyllosilicate was confirmed on the surface of reacted olivine. This result could imply that organic-induced alteration of silicates was a possible reaction process in “dry” meteorite parent bodies that accreted inside the H_2O snow line with delivery of organic compounds with hydroxyl groups and without water ice onto them, although additional works will be needed to evaluate different conditions in the future. Alteration characteristics in some ordinary chondrites could be partially derived from these processes. In that case, significantly heterogeneous D/H distribution and highly D-rich water in ordinary chondrites could also explained by the production of water from D-rich organic matter.

4. Synthesis of Fe-bearing olivine for experiments simulating extraterrestrial conditions.

4.1. Introduction

Olivine is one of the most abundant Earth forming minerals. Many parts of the rocks in upper mantle are considered to be formed from forsterite (Anderson 1970). In case of natural olivine, there are several obtainable samples with high Mg/Fe ratios, for example, forsterite number (Fo# = 100 × Mg/(Mg + Fe)) of natural olivine from San Carlos in Arizona, USA, from Kamuikotan Zone in Hokkaido, Japan and from Sado Island in Niigata prefecture, Japan show Fo89.2-91.1 (Fourrnelle 2011), Fo85-87 (Niida 1977) and Fo79-89 (Yokoyama et al. 1992), respectively. On the other hand, natural obtainable fayalitic olivine sample from northern Newfoundland-Labrador in Canada show Fo6-13 (Wheeler 1965).

Olivine is also abundant in a number of meteorites and other extraterrestrial materials. The natural olivine samples obtained on Earth have been utilized for experiments simulating some extraterrestrial conditions (e.g. Sekine et al. 2015; Vacher et al. 2019; Giese et al. 2019). However, meteoritical olivine usually show more various Mg/Fe ratios (Menzies et al. 2005; Howard et al. 2010, 2014; Lercorre et al. 2015) compared with Earth samples. Since Fe ions in olivine could be significant indicator of alteration and metamorphism of them (Tomeoka et al. 1989), use of olivine with various Mg/Fe ratios is necessary for the experiments simulating extraterrestrial conditions. Such experimental approaches could, for example, reveal the alteration processes in-situ based on the Mg/Fe ratios. Some experimental studies have been prepared artificial olivine with aimed Fo# (e.g. Takatori et al. 1993; Isobe and Yoshizawa 2014) through synthesizing methods.

Synthetic experiments of olivine have been conducted with various methods (Brindley and Hayami 1965; Mitchell et al. 1998; Ando et al. 2007; Ni et al. 2007; Tsubokawa and Ishikawa 2017; Wang et al. 2017). The solid state reaction has been generally conducted for the synthesis of forsterite (Mg_2SiO_4) crystal using MgO and SiO_2 powder for a long time (e.g. Brindley and Hayami 1965). Comparing with the synthesis of forsterite single crystals, synthesis of iron-bearing olivine could be more complex, since there are several parameters which control the generation of olivine crystal such as oxygen fugacity, growth rate, time and temperature (Ito et al. 2003). Hanson et al. (1991) synthesized a Fe-bearing olivine single crystal by a floating-zone method at 1100 °C in 2-5 h, although the method demanded an olivine seed crystal. Nash et al. (2016) recovered Fo#70 polycrystalline olivine capsules in a gas-mixing furnace starting with analytical grade SiO_2, MgO and Fe_2O_3 reagent mixture at 800-1350 °C in 30 minutes with f_{O2} of quartz-fayalite-magnetite (QFM) -1 log units, which was a little redox state compared with QFM buffer, they found that Fe-rich olivine does not demand a

long sintering duration.

Solidus temperature and <24 h heating duration with f_{O2} of QFM-1 log units could be adequate for the preparation of Fe-rich olivine based on Nash et al. (2016). Temperature and the heating duration could be significant parameters to obtain aimed mineral. For the future experiments, it is significant to know the suitable conditions in the present system and to know what phenomena occur during the heating. Synthesizing experiments of Fe-bearing olivine (Fo60) to prepare for the simulating experiments of meteorite parent bodies were performed with various near-solidus line temperatures (1350 °C, 1450 °C and 1500 °C) and two heating durations (1.5 h and 15 h). The manufactured products were analyzed using X-ray diffraction (XRD) and secondary electron microscopy with energy-dispersive X-ray spectroscopy (SEM/EDS) to investigate the phenomena during heating and to evaluate whether the product could be available for future experiments.

4.2. Experiment

4.2.1. Synthetic method

Olivine was synthesized by sintering chemical reagents in a electronic furnace maintaining at solidus temperature. Desired olivine composition (Fo60) was prepared by mixing analytical grade SiO_2 (99.9 %, Wako chemicals Ltd., Japan), MgO (98.0 %, Wako chemicals Ltd., Japan) and Fe_2O_3 (99.9 %, Wako chemicals Ltd., Japan) (1.0: 1.3: 0.4 in molar ratio) reagent powders using an agate mortar, excessive MgO was added following the procedure in Arai and Nagai (1963). The chemical mixture was pressed into pellets of approximately 10 mm diameter and 4 mm thickness at 20 MPa, only pellets for heating at 1500 °C for 15 h were prepared by pressing at 40 MPa, for 3 minutes. The pellets were placed in a Pt-Rh crucible and heated in a electronic furnace under 1 atm at the oxygen fugacity of -log unit below the QFM buffer regulated by a H_2-CO_2 gas mixture (Canil 1997). The pellets were initially placed in the furnace at 1000 °C, then the temperature was increased to an intended temperature (1350, 1450 and 1500 °C) at the rate of 3 °C/min. After maintaining the temperature for 1.5 h or 15 h, samples were recovered to the outside of the furnace and quenched to room temperature. Hereafter each sample is called with the maintained temperature and the heating duration such as “pellets-1500-1.5”. In this study, olivine was synthesized by controlling the heating temperature and duration under the constant oxygen fugacity of QFM-1 log units.

4.2.2. Characterization techniques

4.2.2.1. X-ray diffraction

One pellet of synthesized olivine was grinded to analyze by powder X-ray diffraction (XRD) using a SmartLab diffractometer, with a Hypix-3000 detector (Rigaku, Ltd., Japan) at 40 kV and 45 mA, by Cu Kα radiation, with a scan speed of 5.0 °/min and a resolution of 0.01. Identification of mineral

phase was performed using the SmartLab Studio II by searching the diffraction patterns from ICDD card data through the Hanawalt search method.

4.2.2.2. Scanning electron microscopy with energy dispersive X-ray spectroscopy

Before analysis of chemical composition of each pellet, the surface was polished by diamond powder to obtain the flat surface. The elemental compositions of the synthesized olivine were characterized using a scanning electron microscopy (SEM; JSM-6510LA; JEOL) equipped with an energy dispersive X-ray spectroscopy (EDS; JED2300; JEOL). The sample pellets were fixed on 10-mm brass stub using a carbon tape and were coated by Au spattering. Samples were observed by secondary electron imaging at 15 kV. An elemental analysis was conducted at 20 kV using EDS.

4.3. Results

4.3.1. XRD

Different temperature experiments (1350, 1450 and 1500 °C) were performed with maintaining the temperature for 1.5 h. While the pellets-1500-1.5 showed completely crystalline olivine, strong peaks of quartz and magnesium oxide existed in the XRD pattern of pelletes-1350-1.5 and pellets-1450-1.5 (Figure 4-1a). The relative intensities of quartz and magnesium oxide to the other peaks in pellets-1450-1.5 were weaker than in pellets-1350-1.5. Both quartz and magnesium oxides were initial compounds in the starting chemical mixture, thus unreacted materials could be left in these lower temperature experiments.

To investigate the ratio of Mg and Fe in the synthesized olivine, (130) lattice spacings (d_{130}) of olivine in the pellets were compared based on each XRD pattern. The d_{130} of olivine in pellets-1500-1.5 was 2.879 Å, in pellets-1450-1.5 was 2.790 Å and in pellets-1350-1.5 was 2.773 Å (Figure 4-1b). Based on the Vegard's law, width of the d_{130} linearly changes depending on the chemical compositions of the solid solution. The calculated Fo# of them were 64.5, 61.9 and 88.5, respectively (Yonder and Sahama 1957). Fo60 olivine could be formed at 1500 °C and 1450 °C for 1.5 h, however unreacted materials were left in pellets-1450-1.5. Thus, the sintering condition of pellets-1500-1.5 was the most appropriate for synthesizing the aimed olivine in bulk in this study. The pattern of San Carlos olivine (Fo90.1) was additionally analyzed and also showed in Figure 4-1a and b.

Peaks of magnetite and pyroxene appeared in both pellets-1450-15 and pellets-1500-15 (Figure 4-1a). The other peaks in these pellets were only olivine. Pellets-1500-1.5 contained only olivine, thus at least magnetite and pyroxene in pellets-1500-15 could be formed during 1.5-15 h heating after forming of olivine.

The d_{130} of olivine in pellets-1500-15 and in pellets-1450-15 were 2.768 Å and 2.770 Å (Figure 4-1b). The calculated Fo# of them based on Yonder and Sahama (1957) were 97.7 and 93.8. Thus, the forsterite number of synthesized olivine at 1500 °C or 1450 °C for 1.5 h could become less in iron

during 15 h at these temperatures.

The crystallinity of olivine can be evaluated by the height and narrowness of peaks in X-ray diffraction patterns. In order to compare the degree of crystallinity of each synthesized olivine, full width at half maxima (FWHM) of (021) and (130) reflections were obtained (Figure 4-2) based on Nakato et al. (2008). With increase of temperature and time, both peaks became higher and narrower. Thus, both heating temperature and time depended on the crystallinity of synthesized olivine. The crystallinity of pellets-1450 °C-15 h was higher than pellets-1450-1.5, although the crystallinity of pellets-1500-1.5 and pellets-1500-1.5 were the same degree. The crystallinity of pellets-1500-1.5 and pellets-1500-15 were also the same degree as the crystallinity of natural San Carlos olivine.

4.3.2. SEM/EDS

The surface of pellets-1500-1.5 was porous (Figure 4-3). Grain boundaries were sintered each other. The EDS mapping (Figure 4-3) showed homogeneous distribution of Mg, Al, Si, Fe and O in the analyzed area. Some points showed Fe-rich composition and they were not the olivine. Unreacted Fe_2O_3 from the initial mixture or formation of magnetite during the experiments could be the points. Fe-rich points were also appeared in the ternary diagram (Figure 4-4). Fo64.5 of olivine in the pellets-1500-1.5 was slightly higher value than aimed value (Fo60), which could be due to such unreacted or formation of iron-oxides. However, the XRD pattern did not show such iron-rich minerals in the pellet. Thus, these iron-rich points could be minor inclusions in the pellets.

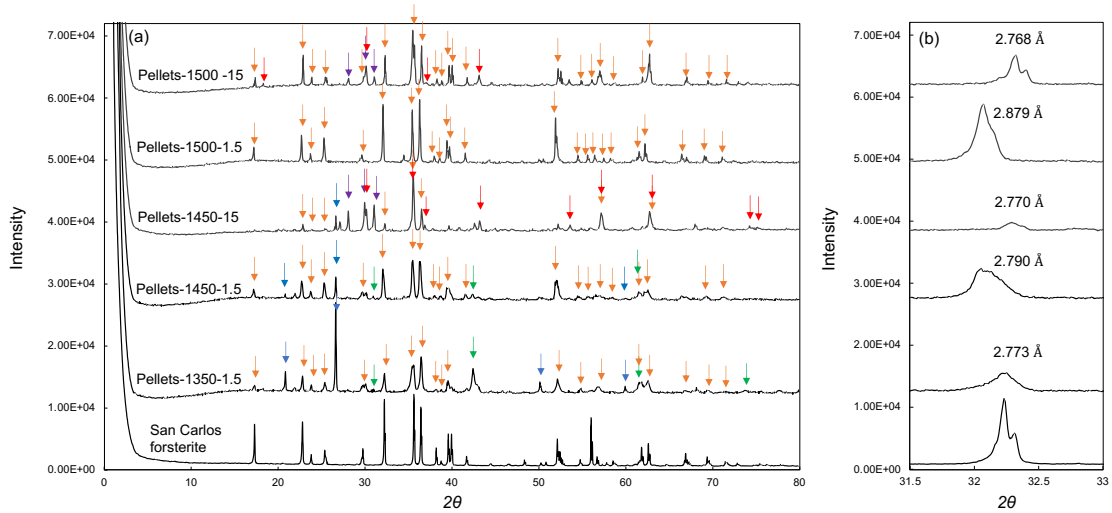

Figure 4-1. (a) XRD patterns of pelets-1500-1.5, pellets-1500-15, pelletes-1450-1.5, pellets-1450-15, pellets-1350-1.5 and San Carlos olivine. (b) XRD patterns of them between 31.5 °-33.0 ° with the apace of $d_{(130)}$. Attribution of minerals was indicated with arrows, orange: olivine, blue: quartz (SiO_2), green: periclase (MgO), purple: pyroxene and red: magnetite.

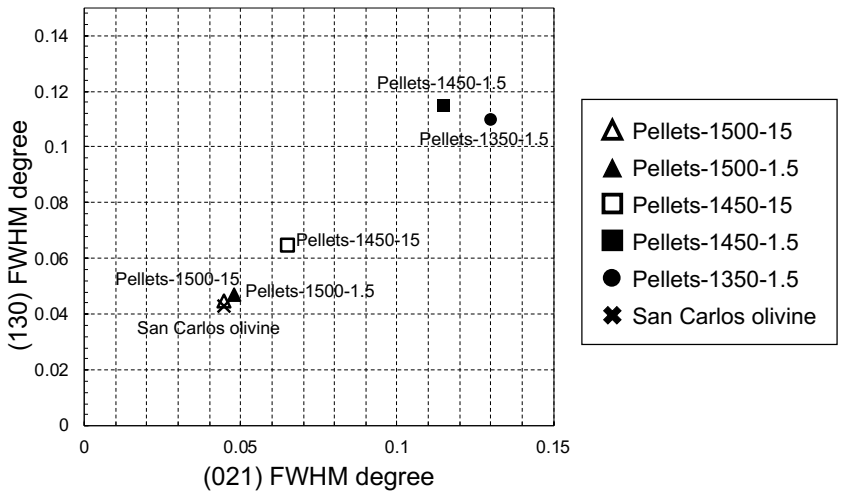

Figure 4-2 Comparison of crystallinity of each pellet based on FWHM (Full Width at Half Maximum) of (021) and (130) reflections determined from X-ray diffraction patterns (Figure 4-1).

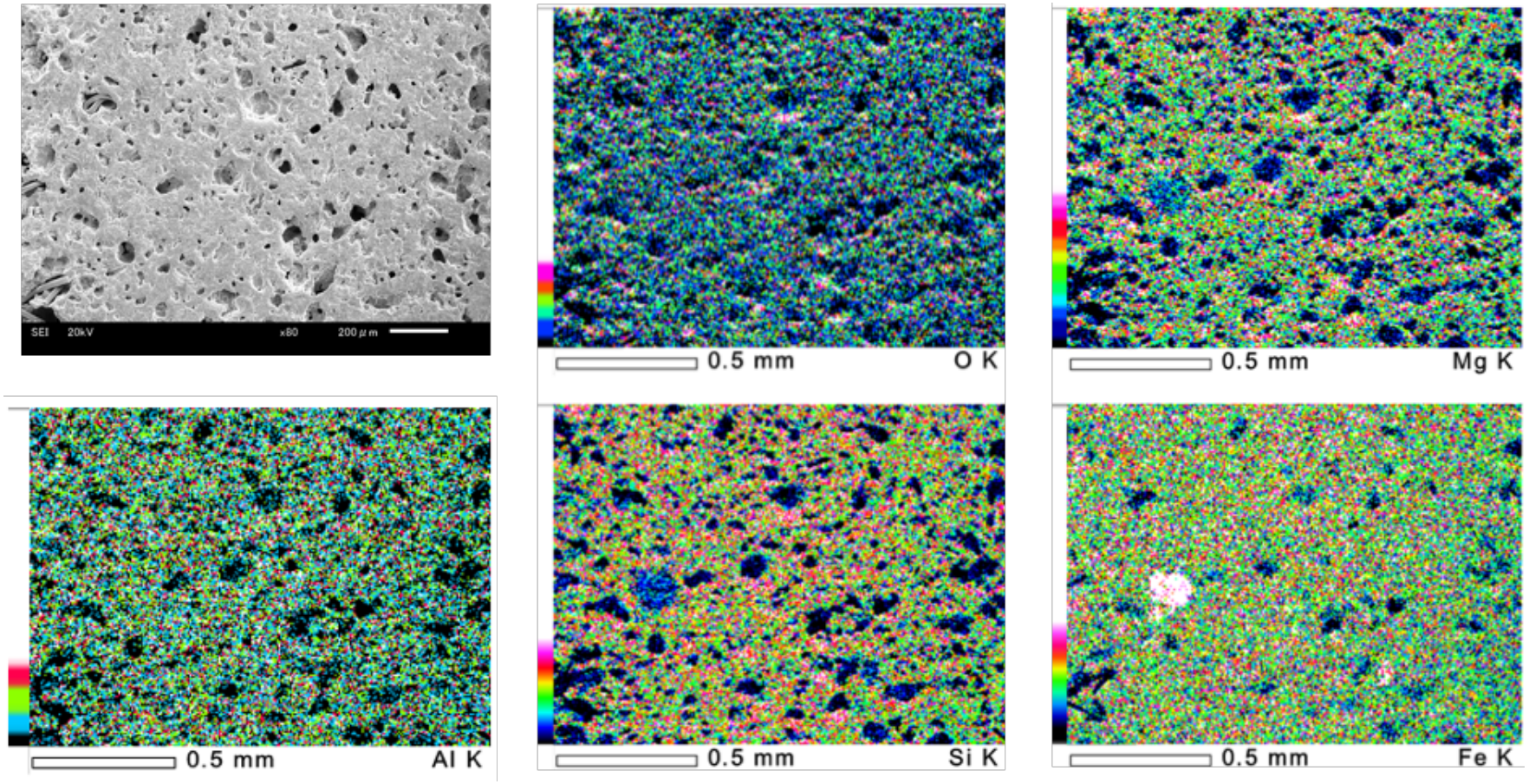

Figure 4-3. Elemental mappings (O, Mg, Al, Si and Fe) of observed area on pellets-1500-1.5.

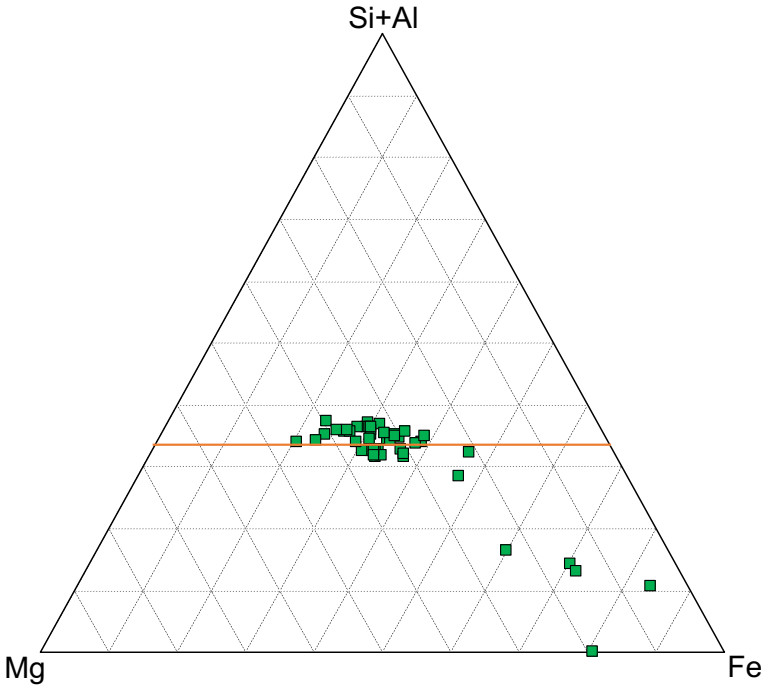

Figure 4-4. A ternary diagram (Si+Al-Mg-Fe) of the analyzed points on pellets-1500-1.5. Solid squares were the composition of analyzed points. The ideal composition of olivine could be on the orange line in the diagram.

4.4. Discussion

In this study, Fo64.5 olivine was synthesized in heating near solidus line temperature (1500 °C) for short time (1.5 h). The crystallinity of the olivine was the same degree as the natural olivine. However, it included small amount of Fe-oxide.

4.4.1. Formation of Fe-bearing olivine

The melting points of SiO_2, MgO and Fe_2O_3 were 1710 °C, 2852 °C and 1565 °C respectively. Thus, the formation reaction of olivine was initially proceeded under sub-solidus conditions by solid-solid reaction under each temperature (1350 °C, 1450 °C and 1500 °C). Fo60 olivine demands Fe^{2+}, thus reduction of Fe^{3+} in Fe_2O_3 to Fe^{2+} could have occurred at high temperature (1450 °C and 1500 °C), then the Fe^{2+} ion could be captured in olivine sites. Mg/Fe ratios of the olivine in the pellets-1350-1.5 showed higher value (Fo88.5) than olivine in 1450 °C (Fo61.9) and 1500 °C (Fo64.5). Higher temperature could be more efficient for reduction of Fe_2O_3 (Chen et al. 2020), thus 1350 °C for 1.5 h was insufficient condition for the reduction of Fe^{3+} to Fe^{2+}.

At 1450 °C, the crystallinity after 15 h was superior to 1.5 h. However, the forsterite number increased from 61.9 to 93.8 accompanied with the formation of pyroxene and magnetite during the heating. At 1500 °C, the crystallinity did not depend on the heating duration, on the other hand the long heating duration lead to the increase of forsterite number (from 64.5 to 97.7) and formation of pyroxene and magnetite. Thus, the best condition for formation of aimed olivine was pellets-1500-1.5 in this experiment.

4.4.2. Oxidation of olivine during heating

High temperature oxidation process of olivine could form the decomposition products such as pyroxene and iron oxides from olivine at approximately 820-1150 °C (Koltermann 1962; Haggerty and Baker (1967); Kohlstedt and Vander Sande 1975; Ashworth and Chambers 2000; Gualtieri et al. 2003; Ejima et al. 2013). Magnetite demands Fe^{3+} ions, however ideal chemical formulae of olivine does not contain Fe^{3+}. Oxidation of olivine can be accomplished by diffusion of electrons and cations without adding oxygen (Ashworth and Chambers 2000) in accordance with:

$$4Fe^{2+}\,SiO_4 \rightarrow 4Fe^{2+}SiO_3 + Fe^{2+}Fe^{3+}{}_2O_4 + 2e^- + Fe^{2+}$$

Olivine Pyroxene Magnetite

thus, oxidation of olivine could contribute to the formation of magnetite.

Additionally, heating temperature in present study was over 1150 °C and near the melting point of Fo60 olivine. Once the olivine was formed, partial melting of olivine could occur. Fe^{2+} ions could concentrate in the partial melt, since the smaller ion, in this case Mg^{2+}, is known to be preferentially

incorporated into the solid lattice rather than the liquid (Goldschimit 1937). Thus, both Fe^{3+} ion by high temperature oxidation process and concentration of Fe^{2+} ions in partial melt could be the source of magnetite during heating for 15 h. Increasing of Mg/Fe ratio in olivine residue from 1.5 h to 15 h heating (Figure 4-1b) should indicate the removal of Fe ions and remaining of Mg ions in residual olivine. Losing Fe ion could also lead to the higher Si composition of the residue, which could, then, form pyroxene.

The same oxidation process of olivine is known as geological phenomena in a lava from some volcano (Ejima et al. 2013; Ueki et al. 2020). The olivine from the lava in Kasayama volcano had Mg-rich core (Fo95-97) and Fe^{3+}-bearing precipitated minerals on the surface (Ejima et al. 2013). Thus, high temperature oxidation of primary synthesized olivine for 15 h accompanied with the partial melting commonly results in the formation of magnetite and pyroxene with Mg-rich relict olivine in nature. To avoid the unnecessary oxidation of formed olivine in this study, maintaining the high temperature for a long time should not be conducted. Formation of olivine at high temperature in short time such as 1500 °C and ~1.5 h could be adequate to obtain approximately Fo60 olivine. Effect of small amount of the impurities in the pellets depends on the precision of the future experiments. The unnecessary magnetite or some iron oxides in pellet-1500-1.5 could be eliminated through magnetic separation (e.g. Buchmann et al. 2018), if highly pure olivine samples are required for some experiments.

4.5. Conclusion

In this study, Fe-rich olivine was synthesized through the heating experiments of the mixture of analytical grade SiO_2, MgO and Fe_2O_3 reagents. To obtain the Fo60 olivine, temperature (1350 °C-1500 °C) and heating duration (1.5 h or 15 h) were controlled under constant oxygen fugacity of QFM-1 log units. As the result, Fo64.5 olivine was obtained by heating near solidus line temperature (1500 °C) for 1.5 h, which could be available for the future experiments simulating extraterrestrial condition. During the heating, olivine could be initially synthesized by solid-solid reaction of each reagent. Fe^{2+} could be supplied from the reduction of Fe_2O_3 at high temperature. However, after maintaining the high temperature for 15 h, initially formed olivine was partially replaced by magnetite and pyroxene. Magnetite demands Fe^{3+}, thus Fe^{2+} in olivine could be, in turn, oxidized to form magnetite. Forsterite number of residual olivine after heating for 15 h was much higher than olivine at 1.5 h, which could support the hypothesis of high temperature oxidation of olivine. Pyroxene could be left as the residue of losing some amount of Fe from olivine.

5. Conclusion remarks

The early stages of our Solar System evolved along a molecular cloud and protoplanetary disk to form the present Solar System. The building blocks of our Solar System was dust particles consisting of mineral core, organic matter and ice mantles. Dusts captured in the protoplanetary disk adhered each other to form planetesimals, the planetesimals collided each other to form various Solar System bodies. Most of the meteorites are originated from asteroids that are often called meteorite parent bodies. Materials accumulated on meteorite parent bodies had been altered and/or metamorphosed by some physicochemical processes, which were recorded in many meteorites. Chondrites, which are one of meteorite groups, are particularly suitable to investigate the evolution of materials in early Solar System, since they could avoid igneous processes in the parent bodies. To understand the evolution of materials through interactions between minerals and organic matter, experiments particularly simulated the conditions in meteorite parent bodies inside a H_2O snow line were performed. Additionally, preparing method of Fe-bearing olivine (Fo60) samples for future experiments was also developed in this study.

In chapter 1, evolution of early Solar System materials was summarized. Some studies have indicated the delivery and survival of some organic matter on grain surface inside H_2O snow line (Nakano et al. 2003; Herbst and van Dishoeck 2009; Welsh et al. 2014; Gail and Trieloff 2017). These grains with organic mantle, but without H_2O ice, could have had significant influences for formation of rocky planetesimals due to their sticky nature (Kudo et al. 2002; Homma et al. 2019). The planetesimals, then, could form rocky parent bodies, which some “dry” chondrites, such as ordinary, CV and CO chondrites, could be originated from. The evolution of organic matter in the meteorite parent bodies has been investigated in various studies (Alexander et al. 2007; Bonal et al. 2006; Busemann et al. 2007; Cody and Alexander 2005; Cody et al. 2008; Homma et al. 2015; Kebukawa et al. 2010b, 2011; Quirico et al. 2003, 2009). In addition to these studies, Nakano et al. (2020) has recently suggested that dehydration of primordial organic matter accumulated on meteorite parent bodies could have become significant water source even in some rocky parent bodies. This fact was also essential for present study, thus the report was summarized in detail. To provide fundamental insights into co-evolution of minerals and organic matter in early Solar System through experiments simulating thermal processes in meteorite parent bodies was aimed as the purpose of this study.

In chapter 2, effects of olivine and montmorillonite on structural changes of organic matter during thermal metamorphism in the meteorite parent bodies were investigated. Heating experiments were performed using an autoclave simulating the co-evolution of organic matter and silicate minerals in the “dry” chondrites’ parent bodies. Primordial organic matter analog was prepared following the procedure of Nakano et al. (2020). The organic matter was heated with silicate minerals in the

autoclave at 25-400 °C for 5 hours, and the experimental products were analyzed in terms of structural changes of organic matter under the co-existence of some minerals. Montmorillonite and olivine, particularly montmorillonite, enhanced decomposition of oxygen containing species due to decarboxylation and/or cracking, while olivine enhanced esterification at lower temperature. The strong degradation effects of montmorillonite could be due to the wide contact surface area and the presence of two acid sites (Lewis acid sites and Brønsted-Lowry acid sites). Olivine, on the other hand, does not have wide contact surface area and not have Brønsted-Lowry acid sites. The results could imply that decreases in O-bearing functional groups in organic matter in chondrites were enhanced by co-existing minerals during thermal processes in CV, CO, and type 3 ordinary chondrite parent bodies, which could induce the structural and compositional variations of insoluble organic matter in those chondrites.

In chapter 3, alteration of anhydrous mineral (olivine) induced by co-existed organic matter was investigated. Effect of organic matter on minerals have not been known well simulating extraterrestrial conditions, thus heating experiments of olivine, which was one of the most abundant minerals in "dry" chondrites, with the presence of the primordial organic matter analog for a long time (10 days) at 300 °C were performed using the autoclave. The morphology and chemical compositions of experimental products were analyzed. The initial olivine grains before the heating experiment with organic matter had smooth surface, but the experimental products showed clear dissolution-precipitation features. Results from X-ray diffraction and transmission electron microscope revealed the formation of secondary minerals such as proto-phyllosilicates and magnesium carbonates on the surface of olivine grains. These newly formed minerals were clearly the evidence of aqueous alteration of olivine induced by organic matter. The water was generated through dehydration of the primordial organic matter analog. The carbonation of olivine could be due to the formation of CO_2 through the decomposition of organic matter. The pH of the formed water was confirmed to be alkaline (pH8-9), then the dissolved CO_2 in the water could be ionized to HCO_3^+ or partially CO_3^{2+}, which could react with Mg^{2+} from olivine. Thus, the results indicated the in-situ formation of hydrated silicates through a mineral-organic interaction without the initial presence of water. It further implies that formation of phyllosilicates on the olivine surface in contact with organic matter can occur in meteorite parent bodies which formed inside the H_2O snow line but accreted with organic matter, initially without water. Water formed through decomposition of organic matter could be one candidate for hydrous silicate formation, for example in ordinary chondrites from S-type asteroids inside the H_2O snow line.

In chapter 4, Fe-bearing olivine (Fo60) was synthesized for future experiments. Meteoritical olivine usually show various Mg/Fe ratios than Earth samples, however only natural San Carlos olivine sample (Fo91) was used for experiments simulating meteorite parent bodies in this study. The olivine was synthesized in an electric furnace under high temperature (1500 °C) for short time (1.5 hours) under the constant oxygen fugacity of QFM-1 log units by solid-solid reaction of analytical grade

chemical reagents (SiO_2, MgO and Fe_2O_3). The effects of temperature and heating duration on the experimental products were particularly evaluated. High temperature synthesis could make the formation of olivine in short time possible, however a long heating duration could, in turn, lead to the high temperature oxidation of olivine.

These studies provide significant aspects of the evolution of primordial mineral-organic matter in the parent bodies during early stages of our Solar System, particularly inside H_2O snow line. When some primordial organic matter accumulated on parent bodies without H_2O molecules, the organic matter could become the potential source of H_2O during thermal metamorphism, then alteration of anhydrous silicate could occur (chapter 3). Other by-products such as CO_2 formed through the decomposition of the organic matter, which the reaction could be enhanced by silicate minerals (chapter 2), possibly contribute to the formation of the other minerals. These relationships between silicate minerals and primordial organic matter possibly contribute to developments of some insights into the co-evolution of minerals and organic matter in meteorite parent bodies. Continuous studies involving the other possible mineral, such as Fe-bearing olivine (chapter 4), and organic matter candidates are required to understand the framework of primordial material evolutions in the early Solar System.

References

Alexander, C.M.O'D., 2017. The origin of inner Solar System water. Phylos. Trans. R. Soc. B-Biol. Sci. A 375: 20150384. http://dx.doi.org/10.1098/rsta.2015.0384

Alexander, C.M.O'D., Barber, D.J., Hutchison, R., 1989. Microstructure of Semarkona and Bishunpur. Geochim. Cosmochim. Acta 53, 3045-3057. https://doi.org/10.1016/0016-7037(89)90180-4

Alexander, C.M.O'D., Bowden, R., Fogel, M.L., 2012. The provenances of asteroids, and their contributions to the volatile inventories of the terrestrial planets. Science 337, 721-726. https://doi.org/10.1126/science.1223474

Alexander, C.M.O'D., Fogel, M., Yabuta, H., Cody, G.D., 2007. The origin and evolution of chondrites recorded in the elemental and isotopic compositions of their macromolecular organic matter. Geochim. Cosmochim. Acta 71, 4380-4403. https://doi.org/10.1016/j.gca.2007.06.052

Alexander, C.M.O'D., Newsome, S.D., Fogel, M.L., Nittler, L.R., Busemann, H., Cody, G.D., 2010. Deuterium enrichments in chondritic macromolecular material-Implications for the origin and evolution of organics, water and asteroids. Geochim. Cosmochim. Acta 74, 4417-4437. https://doi.org/10.1016/j.gca.2010.05.005

Alexander, C.M.O'D., Russell, S.S., Arden, J.W., Ash, R.D., Grady, M.M., Pillinger, C.T., 1998. The origin of chondritic macromolecular organic matter: A carbon and nitrogen isotope study. Meteorit. Planet. Sci. 33, 603-622. https://doi.org/10.1111/j.1945-5100.1998.tb01667.x

Alomon, W., Johns, W., 1975. Petroleum forming reactions: the mechanism and rate of clay catalyzed fatty acid decarboxylation. In: Campos, R., Goñi, J.C, Treibs, A. (eds.), Advances in organic geochemistry, 1975 : proceedings of the 7th International Meeting on Organic Geochemistry, Empresa Nacional Adaro de Investigaciones Mineras, Madrid, pp. 157-171.

Anderson, D. L., 1970. Petrology of the Mantle. Mineral. Soc. Amer. Spec. Pap. 3, 85-93.

Arai, Y., Nagai, S., 1963. Synthesis of Olivine and Acid Solubilities of the Products. Gypsum & Lime, 67, 245-252. https://doi.org/10.11451/mukimate1953.1963.245

Ashworth, J. R., Chambers, A. D., 2000. Symplectic Reaction in Olivine and the Controls of Intergrowth Spacing in Symplectites. J. Petrol. 41, 285-304. https://doi.org/10.1093/petrology/41.2.285

Bardyn, A., Baklouti, D., Cottin, H., Fray, N., Briois, C., Paquette, J., Stenzel, O., Engrand, C., Fischer, H., Hornung, K., Isnard, R., Langevin, Y., Lehto, H., Le Roy, L., Ligier, N., Merouane, S., Modica, P., Orthous-Daunay, F. R., Ryno, J., Schulz, R., Silen, J., Thirkell, L., Varmuza, K., Zaprudin, B., Kissel, J., Hilchenbach, M., 2017. Carbon-rich dust in comet 67P/Churyumov-Gerasimenko measured by COSIMA/*Rosetta*. Mon. Notices Royal Astron. Soc. 469, 712-722. https://doi.org/10.1093/mnras/stx2640

Bischoff, A., 1998. Aqueous alteration of carbonaceous chondrites: Evidence for preaccretionary

alteration-A review. Meteorit. Planet. Sci. 33, 1113-1122. https://doi.org/10.1111/j.1945-5100.1998.tb01716.x

Bisschop, S.E., Jørgensen, J.K., Bourke, T.L., Bottinelli, S., van Dishoeck, E.F., 2008. An interferometric study of the low-mass protostar IRAS 16293-2422: small scale organic chemistry. Astron. Astrophys. 488, 959-968. https://doi.org/10.1051/0004-6361:200809673

Block, K.A., Trusiak A., Katz, A., Alimova, A., Wei, H., Gottlieb, P., Steiner, J.C., 2015. Exfoliation and intercalation of montmorillonite by small peptides. Appl. Clay Sci. 107, 173-181. https://doi.org/10.1016/j.clay.2015.01.021

Bonal, L., Quirico, E., Bourot-Denise, M., Montagnac, G., 2006. Determination of the petrologic type of CV3 chondrites by Raman spectroscopy of included organic matter. Geochim. Cosmochim. Acta 70, 1849-1863. https://doi.org/10.1016/j.gca.2005.12.004

Bonal, L., Bourot-Denise, M., Quirico, E., Montagnac, G., Lewin, E., 2007. Organic matter and metamorphic history of CO chondrites. Geochim. Cosmochim. Acta 71, 1605-1623. https://doi.org/10.1016/j.gca.2006.12.014

Bonal, L., Quirico, E., Flandinet, L., Montagnac, G., 2016. Thermal history of type 3 chondrites from the Antarctic meteorite collection determined by Raman spectroscopy of their polyaromatic carbonaceous matter. Geochim. Cosmochim. Acta 189, 312-337. https://doi.org/10.1016/j.gca.2016.06.017

Brearley, A.J., 2006. The action of water. In: Meteorites and the Early Solar System II (eds. Lauretta, D.S., McSween Jr, H.Y.). University of Arizona Press, Tucson. pp. 587-624.

Brindley, G. W., Hayami, R., 1965. Kinetics and mechanism of formation of forsterite (Mg_2SiO_4) by solid state reaction of MgO and SiO_2. Philosophical Magazine, 12:117, 505-514. https://doi.org/10.1080/14786436508218896

Briggs, R.G., Ertem, G., Ferris, J.P., Greenberg, J.M., Mccain, P.J., Mendoza-Gomez, C. X., Schutte, W., 1992. Comet Halley as an aggregate of interstellar dust and further evidence for the photochemical formation of organics in the interstellar medium. Orig. Life Evol. Biosph. 22, 287-307. https://doi.org/10.1007/BF01810858

Bu, H., Yuan, P., Liu, H., Liu, D., Zhou, X., 2017. Thermal decomposition of long-chain fatty acids and its derivative in the presence of montmorillonite A thermogravimetric (TG/DTG) investigation. J. Therm. Anal. Calorim. 128, 1661-1669. https://doi.org/10.1007/s10973-016-6022-5

Buchmann, M., Schach, E., Tolosana-Delgado, R., Leißner, T., Astoveza, J., Kern, M., Möckel, R., Ebert, D., Rudolph, M., van den Boogaart, K. G., Peuker, U. A., 2018. Evaluation of Magnetic Separation Efficiency on a Cassiterite-Bearing Skarn Ore by Means of Integrative SEM-Based Image and XRF–XRD Data Analysis. Minerals 2018, 8, 390. https://doi.org/10.3390/min8090390

Bunin, I.Z., Chanturiya, V.A., Anashkina, N.E., 2017. Non-thermal effect of high-voltage nanosecond pulses on kimberlite rock-forming minerals processing. In: Advanced Materials (eds. Parinov, I.,

Chang, S.H., Jani, M.) Springer Proceedings in Physics 193, pp. 37-53. https://doi.org/10.1007/978-3-319-56062-5_4

Buseck, P.R., Hua, X., 1993. Matrices of carbonaceous chondrite meteorites. Annu. Rev. Earth Planet. Sci. 21, 255-305. https://doi.org/10.1146/annurev.ea.21.050193.001351

Busemann, H., Alexander, C.M.O'D., Nittler, L.R., 2007. Characterization of insoluble organic matter in primitive meteorites by microRaman spectroscopy. Meteorit. Planet. Sci. 42, 1387-1416. https://doi.org/10.1111/j.1945-5100.2007.tb00581.x

Cai, J.G., Bao Y.J., Yang S.Y., Wang X.X., Fan D.D., Xu J.L., Wang A.P., 2007. Research on preservation and enrichment mechanisms of organic matter in muddy sediment and mudstone. Sci. China Ser. D-Earth Sci. 50, 765-775. https://doi.org/10.1007/s11430-007-0005-0

Cecilia, C., 2002. Millimeter and infrared observations of deuterated molecules. Planet. Space Sci. 50, 1267-1273. https://doi.org/10.1016/S0032-0633(02)00093-4

Chen, Z., Zeilstra, C., van der Stel, J., Sietsma, J., Yang, Y., 2020. Review and data evaluation for high-temperature reduction of iron oxide particles in suspension. Ironmak. Steelmak., 47, 741-747. https://doi.org/10.1080/03019233.2019.1589755

Cody, G.D., Alexander, C.M.O'D., 2005. NMR studies of chemical structural variation of insoluble organic matter from different carbonaceous chondrite groups. Geochim. Cosmochim. Acta 69, 1085-1097. https://doi.org/10.1016/j.gca.2004.08.031

Cody, G.D., Alexander, C.M.O'D., Yabuta, H., Kilcoyne, A.L.D., Araki, T., Ade, H., Dera, P., Fogel, M., Militzer, B., Mysen, B.O., 2008. Organic thermometry for chondritic parent bodies. Earth Planet. Sci. Lett. 272, 446-455. https://doi.org/10.1016/j.epsl.2008.05.008

Cody, G.D., Heying E., Alexander, C.M.O'D., Nittler, L.R., Kilcoyne, A.L.D., Sandford, S.A., Stroud, R.M., 2011. Establishing a Molecular Relationship between Chondritic and Cometary Organic Solids. Proc. Natl. Acad. Sci. U.S.A. 108, 19171-19176. https://doi.org/10.1073/pnas.1015913108

Ciesla, F.J., Lauretta, D.S., Cohen, B.A., Hood, L.L., 2003. A nebular origin for chondritic fine-grained phyllosilicates. Science 299, 549-552. https://doi.org/10.1126/science.1079427

Davis, J.B., Stanley, J.P., 1982. Catalytic effect of smectite clays in hydrocarbon generation revealed by pyrolysis-gas chromatography. J. Anal. Appl. Pyrol. 4, 227–240. https://doi.org/10.1016/0165-2370(82)80033-8

Derenne, S., Robert, F. 2010. Model of Molecular Structure of the Insoluble Organic Matter Isolated from Murchison Meteorite. Meteorit. Planet. Sci. 45, 1461-1475. https://doi.org/10.1111/j.1945-5100.2010.01122.x

Djomgoue, P., Njopwouo, D., 2013. FT-IR spectroscopy applied for surface clays characterization. J. Surf. Eng. Mater. Adv. Tech. 3, 275-282. http://dx.doi.org/10.4236/jsemat.2013.34037

Dobrica, E., Brearley, A.J., 2020. Amorphous silicates in the matrix of Semarkona: The first evidence for the localized preservation of pristine matrix materials in the most unequilibrated ordinary

chondrites. Meteorit. Planet. Sci., 55, 649-668. https://doi.org/10.1111/maps.13458

Doyle, P.M., Jogo, K., Nagashima, K., Krot, A.N., Wakita, S., Ciesla, F.J., Hucheon, I.D., 2015. Early aqueous activity on the ordinary and carbonaceous chondrite parent bodies recorded by fayalite. Nat. Commun. 6, 7444. https://doi.org/10.1038/ncomms8444

Ejima, T., Akasaka, M., Nagao, T., Ohfuji, H., 2013. Oxidation states of Fe and precipitates within olivine from orthopyroxene-olivine-clinopyroxene andesite lava from Kasayama volcano, Hagi, Yamaguchi, Japan. J. Mineral. Petrol. Sci. 108, 25-36. https://doi.org/10.2465/jmps.120621a

Favre, C., Fedele, D., Semenov, D., Parfenov, S., Codella, C., Ceccarelli, C., Bergin, E.A., Chapillon, E., Testi, L., Hersant, F., 2018. First detection of the simplest organic acid in a protoplanetary disk. Astrophys. J. 862, L2-9. https://doi.org/10.3847/2041-8213/aad046

Fuchida, S., Naraoka, H., Masuda, H., 2017. Formation of Diastereoisomeric Piperazine-2,5-dione from DLAlanine in the Presence of Olivine and Water. Orig. Life Evol. Biosph. 43, 83-92. https://doi.org/10.1007/s11084-016-9500-7

Gail, H., Trieloff, M., 2017. Spatial distribution of carbon dust in the early solar nebula and the carbon content of planetesimals. Astron. Astrophys. 606, A16. https://doi.org/10.1051/0004-6361/201730480

Garvie, L.A.J., Buseck, P.R., 2007. Prebiotic carbon in clays from Orgueil and Ivuna (CI), and Tagish Lake (C2 ungrouped) meteorites. Meteorit. Planet. Sci. 42, 2111-2117. https://doi.org/10.1111/j.1945-5100.2007.tb01011.x

Giese, C., Ten Kate, I. L., Plumper, O., KING, H. E., Lenting, C., Liu, Y., Tielens, A. G. G., 2019. The evolution of polycyclic aromatic hydrocarbons under simulated inner asteroid conditions. Meteorit. Planet. Sci. 54, 1930–1950. https://doi.org/10.1111/maps.13359

Goesmann, F., Rosenbauer, H., Bredehöft, J.H., Cabane, M., Ehrenfreund, P., Gautier, T., Giri, C., Krüger, H., Roy, L.L., MacDermott, A.J., McKenna-Lawlor, S., Meierhenrich, U.J., Muñoz Caro, G.M., Raulin, F., Roll, R., Steele, A., Steininger, H., Sternberg, R., Szopa, C., Thiemann, W., Ulamec, S., 2015. Organic compounds on comet 67P/Churyumov-Gerasimenko revealed by COSAC mass spectrometry. Science, 349, 6247. https://doi.org/10.1126/science.aab0689.

Goldschmidt, V. M., The Principles of Distribution of Chemical Elements in Minerals and Rocks. J. Chem. Soc., 655-673. https://doi.org/10.1039/JR9370000655

Grady, M.M., Wright, I.P., Engrand, C., Siljeström, S., 2018. The Rosetta mission and the chemistry of organic species in Comet 67P/Churyumov–Gerasimenko. Elements, 14, 95–100. https://doi.org/10.2138/gselements.14.2.95.

Greenberg, J.M., Mendoza-Gómez, C.X., 1993. Interstellar dust evolution: A reservoir of prebiotic molecules. In: The Chemistry of Life's Origin (eds. Greenberg, J.M., Mendoza-Gómez, C.X., Pirronello, V.). Kluwer Accademic, Boston. pp. 1–32.

Grimm, R.E., Mcsween, H.Y. Jr., 1989. Water and the thermal evolution of carbonaceous chondrite

parent bodies. Icarus 82, 244-280. https://doi.org/10.1016/0019-1035(89)90038-9

Hanson, D. R., Young, M., Ryerson, F. J., 1991. Growth and Characterization of Synthetic Iron-Bearing Olivine. Phys. Chem. Minerals, 18, 53-63. https://doi.org/10.1007/BF00199044

Haresnape, J.N., 1948. The use of montmorillonite catalysts in the cracking of petroleum fractions. Clay Miner. Bull. 1 (2), 59-61. https://doi.org/10.1180/claymin.1948.000.2.07

Hayashi, C., Nakazawa, K., Nakagawa, Y., 1985. Formation of the Solar System. In: Protostars and Planets II (eds. Black, D.C., Matthews, M.S.). University of Arizona Press, Tucson. pp. 1100-1153.

Hayatsu, R., Anders, E., 1981. Organic Compounds in Meteorites and Their Origins. In: Topics in Current Chemistv, Vol. 99 (eds. Boschke, F. L.) Springer-Verlag., pp.l-37.

Heller-Kallai, L., Aizenshtat, Z., Miloslavski, I., 1984. The effect of various clay minerals on the thermal decomposition of stearic acid under 'Bulk Flow' conditions. Clay Miner. 19, 779-788. https://doi.org/10.1180/claymin.1984.019.5.08

Hendricks, S. B., 1941. Base exchange of the clay mineral montmorillonite for organic cations and its dependence upon adsorption due to van der Waals forces. J. Phys. Chem. 45, 65-81. https://doi.org/10.1021/j150406a006

Herbst, E., van Dishoeck, E.F., 2009. Complex organic interstellar molecules. Ann. Rev. Astron. Astrophys. 47, 427-480. https://doi.org/10.1146/annurev-astro-082708-101654

Homma, Y., Kouketsu, Y., Kagi, H., Mikouchi, T., Yabuta, H., 2015. Raman spectroscopic thermometry of carbonaceous material in chondrites: four–band fitting analysis and expansion of lower temperature limit. J. Mineral. Petrol. Sci. 110, 276-282. https://doi.org/10.2465/jmps.150713a

Homma, K.A., Okuzumi, S., Nakamoto, T., Ueda, Y., 2019. Rocky Planetesimal Formation Aided by Organics. Astrophys. J. 877, 128. https://doi.org/10.3847/1538-4357/ab1de0

Howard, K.T., Benedix, G.K., Bkand, P.A., Cressay, G., 2010. Modal mineralogy of CV3 chondrites by X-ray diffraction (PSD-XRD). Geochim. Cosmochim. Acta 74, 5084-5097. https://doi.org/10.1016/j.gca.2010.06.014

Howard, K.T., Alexander, C.M.O'D., Dyl, K.A., 2014. PSD-XRD modal mineralogy of type 3.0 CO chondrites: initial asteroidal water mass fractions and implications for CM chondrites. In: Lunar and Planetary Science Conference XXXXV Abstract #1830.

Huss, G.R., Rubin, E.A., Grossman, J.N., 2006. Thermal metamorphism in chondrites. In: Meteorites and the Early Solar System II (eds. Lauretta, D.S., McSween Jr, H.Y.). University of Arizona Press, Tucson. pp.567-586.

Hutchison, R., Alexander, C.M.O'D., Barber, D.J., 1987. The Semarkona meteorite: First recorded occurrence of smectite in an ordinary chondrite, and its implications. Geochim. Cosmochim. Acta 51, 1875- 1882. https://doi.org/10.1016/0016-7037(87)90178-5

Isobe, H., Yoshizawa, M., 2014. Formation of iron mineral fine particles by acidic hydrothermal

alteration experiments of synthetic martian basalt. Journal of Mineral. Petrol. Sci., 109, 62-73. https://doi.org/10.2465/jmps.121207

Ito, K., Sato, H., Kanazawa, H., Kawame, N., Tamada, O., Miyazaki, K., Uehara, S., Iio, Y., Takei, H., Kitazawa, T., Koike, M., Matsushita, Y., Ito, Y., 2003. First Synthesis of Olivine Single Crystal as Large as 250 Carats. J. Cryst. Growth 253, 557-561. https://doi.org/10.1016/S0022-0248(03)01029-7

Iwakami, Y., Takazono, M., Tsuchiya, T., 1968. Thermal decomposition of hexamethylenetetramine. Bull. Chem. Soc. Jpn. 41, 813-817. https://doi.org/10.1246/bcsj.41.813

Johns, W.D., 1979. Clay mineral catalysis and petroleum generation. Ann. Rev. Earth Planet. Sci. 7, 183-198. https://doi.org/10.1146/annurev.ea.07.050179.001151

Jacquet, E., Robert, F., 2013. Water transport in protoplanetary disks and the hydrogen isotopic composition of Chondrites. Icurus 2, 722-732. https://doi.org/10.1016/j.icarus.2013.01.022

Jerry Shiao, Y.S., Looney, L.W., Remijan, A.J., Snyder, L.E., Friedel, D.N., 2010. First acetic acid survey with CARMA in hot molecular cores. Astrophys. J. 716, 286. https://doi.org/10.1088/0004-637X/716/1/286 Page 14/21

Jørgensen, J.K., Favre, C., Bisschop, S.E., Bourke, T.L., van Dishoeck, E.F., Schmalzl, M., 2012. Detection of the simplest sugar, glycolaldehyde, in a solar-type protostar with ALMA. Astrophys. J. Lett. 757, L4. https://doi.org/10.1088/2041-8205/757/1/L4

Kazakos, A., Komarneni, S., Roy, R., 1990. Preparation and Densification of Forsterite (Mg_2SiO_4) by Nanocomposite Sol-Gel Processing. Matter. Lett. 9: 10, 405-409. https://doi.org/10.1016/0167-577X(90)90075-W

Kebukawa, Y., Alexander, C.M.O'D., Cody, G.D., 2011. Compositional diversity in insoluble organic matter in type 1, 2 and 3 chondrites as detected by infrared spectroscopy. Geochim. Cosmochim. Acta 75, 3530-3541. https://doi.org/10.1016/j.gca.2011.03.037

Kebukawa, Y., Alexander, C.M.O'D., Cody, G.D., 2019b. Comparison of FT-IR spectra of bulk and acid insoluble organic matter in chondritic meteorites: An implication for missing carbon during demineralization. Meteorit. Planet. Sci., 54, 1632-1641. https://doi.org/10.1111/maps.13302

Kebukawa, Y., Kilcoyne, A.L.D., Cody, G.D., 2013. Exploring the Potential Formation of Organic Solids in Chondrites and comets through Polymerization of Interstellar Formaldehyde. Astrophys. J. 771, 19. https://doi.org/10.1088/0004-637X/771/1/19

Kebukawa, Y., Kobayashi, H., Urayama, N., Baden, N., Kondo, M., Zolensky, M.E., Kobayashi, K., 2019a. Nanoscale infrared imaging analysis of carbonaceous chondrites to understand organic-mineral interactions during aqueous alteration. Proc. Natl. Acad. Sci. U.S.A, 116, 753-758. https://doi.org/10.1073/pnas.1816265116

Kebukawa, Y., Nakashima, S., Ishikawa, M., Aizawa, K., Inoue, T., Nakamura-Messenger, K. and Zolensky, M.E., 2010a. Spatial distribution of organic matter in the Bells CM2 chondrite using

near-field infrared microspectroscopy. Meteorit. Planet. Sci. 45, 394-405. https://doi.org/10.1111/j.1945-5100.2010.01030.x

Kebukawa, Y., Nakashima, S., Zolensky, M.E., 2010b. Kinetics of organic matter degradation in the Murchison meteorite for the evaluation of parent-body temperature history. Meteorit. Planet. Sci. 45, 99-113. https://doi.org/10.1111/j.1945-5100.2009.01008.x

King, A.J., Schoeld, P.F., Russell, S.S., 2017. Type 1 aqueous alteration in CM carbonaceous chondrites: Implications for the evolution of water-rich asteroids. Meteorit. Planet. Sci. 52, 1197-1215. https://doi.org/10.1111/maps.12872

Kissel, J., Krueger, F.R., 1987. The organic component in dust from comet Halley as measured by the PUMA mass spectrometer on board Vega 1. Nature 326, 755-760. https://doi.org/10.1038/326755a0

Kitajima, F., Nakamura, T., Takaoka, N., Marue, T., 2002. Evaluating the thermal metamorphism of CM chondrites by using the pyrolytic behavior of carbonaceous macromolecular matter. Geochim. Cosmochim. Acta 66, 163-172. https://doi.org/10.1016/S0016-7037(01)00758-X

Kluger, R., Howe, G.W., Mundle, S.O.C., 2013. Avoiding CO_2 in catalysis of decarboxylation. In: Williams, I.H., Williams, N.H. (eds.), Advances in Physical Organic Chemistry. Academic Press, New York, 47, pp. 85-128. https://doi.org/10.1016/B978-0-12-407754-6.00002-8

Kohlstedtand, D. L., Vander Sande, J. B., 1975. An Electron Microscopy Study of Naturally Occurring Oxidation ProducedPrecipitates in Iron-Bearing Olivines. Contrib. Mineral. Petrol., 53, 13-24. https://doi.org/10.1007/BF00402451

Kouchi, A., Kudo, T., Nakano, H., Arakawa, M., Watanabe, N., Sirono, S., Higa, M., Maeno, N., 2002. Rapid growth of asteroids owing to very sticky interstellar organic grains. Astrophys. J. 566, 121-124. https://doi.org/10.1086/339618

Kracher, A., Keil, K., Kallemeyn, G.W., Wasson, J.T., Clayton, R.N., Huss, G.I., 1985. The Leoville (CV 3) accrecionary breccia. J. Geochem. Res. 90, 123-135. https://doi.org/10.1029/JB090iS01p00123Lancee, R.J., 2014. Characterization and reactivity of olivine and model catalysts for biomass gasification. Ph. D. thesis, Technische Universiteit Eindhoven, https://doi.org/10.6100/IR781405.

Krot, A.N., Keil, K., Scott, E.R.D., Goodrich, C.A., Weisberg, M.K., 2014. Classification of Meteorites and Their Genetic Relationships. In: Treatise on Geochemistry Second Edition Volume 1 (eds. Davis, A.M.) Elsevier Ltd. pp.1-63

Kudo, T., Kouchi, A., Arakawa, M., Nakano, H., 2002. The role of sticky interstellar organic material in the formation of asteroids. Meteorit. Planet. Sci. 37, 1975-1983. https://doi.org/10.1111/j.1945-5100.2002.tb01178.x

Laine, M., Balan, E., Allard, T., Paineau, E., Jeunesse, P., Mostafavi, M.J.-L., Le, S. 2016. Reaction mechanisms in swelling clays under ionizing radiation: influence of the water amount and of the

nature of the clay. RSC Adv. 7, 526-534. https://doi.org/10.1039/C6RA24861F

Lafay, R., Montes-Hernandez, G., Janots, E., Chiriac, R., Findling, N., Toche, F., 2012. Mineral replacement rate of olivine by chrysotile and brucite under high alkaline conditions. J. Cryst. Growth 347, 62-72. https://doi.org/10.1016/j.jcrysgro.2012.02.040

Lafey, R., Montes-Hernandez, G., Janots, E., Chiriac, R., Findling, N., Toche, F., 2014. Simultaneous precipitation of magnesite and lizardite from hydrothermal alteration of olivine under high-carbonate alkalinity. Chem. Geol. 368, 63-75. https://doi.org/10.1016/j.chemgeo.2014.01.008

Lafey, R., Fernandez-Martinez, J., Montes-Hernandez, G., Auzende, A.L., Poulain, A., 2016 Dissolutionreprecipitation and self-assembly of serpentine nanoparticles preceding chrysotile formation: Insights into the structure of proto-serpentine. Am. Mineral. 101, 2666-2676. https://doi.org/10.2138/am-2016- 5772

Le Corre, L., Reddy, V., Sanchez, J. A., Dunn, T., Cloutis, E. A., Izawa, M. R. M., Mann, P., Nathues, A., 2015. Exploring exogenic sources for the olivine on Asteroid (4) Vesta. Icarus, 258, 483-499. https://doi.org/10.1016/j.icarus.2015.01.018

Le Guillou, C., Bernard, S., Brearley, A.J., Remusat, L. 2014. Evolution of organic matter in Argueil, Murchicson and Renazzo during parent body aqueous alteration: *In situ* investigation. Geochim. Cosmochim. Acta 131, 368-392. https://doi.org/10.1016/j.gca.2013.11.020

Liu, H., Yuan, P., Qin, Z., Liu, D., Tan, D., Zhu, J., He, H., 2013. Thermal degradation of organic matter in the interlayer clay–organic complex: a TG-FTIR study on a montmorillonite/12-aminolauric acid system. Appl. Clay Sci. 80, 398-406. https://doi.org/10.1016/j.clay.2013.07.005

Lisabeth, H., Zhu, W., Xing, T., De Andrade, V., 2017. Dissolution-assisted pattern formation during olivine carbonation. Geophys. Res. Lett. 44, 9622-9631. https://doi.org/10.1002/2017GL074393

Luce, R.W., Bartlett, R.W., Parks, G.A., 1972. Dissolution kinetics of magnesium silicates. Geochim. Cosmochim. Acta 36, 35-50. https://ui.adsabs.harvard.edu/abs/1972GeCoA..36...35L/abstract

Maina, E.W., Wanyika, H.J., Gacanja, A.N., 2015. Instrumental characterization of montmorillonite clay by FT-IR and XRD from J.K.U.A.T farm, in the republic of Kenya. Chem. Mater. Res. 7, 43-49.

Malvoisin, B., Brunet, F., Carlut, J., Rouméjon, S., Cannat, M., 2012. Serpentinization of oceanic peridotites: 2. Kinetics and processes of San Carlos olivine hydrothermal alteration. J. Geophys. Res. Solid Earth 117: B04102. https://doi.org/10.1029/2011JB008842

Marrocchi, Y., Bekaert, D.V., Piani, L., 2018. Origin and abundance of water in carbonaceous asteroids. Earth Planet. Sci. Lett. 482, 23-32. https://doi.org/10.1016/j.epsl.2017.10.060 Page 15/21

Mauersberger, R., Henkel, C., Jacq, T., Walmsley, C.M., 1988. Deuterated methanol in Orion. Astron. Astrophys. 194, L1-4.

McAdam, M.M., Sunshine, J.M., Howard, K.T., Alexander, C.M.O'D., McCoy, T.J., Bus, S.J., 2018. Spectral evidence for amorphous silicates in least-processed CO meteorites and their parent bodies.

Icarus 306, 32-49. https://doi.org/10.1016/j.icarus.2018.01.024

Mendoza-Gómez, C.X., Greenberg, J.M., 1993. Laboratory simulation of organic grain mantles. Orig. Life Evol. Biospheres 23, 23–28. https://doi.org/10.1007/BF01581987

Mitchell, M. B. D., Jackson, D., James, P. F., 1998. Preparation and characterisation of forsterite (Mg_2SiO_4) aerogels. J. Non-Cryst. Solids, 225, 125–129. https://doi.org/10.1016/S0022-3093(98)00017-9

Michels, L., Fossum, J.O., Rozynek, Z., Hemmen, H., Rustenberg, K., Sobas, P.A., Kalantzopoulos, G.N., Knudsen, K.D., Janek, M., Plivelic, T.S., da Silva, G.J., 2015. Intercalation and retention of carbon dioxide in a smectite clay promoted by interlayer cations. Sci. Rep. 5, 8775. https://doi.org/10.1038/srep08775

Millar, T.J., 2003. Deuterium Fractionation in Interstellar Clouds. Space Sci. Rev. 106, 73. https://doi.org/10.1023/A:1024677318645

Moore, D.E., Rymer, M.J., 2007. Talc-bearing serpentinite and the creeping section of the San Andreas fault. Nature 448, 795-797. https://doi.org/10.1038/nature06064

Milliken, T.H., Oblad, A.G., Mills, G.A., 1952. Use of clays as petroleum cracking catalyst. Clays and Clay Technology, Proc. of the First National Conference on Clays and Clay Technology. Dep. of National Resources, State of California Bull. 169, 314-326. https://ui.adsabs.harvard.edu/link_gateway/1952CCM.....1..314M/doi:10.1346/CCMN.1952.0010127

Mumma, M.J., Charnley, S.B., 2011. The chemical composition of comets—emerging taxonomies and natal heritage. Annu. Rev. Astron. Astrophys., 49, 471-524. https://doi.org/10.1146/annurev-astro-081309-130811.

Nagahara, H., Ozawa, K., 2011. Phyllosilicate formation and its role on the formation of organic materials in the early solar nebula. In: Lunar and Planetary Science Conference XXXXII Abstract #2838.

Nagaoka, A., Watanabe, N., Kouchi, A., 2005. H-D substitution in interstellar solid methanol: A key route for D enrichment. Astrophys. J. 624, L29-32. https://doi.org/10.1086/430304

Nakamura, T., 2005. Post-hydration thermal metamorphism of carbonaceous chondrites. J. Miner. Petrol. Sci. 100, 260-272. https://doi.org/10.2465/jmps.100.260

Nakano, H., Kouchi, A., Arakawa, M., Kimura, Y., Kaito, C., Ohno, H., Hondoh, T., 2002. Alteration of interstellar organic materials in meteorites' parent bodies: a novel route for diamond formation. Proc. Jpn. Acad., Ser. B 78, 277-281. https://doi.org/10.2183/pjab.78.277

Nakano, H., Kouchi, A., Tachibana, S., Tsuchiyama, A., 2003. Evaporation of interstellar organic materials in the solar nebula. Astrophys. J. 592, 1252-1262. https://doi.org/10.1086/375856

Nakano, H., Hirakawa, N., Matsubara, Y., Yamashita, S., Okuchi, T., Asahina, K., Tanaka, R., Suzuki, N., Naraoka, H., Takano, Y., Tachibana, S., Hama, T., Oba, Y., Kimura, Y., Watanabe, N., Kouchi,

A., 2020. Interstellar organic matter: A hidden reservoir of water inside the snow line. Si. Rep. 10, 7755. https://doi.org/10.1038/s41598-020-64815-6

Nakato, A., Nakamura, T., Kitajima, F., Noguchi, T., 2008. Evaluation of dehydration mechanism during heating of hydrous asteroids based on mineralogical and chemical analysis of naturally and experimentally heated CM chondrites. Earth Planet. Sci. 60, 855-864. https://doi.org/10.1186/BF03352837

Naraoka, H., Shimoyama, A., Harada, K., 2000. Isotopic evidence from an Antarctic carbonaceous chondrite for two reaction pathways of extraterrestrial PAH formation. Earth Planet. Sci. Lett. 184, 1-7. https://doi.org/10.1016/S0012-821X(00)00316-2.

Naraoka, H., Yamashita, Y., Koga, T., Ishibashi, Y., Mita, H., 2015. Meteoritic organic matter synthesis inferred from aldehydes and ammonia with olivine. In: Astrobiology Science Conference 2015 Abstract #7146.

Nash, W., Smythe, D., Wood, B. J., 2016. Synthetic olivine capsules for use in experiments. Am. Mineral., 101, 2260–2263. https://doi.org/10.2138/am-2016-5549CCBY

Ni, S., Chou, L., Chang, J., 2007. Preparation and characterization of forsterite (Mg_2SiO_4) bioceramics. Ceram. Int., 33, 83-88. https://doi.org/10.1016/j.ceramint.2005.07.021

Niida, K., 1977. Olivine Clinopyroxenite in Serpentinized Dunite - Harzburgite Masses of the Kamuikotan Zone, Hokkaido. J. Fac. Sci., Hokkaido Univ., Ser. IV, 17, 517-525.

Nuth III, J.A., Johnson, N.M., Manning, S., 2008. A Self-Perpetuating Catalyst for the Production of Complex Organic Molecules in Protostellar Nebulae. Astrophys. J. 673, 225-228. https://doi.org/10.1086/528741

Oba, Y., Osaka, K., Chigai, T., Kouchi, A., Watanabe, N., 2016. Hydrogen–deuterium substitution in solid ethanol by surface reactions at low temperatures. Mon. Notices Royal Astron. Soc. 462, 689-695. https://doi.org/10.1093/mnras/stw1714

Oelkers, E.H., Declercq, J., Saldi, G.D., Gislason, S.R., Schott, J., 2018. Olivine dissolution rates: A critical review. Chem. Geol. 500, 1-19. https://doi.org/10.1016/j.chemgeo.2018.10.008

Ootsubo, T., Kawakita, H., Shinnaka, Y., Watanabe, J., Honda, M., 2020. Unidentified infrared emission features in mid-infrared spectrum of comet 21P/Giacobini-Zinner. Icarus, 338, 113450. https://doi.org/10.1016/j.icarus.2019.113450.

Owen, T., Lutz, B.L., de Bergh, C., 1986. Deuterium in the outer Solar System: evidence for two distinct reservoirs. Nature 320, 244-246. https://doi.org/10.1038/320244a0

Parise, B., Castets, A., Herbst, E., Caux, E., Ceccarelli, C., Mukhopadhyay, I., Tielens, A.G.G.M., 2004. First detection of triply-deuterated methanol. Astron. Astrophys. 416, 159-163. https://doi.org/10.1051/0004- 6361:20034490

Pearson, V.K., Sephton, M., Kearsley, A.T., Bland, P.A., Franchi, I.A., Gilmour, I., 2002. Clay mineral-organic matter relationships in the early solar system. Meteorit. Planet. Sci. 37, 1829-1833.

https://doi.org/10.1111/j.1945-5100.2002.tb01166.x

Pearson, V.K., Kearsley, A.T., Sephton, M.A., Gilmour, I.G., 2007. The labelling of meteoritic organic material using osmium tetroxidevapour impregnation. Planet. Space Sci. 55, 1310-1318. https://doi.org/10.1016/j.pss.2007.04.005

Piani, L., Robert, F., Remusat, L., 2015. Micron-scale D/H heterogeneity in chondrite matrices: A signature of the pristine solar system water? Earth Planet. Sci. Lett. 415, 154-164. https://doi.org/10.1016/j.epsl.2015.01.039

Plümper, O., Royne, A., Magraso, A., Jamtveit, B., 2012. The interface-scale mechanism of reaction-induced fracturing during serpentinization. Geol. 40, 1103-1106. https://doi.org/10.1130/G33390.1

Postizil, C., Montgomery, W., Sephton, M.A., 2017. Effects of pressure on model compounds of meteorite organic matter. ACS Earth Space Chem. 1, 475-482. https://doi.org/10.1021/acsearthspacechem.7b00053

Putnis, A., 2002. Mineral replacement reactions: from macroscopic observations to microscopic mechanisms. Mineral. Mag. 66, 689-708. https://doi.org/10.1180/0026461026650056

Quirico, E., Raynal, P.I., Bourot-Denise, M., 2003. Metamorphic grade of organic matter in six unequilibrated ordinary chondrites. Meteorit. Planet. Sci. 38, 795-811. https://doi.org/10.1111/j.1945-5100.2003.tb00043.x

Quirico, E, Montagnac, G., Rouzaud, J.-N., Bonal, L., Bourot-Denise, M., Duber, S., Reynard, B., 2009. Precursor and metamorphic condition effects on Raman spectra of poorly ordered carbonaceous matter in chondrites and coals. Earth Planet. Sci. Lett. 287, 185-193. https://doi.org/10.1016/j.epsl.2009.07.041

Quirico, E., Bonal, L., Beck, P., Alexander, C.M.O'D., Yabuta, H., Nakamura, T., Nakato, A., Fladndinet, L., Montagnac, G., Schmitt-Kopplin, P., Herd, C.D.K., 2018. Prevalence and nature of heating processes in CM and C2-ungrouped chondrites as revealed by insoluble organic matter. Geochim. Cosmochim. Acta 241, 17-37. https://doi.org/10.1016/j.gca.2018.08.029

Remsat, L., Piani, L., Bernard, S., 2016. Thermal recalcitrance of the organic D-rich component of ordinary chondrites. Earth Planet. Sci. Lett. 435, 36-44. https://doi.org/10.1016/j.epsl.2015.12.009

Rotelli, L., Trigo-Rodríguez, J.M., Moyano-Cambero, C.E., Carota, E., Botta, L., Di Mauro, E., Saladino, R., 2016. The key role of meteorites in the formation of relevant prebiotic molecules in a formamide/water environment. Sci. Rep. 6: 38888. https://doi.org/10.1038/srep38888

Rubin, A.E., 2004. Postshock annealing and postannealing shock in equilibrated ordinary chondrites: Implications for the thermal and shock histories of chondritic asteroids. Geochim. Cosmochim. Acta 68, 673-689. https://doi.org/10.1016/S0016-7037(03)00452-6

Rubin, A.E., Trigo-Rodríguez, J.M., Huber, H., Wasson, J.T., 2007. Progressive aqueous alteration of CM carbonaceous chondrites. Geochim. Chosmochim. Acta 71, 2361-2382. https://doi.org/10.1016/j.gca.2007.02.008

Sandford, S.A., Aléon, J., Alexander, C.M.O'D., Araki, T., Bajt, S., Baratta, G.A., Borg, J., Bradley, J.P., Brownlee, D.E., Brucato, J.R., Burchell, M.J., Busemann, H., Butterworth, A., Clemett, S. J., Cody, G., Colangeli, L., Cooper, G., D'Hendecourt, L. Djouadi, Z., Dworkin, J. P., Ferrini, G., Fleckenstein, H., Flynn, G.J., Franchi, I.A., Fries, M., Gilles, M.K., Glavin, D.P., Gounelle, M., Grossemy, F., Jacobsen, C., Keller, L.P., Kilcoyne, A.L.D., Leitner, J., Matrajt, G., Meibom, A., Mennella, V., Mostefaoui, S., Nittler, L.R., Palumbo, M.E., Papanastassiou, D.A., Robert, F., Rotundi, A., Snead, C.J., Spencer, M.K., Stadermann, F.J., Steele, A., Stephan, T., Tsou, P., Tyliszczak, T., Westphal, A.J., Wirick, S., Wopenka, B., Yabuta, H., Zare, R.N., Zolensky, M.E., 2006. Organics captured from comet 81P/Wild 2 by the stardust spacecraft. Science, 314, 1720-1724. DOI: 10.1126/science.1135841.

Sanna, A., Andrésen, J.M., 2012. Bio-oil deoxygenation by catalytic pyrolysis: novel catalysts for the conversion of biomass into densified and deoxygenated bio-oil. ChemSusChem 1-26.

Sayah, A., Habelhames, F., Bahloul, A., Nessark, B., Bonnassieux, Y., Tendelier, D., Joua, M.E., 2018. Electrochemical synthesis of polyaniline-exfoliated graphene composite films and their capacitance properties. J. Electroanal. Chem., 818, 26–34. https://doi.org/10.1016/j.jelechem.2018.04.016

Sekine, Y., Shibuya, T., Postberg, F., Hsu, H., Suzuki, K., Masaki, Y., Kuwatani, T., Mori, M., Hong, P. K., Yoshizaki, M., Tachibana, S., Sirono, S., 2015. High-Temperature Water–Rock Interactions and Hydrothermal Environments in the Chondrite-like Core of Enceladus. Nat. Commun., 6:8604. https://doi.org/10.1038/ncomms9604

Shankland, R.V., 1954. Industrial catalytic cracking. In: Frankenburg, W.G., Rideal, E.K., Komarewsky, V.I. (eds.), Advances in Catalysis and related subjects. Academic Press, New York, pp. 271-434. https://doi.org/10.1016/S0360-0564(08)60393-4

Socrates, G., 2001. Infrared and Raman characteristic group frequencies, third ed. John Wiley & Sons, Chichester. https://doi.org/10.1002/cssc.201200245

Takatori, K., Tomeoka, K., Tsukimura, K., Takeda, H., 1993. Hydrothermal Alteration Experiments of Olivine with Varying Fe Contents: an Attempt to Simulate Aqueous Alteration of the Carbonaceous Chondrites. In: Lunar and Planetary Science Conference XXIV Abstract #1389.

Taquet, V., Ceccarelli, C., Kahane, C., 2012. Formaldehyde and methanol deuteration in protostars: fossils from a past fast high-density Pre-collapse phase. Astrophys. J. Lett. 748, L3. https://doi.org/10.1088/2041- 8205/748/1/L3

Tao, Y., Dreger, Z.A., Gupta, Y.M., 2014. High pressure effects on benzoic acid dimers: vibrational spectroscopy. Vib. Spectrosc. 73, 138-143. https://doi.org/10.1016/j.vibspec.2014.06.002

Tian, M., Liu, B.S., Hammonds, M., Wang, N., Sarre, P.J., Cheung, A.S.-C., 2012. Formation of polycyclic aromatic hydrocarbons from acetylene over nanosized olivine-type silicates. Phys. Chem. Chem. Phys. 14, 6603-6610. https://doi.org/10.1039/C2CP23309F

Tomeoka, K., Mcsween Jr, H. Y., Buseck, P. R., 1989. Mineralogical Alteration of CM Carbonaceous Chondrites: A Review. Proc. NIPR Symp. Antarct. Meteorites, 2, 221-234.

Tomeoka, K., Tanimura, I., 2000. Phyllosilicate-rich chondrule rims in the Vigarano CV3 chondrite: Evidence for parent-body processes. Geochim. Cosmochim. Acta 64, 1971-1988. https://doi.org/10.1016/S0016-7037(00)00332-X

Trejda, M., Nurwita, A., Kryszac, D., 2019. Synthesis of solid acid catalysis for esterification with the assistance of elevated pressure. Microporous Mesoporous Mater. 278, 115-120. https://doi.org/10.1016/j.micromeso.2018.11.009

Trigo-Rodríguez, J.M., Rimola, A., Tanbakouei, S., Soto, V.C., Lee, M., 2019. Accretion of Water in Carbonaceous Chondrites: Current Evidence and Implications for the Delivery of Water to Early Earth. Space Sci. Rev. 215, 18. https://doi.org/10.1007/s11214-019-0583-0

Trigo-Rodríguez, J.M., Rubin, A.E., Wasson, J.T., 2006. Non-nebular origin of dark mantles around chondrules and inclusions in CM chondrites. Geochim. Cosmochim. Acta 70, 1271-1290. https://doi.org/10.1016/j.gca.2005.11.009

Tsubokawa, Y., Ishikawa, Y., 2017. Sintering polycrystalline olivine and polycrystalline clinopyroxene containing trace amount of graphite from natural crystals. Earth Planets Space, 69: 128. https://doi.org/10.1186/s40623-017-0717-0

Ueki, K., Inui, M., Matsunaga, K., Okamoto, N., Oshio, K., 2020. Oxidation during Magma Mixing Recorded by Symplectites at Kusatsu–Shirane Volcano, Central Japan. Earth Planets Space, 72:68. https://doi.org/10.1186/s40623-020-01192-4

Ulrich, M., Muñoz, M., Guillot, S., Cathelineau, M., Picard, C., Quesnel, B., Boulvais, P., Couteau, C., 2014. Dissolution-precipitation processes governing the carbonation and silicication of the serpentinite sole of the New Caledonia ophiolite. Contrib. to Mineral. Petrol. 167, 952. https://dx.doi.org/10.1007/s00410-013- 0952-8

Vacher, L. G., Truche, L., Faure, F., Tissandier, L., Mosser-Ruck, R., Marrocchi, Y., 2019. Deciphering the Conditions of Tochilinite and Cronstedtite Formation in CM chondrites from Low Temperature Hydrothermal Experiments. Meteorit. Planet. Sci. 54, 1-20. https://doi.org/10.1111/maps.13317

Varma, R.S., 2002. Clay and clay-supported reagents in organic synthesis. Tetrahedron 58, 1235-1255.

Velvel, M.A., 2009. Dissolution of olivine during natural weathering. Geochim. Cosmochim. Acta 73, 6098- 6113. https://doi.org/10.1016/j.gca.2009.07.024

Vinogradoff, V., Le Guillou, C., Bernard, S., Viennet, J.C., Jaber, M., Remusat, L., 2020. Influence of phyllosilicates on the hydrothermal alteration of organic matter in asteroids: Experimental perspectives. Geochim. Cosmochim. Acta 269, 150-166. https://doi.org/10.1016/j.gca.2019.10.029

Vinogradoff, V., Remusat, L., McLain, H.L., Aponte, J.C., Bernard, S., Danger, G., Dworkin, J.P., Elsila, J.E., Jaber, M., 2020. Impact of phyllosilicates on amino acid formation under asteroidal

conditions. ACS Earth Space Chem. 4, 1398-1407. https://doi.org/10.1021/acsearthspacechem.0c00137

Walsh, C., Millar, T.J., Nomura, H., Herbst, E., Weaver, S.W., Aikawa, Y., Laas, J.C., Vasyunin, A.I., 2014. Complex organic molecules in protoplanetary disks. Astron. Astrophys. 563, A33. https://doi.org/10.1051/0004- 6361/201322446

Walsh, C., Loomis, R.A., Öberg, K.I., Kama, M., van 't Hoff, M.L.R., Millar, T.J., Aikawa, Y., Herbst, E., Weaver, S.L.W., Nomura, H. 2016. First detection of gas-phase methanol in a protoplanetary disk. Astrophys. J. Lett. 823, L10. https://doi.org/10.3847/2041-8205/823/1/L10

Wang, W. B., Shi, Z. M., Wang, X. G., Wang, Z. X., Cao, Z., Fan, W., 2017. The synthesis and properties of high-quality forsterite ceramics using desert drift sands to replace traditional raw materials. J. Ceram. Soc. Japan, 125, 88-94. https://doi.org/10.2109/jcersj2.16268

Watanabe, N., Kouchi, A., 2008. Ice surface reactions: A key to chemical evolution in space. Prog. Surf. Sci. 83, 439-489. https://doi.org/10.1016/j.progsurf.2008.10.001

Wegner, W.W., Ernst, W.G., 1983. Experimentally determined hydration and dehydration reaction rates in the system MgO-SiO_2-H_2O. Am. J. Sci. 283-A, 151-180.

Wheeler, E. P., 1965. Fayalitic Olivine in Northern Newfoundland-Labrador. Can. Mineral., 8, 339–346.

Yabuta, H., Williams, L.B., Cody, G.D., Alexander, C.M.O'D., Pizzarello, S., 2007. The insoluble carbonaceous material of CM chondrites: A possible source of discrete organic compounds under hydrothermal conditions. *Meteorit. Planet. Sci.* 42, 37-48. https://doi.org/10.1111/j.1945-5100.2007.tb00216.x

Yada, K., Iishi, K., 1974. Serpentine minerals hydrothermally synthesized and their microstructures. J. Cryst. Growth 24/25, 627-630. https://doi.org/10.1016/0022-0248(74)90393-5

Yada, K., Iishi, K., 1977. Growth and microstructure of synthetic chrysotile. Am. Mineral. 62, 958-965.

Yamashita, Y., Naraoka, H., 2014. Two homologous series of alkylpyridines in the Murchison meteorite. Geochem. J. 48, 519-525. https://doi.org/10.2343/geochemj.2.0340Vinogradoff, V., Le Guillou, C., Bernard, S., Vinnet, J.C., Jaber, M., Remusat, L., 2020. Influence of phyllosilicates on the hydrothermal alteration of organic matter in asteroids: experimental perspectives. Geochim. Cosmochim. Acta 269, 150-166. https://doi.org/10.1016/j.gca.2019.10.029

Yesiltas, M., Peale, R.E., Unger, M., Sedlmair, J., Hirschmugl, C.J., 2015. Organic and inorganic correlations for Northwest Africa 852 by synchrotron-based Fourier transform infrared microspectroscopy. Meteorit. Planet. Sci. 50, 1684-1696. https://doi.org/10.1111/maps.12498

Yesiltas, M., Kebukawa, Y., 2016. Associations of organic matter with minerals in Tagish Lake meteorite via highspatial resolution synchrotron-based FTIR microspectroscopy. Meteorit. Plaet. Sci. 51, 584-595. https://doi.org/10.1111/maps.12609

Yoder Jr., H. S., Sahama, T. G., 1957. Olivine X-ray Determinative Curve. Am. Mineral. 42, 475-491.

Yokoyama, K., Tiba, T., Chihara, K., 1992. Picrite sill in the Sado Island, Japan. Bull. Natn. Sci. Mus., Tokyo, Ser. C, 18, 1-11.

Acknowledgements

I would like to express my sincere gratitude to the supervisor, associate Professor Y. Kebukawa of Graduate School of Engineering Science, Yokohama National University. She gave me a lot of comments and significant ideas to develop my studies. She was always supportive for performing experiments, discussing problems and summarizing reports as journals. Without her kind cooperation, my researches could not reach to the sufficient qualities as planetary science.

I also specially appreciate Professor emeritus K. Kobayashi of Graduate School of Engineering Science, Yokohama National University giving me a lot of suggestive and technical comments for performing experiments. His comments, and also his scientifically interesting ideas, encouraged and excited me a lot of times. My interests and my researches were strongly stimulated by his considerings.

I would also show my great appreciation to my collaborator, Professor H. Nakano of Faculty of Culture and Sport Policy, Toin University of Yokohama, Associate Professor Y. Furukawa of Department of Earth Science, Tohoku University, Mr. M. Kondo of Instrumental Analysis Center, Yokohama National University, Dr. T. Shibuya of Institute for Extra-cutting-edge Science and Technology Avant-garde Research (X-star), Super-cutting-edge Grand and Advanced Research (SUGAR) Program, Japan Agency for Marine-Earth Science and Technology (JAMSTEC) and Dr. H. Ueda of Institute for Extra-cutting-edge Science and Technology Avant-garde Research (X-star), Super-cutting-edge Grand and Advanced Research (SUGAR) Program, Japan Agency for Marine-Earth Science and Technology (JAMSTEC) for performing and teaching significant experiments, analyses. All my works were strongly supported by their very kind cooperation.

In addition to them, I thank Dr. Naoki Yoshihara of Instrumental Analysis Center, Yokohama National University for providing access to the XRD, Dr. Yoshihiro Kubota and Dr. Satoshi Inagaki of Graduate School of Engineering Science, Yokohama National University for providing access to the GC/MS, Dr. George D. Cody of Earth and Planets Laboratory, Carnegie Institution for Science for providing San Carlos olivine, Dr. Ellen Yvette Aguilar Ovando of Instituto de Ciencias Nucleares, Universidad Nacional Auto´noma de Me´xico for providing montmorillonite, Professor Shungo Kawagata of Department of Education, Yokohama National University for providing access to the SEM/EDS equipment, Dr. Aiko Nakato and Dr. Miwa Yoshitake of Astromaterials Science Research Group (ASRG), Japan Aerospace Exploration Agency for supporting the FIB processing, Mr. Takamichi Miyazaki Instrumental Analysis Group, Graduate School of Engineering, Tohoku University for supporting the TEM analysis.

I would acknowledge Professor C. Kojima, Professor H. Yoshitake, Associated Professor R. Inagaki, Professor emeritus K. Kobayashi for my thesis examination.

21th Jan. 2021 Naoki Hirakawa